UNIVERSITÀ DI PARMA

UNIVERSITÁ DEGLI STUDI DI PARMA

DOTTORATO DI RICERCA IN SCIENZE DELLA TERRA CICLO XXXVI

Modelling of Hydro-Geomorphological Processes Related to Sediment Transport:

Case Study of the Baganza River (Italy)

Coordinatore:

Chiar.mo Prof. F. Balsamo

Tutore:

Chiar.mo Prof. R. Valentino

Co-Tutori:

Chiar.mo Prof. A. Chelli

Chiar.mo Prof.ssa S. Dazzi

Chiar.mo Prof.ssa A. Ferrari

Chiar.mo Prof. R. Vacondio

Dottorando: Usman Ali Khan

Anni Accademici 2020/2021 – 2022/2023

Abstract

Sediment transport and the processes that shape river landscapes have a significant impact on flood dynamics. This interdisciplinary study combines Earth Sciences and Hydraulic Engineering principles to investigate sediment bahaviour within the Baganza River catchment in Northern Italy. The research particularly focuses on developing a robust sediment transport numerical model, which is essential for simulating the bed morphological changes in river systems.

It's imperative to note that while numerical models are valuable tools, their effectiveness depends on addressing various limitations, such as spatial and temporal scales, data requirements, model complexity, numerical stability, and computational demands. This research aims to overcome these constraints by examining a 2D numerical model specifically designed for simulating bedload transport in real-world applications. The model incorporates weak coupling of shallow water and Exner equations, which represent the liquid and solid phases, respectively.

Besides the modification and improvement of the pre-existing numerical model, one of the novelties of this research lies in the fact that it incorporates actual grain size obtained from field-derived data, used as input parameter for the model. The technique employed for obtaining granulometric distribution is of hybrid nature i.e., combining sieve analysis and photogrammetric technique. This offers an efficient and cost-effective approach, enhancing sediment analysis precision while reducing fieldwork demands. By applying the built model to the Baganza River, it provides valuable insights into sediment conveyance, flow-bed interactions, erosion, and deposition.

To estimate sediment discharge, equations by Meyer-Peter and Müller (1948) and Smart (1984) were employed, which are optimized for computational efficiency using Graphics Processing Unit (GPU) parallelization. Hereafter, Smart (1984) will be referred to as the SMART and Meyer-Peter and Müller (1948) as the MPM approach. The model simulates morphological transformations that occurred in the Baganza River between 2008 and 2014, utilizing a high-resolution (4 m x 4 m) Digital Terrain Model (DTM). The model's accuracy is validated by benchmark testing against 1D and 2D dam break scenarios with mobile bed conditions, including sensitivity analyses of model input parameters. In the absence of calibration data, sensitivity analysis explores the influence of key input parameters on the predictive capabilities of the bedload transport model. Three distinct cases are considered, each examining the model's response to alterations in specific parameters, i.e. median grain size D_{50} and manning roughness "n" value while keeping other variables constant. The results of the sensitivity analysis shed light on the performance of the 2D sediment transport model.

The findings contribute to best parameter selection and model enhancements, ultimately improving the model's predictive capabilities. Furthermore, the analysis of 2D model outputs related to the Baganza River delineates eight distinct in-channel bed Morphological Units (MU's), based on thresholds measuring depth and Froude number. These units encompass pools, runs, chutes, riffles, riffle transitions, fast glides, slow glides, and slackwater zones.

In conclusion, this research underscores the significance of an interdisciplinary approach in comprehending the intricate sediment dynamics of riverine environments.

Keywords: sediment transport, sensitivity analysis, geomorphic analysis, flood risk management, granulometric distribution.

Acknowledgements

All praises belong to Allah, who is the Author of all existence, the most magnificent and merciful, for granting me the strength and patience to navigate the challenges of this academic journey.

I extend my heartfelt thanks to my supervisor, Prof. Roberto Valentino, for his consistent guidance, invaluable insights, and unwavering support. His expertise has played a pivotal role in shaping the trajectory of this research.

I am deeply indebted to Prof. Renato Vacondio along with Prof.ssa Susanna Dazzi and Prof.ssa Alessia Ferrari for their steadfast support, which was instrumental in the successful development of this research.

A special appreciation to Prof. Alessandro Chelli for his time-to-time feedback and keen insights from geomorphological perspective, which have been influential in enhancing the depth and quality of this thesis.

To my family and friends, I extend my deepest gratitude for their prayers, support, and encouragement. Undoubtedly, their love has been a constant source of inspiration and strength throughout this doctoral journey. This thesis is a testament to the collective efforts, guidance, and support from all of these.

Contents

List of Figures

List of Tables

Chapter 1: INTRODUCTION

1.1 Background and Motivation

My academic journey is started from a civil engineering background specialization in Water Science and Hydraulics Engineering. Transitioning into Earth Sciences at the University of Parma presented an intriguing challenge due to limited knowledge of the sector. This prompted me to seek interdisciplinary research opportunities, aiming to bridge the gap between Earth Sciences and Hydraulics Engineering. My exploration began with an in-depth study of river geomorphology, flood-related topics, i.e. levee erosion and river training works, focusing on the interface between land and water dynamics.

This pursuit led to the identification of a critical knowledge gap such as necessity for comprehensive guidelines in geomorphic and granulometric data collection for numerical modellers. The objective was to develop robust sediment transport model to support modellers with essential input data requirement. Under the supervision of Prof. Roberto Valentino, I embarked on a collaborative effort by Prof. Renato Vacondio, Prof.ssa Susanna Dazzi and Prof.ssa Alessia Ferrari at the Department of Engineering and Architecture, University of Parma. This collaboration was instrumental in integrating sediment effects into the PARFLOOD model (Inhouse built flood modelling tool at University of Parma) — an essential step towards my interdisciplinary aspirations.

Additionally, my prior experience in analysing sediment transport dynamics in the Piave River (Italy) during my Master's studies provided a strong foundation and motivation for this pursuit. The aspiration to contribute by developing practical guidelines and dependable sediment transport model for flood management remains a driving force. These endeavours propel my research towards addressing significant gaps in understanding sediment dynamics and their implications for effective flood management strategies.

1.2 Research Objectives

The main objective of this thesis is to conduct an interdisciplinary study in Baganza River through numerical modelling. Below are the specific objectives of this thesis.

1. Geomorphological characterization of Baganza River basin for identification of key morphometric parameters.
2. Granulometric characterization of Baganza River by indicating representative grain size distribution that will be used as input parameter for the sediment transport model.
3. Incorporating sediment effects into the 2-D hydrodynamic PARFLOOD model Vacondio et al. (2014, 2017), validating its accuracy and efficiency through benchmark testing.
4. Evaluation of different morphological shapes at key river sections by simulating real floods (2008-2014).
5. Model Validation and Sensitivity Analysis.
6. Application of the model to predict the In-channel Morphological Units (MU's).

1.3 Significance and Scope

The research is important for three key reasons:

Firstly, this is an interdisciplinary study that focuses on geomorphological changes using sediment transport numerical modelling, which is able to highlight areas that show potential morphological changes i.e., erosion and deposition. This could improve significantly flood management strategies locally.

Secondly, the inclusion of actual field data, particularly grain size distribution, enhances the reliability of the sediment transport model by ensuring a realistic representation of sediment characteristics, which are crucial for accurate simulations.

Thirdly, by replicating and confirming the changes that occurred in the Baganza River during significant floods from 2008 to 2014, this research ensures that the model captures real-world scenarios.

1.4 Interdisciplinary Approach

The adoption of an interdisciplinary approach in this research work arises from the recognition that complex phenomena, such as sediment transport, demand a holistic understanding that transcends the boundaries of single disciplines. This research at its core employs a weakly-coupled shallow water Exner approach, integrating actual field data such as grain size distribution, Manning roughness, hydrological and bathymetric information. Including benchmarking through 1D and 2D dam break tests, along with sensitivity analysis, ensures the model's accuracy.

Furthermore, the results of the numerical simulations are utilized to delineate in-channel morphological units. This approach is instrumental in providing a comprehensive understanding of sediment transport and morphodynamics. The reliability of the sediment transport model is fortified through rigorous benchmarking, including 1D and 2D dam break laboratory tests from the literature, as already explained. These tests subject the model to challenging scenarios and assess its performance in simulating morphological changes. This process serves as a robust mechanism for identifying potential limitations and refining the model to enhance its reliability and applicability in real-world river systems. The research employs sensitivity analysis to fine-tune the parameterization of the sediment transport model. By systematically varying input parameters such as grain size distribution and manning roughness, this research gains insights into their influence on model predictions and check model responsiveness.

The interdisciplinary nature of this study and its key components are shown in Figure 1.1. The primary focus, highlighted in yellow, is the construction of the sediment transport model. Other aspects orbit around this central theme, encompassing tasks like collecting data tailored for the chosen sediment transport model. This process also involves selecting the best model parameters to achieve accurate results. Following this, a selected area of the Baganza River is simulated using these refined model parameters, leading to the identification of

in-channel morphological units, based on the obtained results. This flowchart provides a visual representation of the overall approach utilized in this study. Here SO means specific objectives.

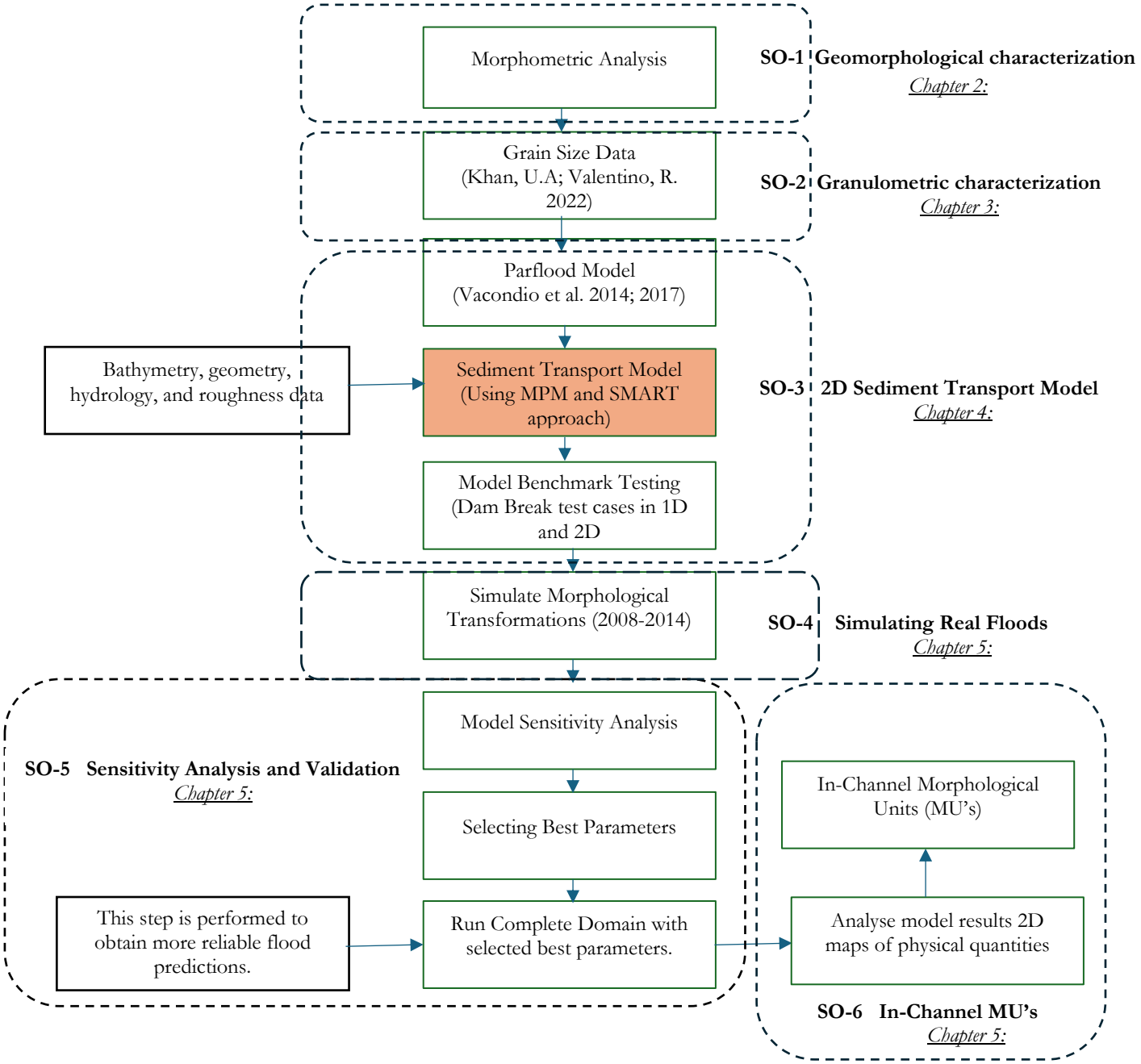

Figure 1.1 Flow chart showing interdisciplinary approach for Baganza River

1.5 Thesis Organization

The structure of this thesis is as follows:

Chapter 1 covers the background and motivation behind the study, aiming to describe the relationship between sediment transport and geomorphology. This chapter explicitly defines research objectives, outlining the goals along with explaining the interdisciplinary approach utilized in this thesis for sediment transport modelling.

Chapter 2 covers detailed characterization of geomorphological features of the Baganza catchment. It begins by introducing the characterization process, summarizing previous studies, methodology utilized, and subsequently presenting and discussing the results. The main objective was achieved by characterizing hydro-geomorphological processes using morphometric approach using a Geographic Information System (GIS) based plugin, analysing the results, and discussing them.

Chapter 3 corresponds to a published research article that is included in this thesis. It probes into the incorporation of sediment granulometric distributions derived from field data. It specifically focuses on a hybrid technique, offering an efficient and cost-effective approach to obtain appropriate granulometric distributions while reducing the demands of extensive fieldwork. The information was used as input parameter for the sediment model.

Chapter 4 contains construction, testing and validation of a sediment transport numerical model. It commences with an introduction to numerical modelling, by studying the hydrodynamic PARFLOOD model, and progresses into detailing the integration of sediment effects into this model. The chapter describes the relevant equations and formulas utilized in hydrodynamic and sediment code. It also discusses river domain discretization, numerical flux computation, and the process of model validation through various benchmark testing cases.

Chapter 5 is centred on the case study of the Baganza River in Italy and includes a detailed analysis of the morphological evolution during a specific flooding period (2008-2014). This chapter aims to present the modelling results, followed by a sensitivity analysis, and concludes with a comprehensive discussion of the derived outcomes. It also describes high-resolution data pertaining to geomorphic processes. It primarily focuses on in-channel bed morphological units, obtained from the post processing results (velocity and depth raster's) of the 2D morphodynamical model, and analysis of erosion and deposition volumes.

Chapter 2: GEOMORPHOLOGICAL CHARACTERIZATION

2.1 Sediment Transport in River Systems

2.1.1 Outline

In the field of sediment transport modelling and fluvial geomorphology, demonstrating the movement of water and sediment is a major challenge, and significant efforts have been made in this context. The complexity arises from constantly changing patterns of fluid flow, high sediment concentrations, and complex interactions between hydraulics and sediment transport, all of which result in morphological changes.

Additionally, rivers have unique characteristics such as irregular topology that changes over time and distance, and differences in the composition of materials in the layers further complicate the modelling process. To enhance this complexity, rivers are often restricted by artificial barriers such as dams and levees, which play an important role in water management such as flood control, but are also vulnerable to natural breaches. For instance, it could be the case of a levee failure, that poses a threat to downstream infrastructure and floodplains due to the powerful energy released by the resulting waves. This phenomenon is characterized by unsteady hydrodynamics, intense sediment transport, and consequent morphological changes.

Sediment transport is a fundamental process that shapes river landscapes and influences basin-scale hydro geomorphological processes. This plays an important role in determining channel morphology, sediment distribution, and overall river bahaviour. Understanding sediment dynamics is important for a variety of applications such as flood risk assessment, river restoration, and catchment management. In gravel-bedded rivers, sediment transport is influenced by a complex interaction between flow dynamics, geological composition (including lithology of clasts), sediment supply, and channel morphology. The movement of particles, from sand to gravel to boulders, is critical in shaping riverbeds and influencing habitat conditions for aquatic life. Innovative methods such as numerical modelling have significantly contributed to improving the understanding of sediment transport processes in river systems.

The effectiveness of a model is determined by the quality of the available data and the numerical scheme the model uses to solve the problem. This limits both the structure and parameters of the model and affects the accuracy of the predictions. Researchers have developed a variety of models that simulate sediment transport under different flow conditions and sediment properties. These models span a wide range of scales, from small-scale laboratory experiments to large-scale basin-scale simulations. Additionally, these numerical models require specific parameters to simulate real river conditions, such as flow velocity, roughness, grain size distribution, and channel bathymetry. These parameters are essential for the model to reproduce the complexity of sediment transport in rivers.

2.1.2 Literature Review

Numerical modelling plays a vital role in understanding complex processes and predicting system bahaviour. Hutton's (2012) study focused on the selection criteria for numerical modelling schemes, addressing uncertainties associated with these processes. This laid the groundwork for subsequent studies, such as exploration of 2D sediment transport modelling in high-energy rivers Zavattero et al. (2016). They employed finite volume schemes with unstructured meshes, providing deeper insights into sediment bahaviour. One of the key advantages of using finite volume schemes with unstructured meshes is their exceptional flexibility in adapting to complex geometries and irregular boundaries, allowing for accurate representation of the physical features of rivers, including meanders, confluences, and irregular bed shapes. Some of the macro-types of numerical models used in geomorphic studies are categorized as follows:

- Process-Based Models

  Process-based models represent the underlying mechanisms governing landscape dynamics, i.e. sediment transport process. These models such as cellular automata models, particle-based models and fluid dynamics simulations, at fine spatio-temporal scales focus on capturing detailed interactions.
- Conceptual Models

  Conceptual models provide a simplified representation of geomorphic system bahaviour. The core concept is to represent the broad pattern and relationship rather than detailed physics of catchment characteristics.
- Empirical Models

  Empirical models rely on observation and statistical relationships. They lack the mechanistic details but offer some practical predictions. For instance, in hydrometry, the rating curve serves as a conceptual model, while regression models fall into this category.
- Hybrid Models

  Hybrid models utilize process-based models and empirical models to optimize the modelling process to get efficient results. Hybrid models strike a balance between accuracy and computational efficiency and are valuable for large scale simulations.

High-resolution spatial data is crucial for numerical modelling, offering precision and accuracy in capturing detailed spatial and temporal variations, thereby enhancing the realism of simulation. In this regard, Williams et al. (2016) conducted a comprehensive review, emphasizing the integration of high-resolution survey data in numerical modelling approaches for braided river morphodynamics. This integration turned out to be crucial for accurate predictions, especially in complex river systems. Dottori et al. (2017) proposed an operational procedure for rapid flood risk estimation in Europe, highlighting the importance of translating flood forecasts into risk estimations for specific river basins during flood events. A GIS-based morphometric indexing approach, showcasing the integration of technology to assess sediment connectivity in small alpine catchments,

was developed by Cavalli et al. (2013). This method, grounded in high-resolution data, provides an effective evaluation of sediment transfer processes, fostering a nuanced comprehension of sediment connectivity.

Dazzi et al. (2019) integrated a levee breach erosion model with a GPU-accelerated 2D shallow water equation code. The suggested model dynamically adjusts the local topography in real-time whenever the levee is overtopped, eliminating the need to predefine the position and shape of the breach. Vanzo et al. (2021) took a modular approach, leading BASEMENT v3, a freeware for river process modelling. This numerical model efficiently simulates large-scale hydrodynamic processes and morphological scenarios, thereby supporting river restoration and basin management. The modular nature encourages a holistic understanding of river systems, emphasizing the interconnectedness of various components. The investigation expands beyond numerical modelling, encompassing studies that contribute to various aspects of sediment transport.

Studies exploring long-term morphological changes resulting from large rock-slope failures, such as that by Korup et al. (2006) contribute valuable insights into the impacts of natural dams on fluvial systems. These insights feed into the broader narrative of understanding river responses to external influences.

Robert et al. (2014) presented an advanced review on geomorphological changes, offering guidelines for sustainable river restoration and catchment management. Kabir et al. (2015) evaluated different sediment transport capacity equations (TCEs) using a process-based sediment dynamic model. Their work, grounded in data from the Abukuma River Basin, contributes to the ongoing refinement of models, demonstrating the need for continuous integration and validation to improve our understanding of suspended sediment dynamics. This review integrates knowledge from various studies, aiding in identifying the underlying causes of geomorphological changes and predicting possible trajectories under different management scenarios.

2.2 Geomorphological Processes

Geomorphological processes are the natural forces that shape and transform the earth's surface over time. These processes are influenced by various geomorphological agents, such as wind, water, gravity, and other environmental factors. These processes play a crucial role in shaping landscapes, altering terrain, and influencing the distribution of land, water, and resources. Some of the key geomorphological processes are captioned in the Figure 2.1.

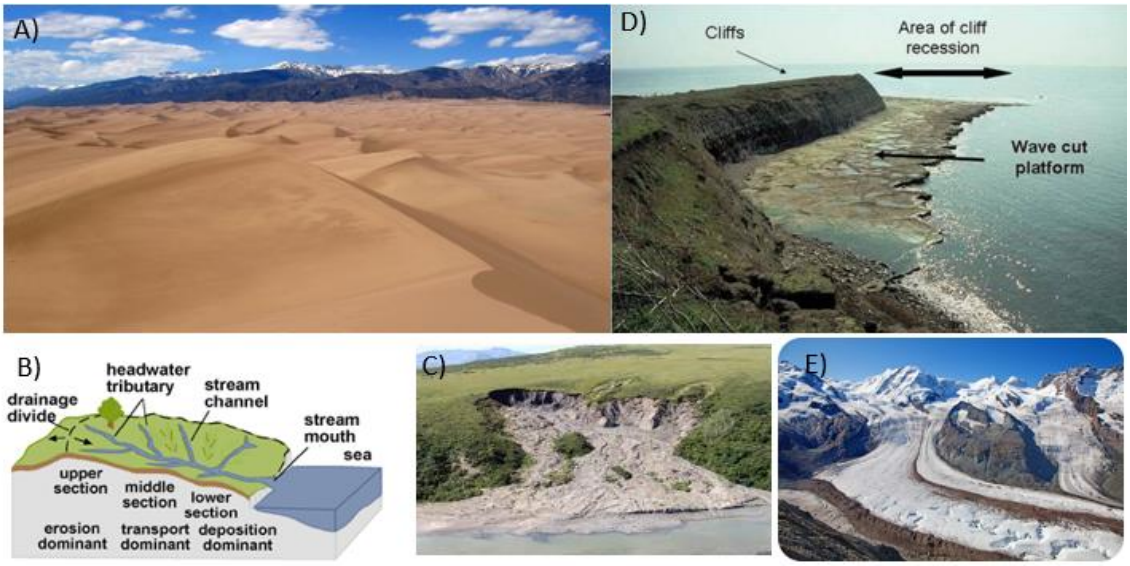

Figure 2.1. Capturing key geomorphological processes: A) Aeolian: Depicting wind-driven erosion, sand movement, and desert landscape, B) Fluvial: Riverine processes segmented into upper, middle and lower section, C) Slope: Representing hillslope instability in the form of landslide, D) Coastal: Showing coastal dynamics, area of cliff recession and beach formulation, and E) Glacial: Portraying glacial movements, and ice deposition (Image sources: Collage created by the author using individual figures obtained from www.google.com)

Understanding hydrogeomorphology involves grasping its core fundamentals, including mechanisms, processes, and the tools required for in-depth analysis. It examines the properties of earth materials, the spatial scales of hydrology, and the dimensions of hydrological units to comprehend the formation and development of landforms.

Moreover, it emphasizes the significance of the hydrological cycle and water budget, showcasing the intricate balance between water inflows, outflows, and storage, which are fundamental to understanding how water interacts with the environment. Historical records on Baganza River shows that an atlas had been developed to know how the river morphology has been changed over time through aerial shots, cartography, and topographical sections etc. The historical atlas consists of three parts. Part I: Planimetric Evolution (1976-2014), which traces the river's planform changes, while Part II: Altimetric Evolution (1972-2014) deals with changes in riverbed elevation in 4 reaches, namely, Reach 1: Calestano – Marzolara, Reach 2: Marzolara - Sala Baganza, Reach 3: Sala Baganza – Parma southern ring road bridge, Reach 4: Parma southern ring road bridge - confluence with the Parma stream. The study area of the current thesis includes all these four reaches. In Part III: Monitoring changes in geomorphological features (2008-2014), captures altimetric fluctuations. The difference lies in the higher spatio-temporal resolution of the analyses performed on this reduced time interval compared to what was reported in Part II. Within the realm of sediment transport modeling, these geomorphological phenomena wield a profound impact. For instance, Ziliani & Surian (2012) reported evolutionary trajectory of the Tagliamento River, a large gravel-bed river in northeastern Italy. By combining historical data and numerical modeling, the research identifies three main phases of channel adjustment over

the last 200 years. Human interventions (sediment mining, channelization) play a significant role, while sediment supply changes have minor effects.

Figure 2.2 Planimetric Evolution (1976-2014) near Collecchio, red line represents the max bank line.

2.2.1 Landforms associated with river morphological processes.

River morphology evolves dynamically with the interaction of water, sediments, and surrounding landscape because of which various landforms built up. The non-exhaustive list of key processes and various landforms mentioned in this thesis are as described as follows:

- Erosion:

  The flowing action of river make gorges and valleys and worn away the earth over a period this process is called erosion. As the river flows, it carries sediment and particles along with it. The friction and impact of these sediments against the riverbed and banks contribute to the erosion process. This

erosive process involves not only the physical force of water but also the gradual disintegration of rocks and sediment along the riverbed and banks.

- Transportation:

  Sediments in the river are transported by different mechanism i.e., traction, saltation or suspension This intermittent movement contributes to the formation of distinctive landforms such as alluvial fans—fan-shaped sediment deposits—and river terraces—elevated, flat surfaces adjacent to rivers.

- Deposition:

  When river velocity decreases, it relinquishes the sediment it has transported as it no longer supports the transport of heavier particles which causes them to settle down and deposition occurs. Deposition in rivers involves understanding the complex interactions between flow velocity, sediment characteristics, channel morphology, and other influencing factors.

- Knickpoints:

  Knickpoints are significant features in river systems that mark sudden changes in the elevation of the riverbed. These changes can occur due to geological variations in the underlying terrain or alterations in the flow regime of the river. Knickpoints play a crucial role in shaping the long-term evolution of river channels and the surrounding landscape. From a modelling perspective, accurately representing these abrupt changes in the riverbed is essential for numerical schemes that aim to simulate real-world scenarios. Numerical models used to study rivers and their behaviour need to account for the presence of knickpoints to ensure accurate and realistic predictions.

- Head Cutting:

  Head cutting denotes the upstream migration of erosion along a river channel, often occurring at waterfalls or steep sections. As the riverbed retreats upstream, it alters the river's profile and drainage patterns, exemplifying the dynamic interplay between erosional processes and landscape evolution.

- Bar:

  Bar refers to an accumulation of sediment within channel in the form of an island containing various particles such as sand, gravel, or rocks. It is a raised or elevated feature that can be found in shallower areas of the river. Bars are created through the deposition of sediment, often influenced by changes in the flow velocity or river morphology. They can take various shapes, such as elongated ridges or islands, and can affect the flow patterns and characteristics of the river.

- Pool:

  Pool is a relatively deep section within a river where the water depth is greater compared to the surrounding areas. Pools are typically characterized by slower flow velocities. They are formed through the deposition of sediment or the presence of natural obstructions that impede the flow. Pools provide areas of refuge and habitat for aquatic organisms, particularly during times of high flow or when the water velocity is swift. They contribute to the diversity and complexity of the river ecosystem.

- Riffle:

  Riffle is a shallower area within a river characterized by fast-flowing water. It is often composed of a rocky or gravelly riverbed, causing the water to flow rapidly and create turbulence. Riffles are typically found in areas with a steeper gradient or where the channel narrows. The turbulent flow over the rough substrate increases oxygenation and aeration of the water, making riffles important habitats for various aquatic organisms. They can also influence sediment transport and erosion processes within the river.

- Glide:

  Glide refers to a relatively smooth and uniform section of a river channel. It is characterized by slower flow velocities and a gentle movement of water. Glides are often located between riffles and pools, serving as transition zones. Glides may contribute to sediment deposition and play a role in shaping the overall hydraulic characteristics of the river channel.

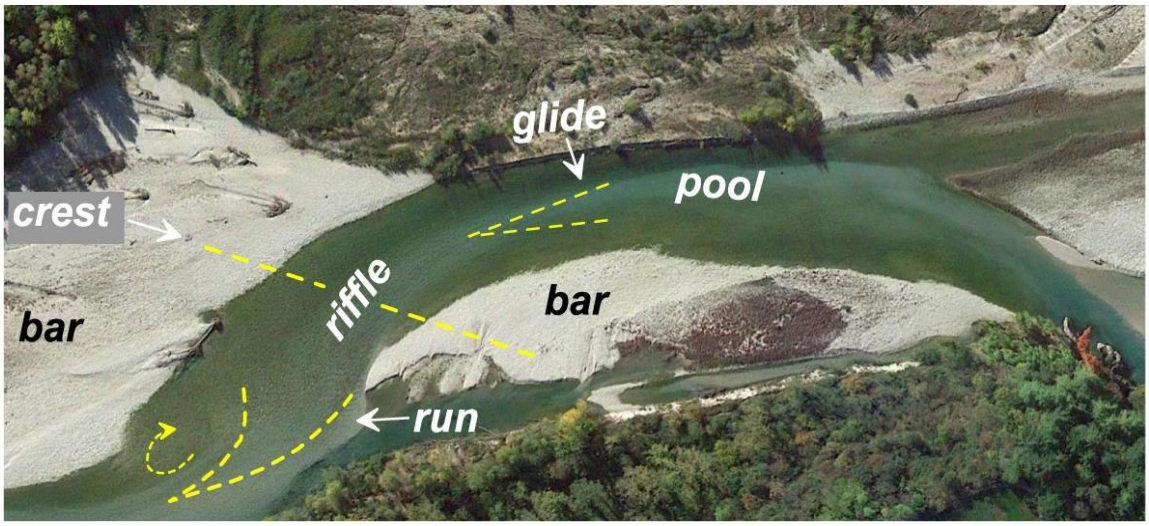

Figure 2.3 Satellite imagery showing different landforms associated with riverine process.

2.2.2 Overview Previous Studies

The Baganza catchment is located in the Emilia Romagna Region (Italy), with an elevation between 1490 and 60 m a.s.l.. It exhibits significant variability in its characteristics along its spatial advancement, ranging from the narrow stretches of the mountain valley, often confined by the slopes, to the wide stretches in the plain. The mountain territory is essentially made up of flyschoid rocks, clayey and arenaceous units combined in a complex structure, controlled by tectonics. To this structure is added the presence of large detrital bodies derived from the glacial phases. From these geological and geomorphological characteristics derives the Predisposing factors to large landslides in hilly and mountainous areas include lithology, tectonic activity, slope morphology, and river erosion. Lithology refers to rock composition, including flysch and other relevant types. Tectonic activity involves faults and seismicity. Slope morphology encompasses shape, steepness, and profile. River erosion undermines slope stability. The strong tectonic action to which the arenaceous-marl and calcareous-marl formations have been subjected and the widespread presence of clayey soils determines a general condition of instability of the slopes and an accentuated susceptibility to surface erosion. ("Variante al Piano per l'assetto idrogeologico del bacino del fiume Po (PAI): torrente Baganza da Calestano a Confluenza Parma e torrente Parma da Parma a confluenza Po", 2015, p.12). The Baganza River flows through this elongated valley, ultimately merging with the Parma River in Parma town. With a length of approximately 34 kilometers and a width varying between 3 to 6 kilometers, the valley features a distinct V-shaped profile, characterized by a gentler eastern slope and a steeper western slope. Predominantly shaped by water and gravity, the valley exhibits remnants of Pleistocene glacial activity in its upper reaches, albeit less pronounced due to the region's geology. Erosion, both from running water and landslides, is visible, particularly on the eastern side. Climatically, the valley experiences significant changes, with rainfall ranging from 800 mm in the lower regions to 2,000–2,500 mm in the higher elevations. Rainfall peaks in late autumn and spring, while winters and summers see comparatively lower rainfall. Temperature distribution is influenced by orography, with lower temperatures at higher elevations compared to the valley floor as highlighted by Clerici et al. (2002)

Mathematical analysis of the geometrical features of terrain, known as morphometric analysis, is a commonly used approach for the geomorphological characterization of any river basin. In our research, we explore key aspects of the Baganza River Basin using morphometry. Specifically, we focus on the linear, areal, and relief aspects of the basin. Linear aspect deals with characteristics related to the length and connectivity of the streams within a drainage basin. Areal aspect deals with shape, size and spatial distribution of the drainage basin. Lastly, the relief aspect deals with elevation variation in elevation etc. Several studies pointed out the significance of morphometric analysis approach for geomorphological characterization. For instance, Mahala (2019), while comparing the morphometric characteristics in two different morpho-climatic settings and after verifying the results with field measurements, found that there is considerable difference of values among morphometric parameters in different morpho-climatic regions.

Hydrologic bahaviour of Qa' Jahran basin, Thamar province (Yemen) was described by Albaroot et al. (2018) using remote sensing and GIS based techniques. They presented a variety of morphometric indices i.e., stream order, bifurcation ratio, drainage density, relief ratio, drainage texture and length of overland flow etc. These parameters confirmed the high susceptibility of the Qa' Jahran basin for flooding. Remotely sensed data and techniques that are based on GIS provide geomorphologists with valuable information that helps them decipher the relationships among different morphometric indices. Similarly, Rai et al. (2017) performed GIS based morphometric analysis of Kanhar river watershed, India. In this case, detailed morphometric study of all sub-watersheds showed dendritic to sub-dendritic drainage patterns, which certified that lithology of the area was homogenous. River management from geomorphological perspective is an important aspect and requires special attention. In this perspective, Mandarino et al. (2020) performed multitemporal analysis of satellite imagery for last 20 years (1999-2019) on Scrivia River (Italy) using a GIS based approach and revealed that the morphological changes are prominent in space and time, whereas the hydro-geomorphological processes like floods are the most important triggering factor causing these morphological changes. The morphometric features of the Kalvari basin (Iran) were studied by Arabameri et al. (2020) to rank sub-basins using multi criteria analysis that were built on their susceptibility to erosion, thus founding that drainage density and slope are the major factors influencing the erosion in the study area. Analysis of the morphometric variables and their relationship with the volume of the sedimentary yield in Wadi Al-Arja (Jordan) was conducted by Salim (2014), who predicted that the ability of sedimentary yield inside the basin depends upon the variation in the climatic conditions and is in direct relationship with the morphometric parameters.

2.2.3 Material and Methods

Morphometric analysis of Baganza River has been performed to identify key morphometric parameters. High quality spatial data containing Digital Elevation Model (DEM) 5m x 5m was obtained from the "Geographic data download service" of the Emilia Romagna Region. The data is available in raster .tiff format in the form of tiles having reference systems: ETRS 1989 UTM Zone 32N, EPSG: 25832.

The following steps were performed for DEM pre-processing.

1. Individual tiles of the study area were inserted in GIS workspace.
2. Tiles were mosaiced to get one raster file having resolution (5 m x 5 m)
3. Using fill command, the sinks/ depressions were filled.
4. Flow direction to find 9 possible directions shown as:

32 64 128
↖ ↑ ↗
16 ← 0 → 1
↙ ↓ ↘
8 4 2

So, a cell with the value '1' means that the flow in that cell goes to the East, while a value of '32' means that the cell's flow goes to the Northwest. The value '0' implies that the cell is a sink and flow does not leave it.

5. Afterwards, flow accumulation command is used, which ensures that the total upstream flow contributing to each cell in a raster grid based on flow direction.
6. Clip basin boundary command is used to limit the extent of a spatial dataset to the boundaries of Baganza basin.
7. Raster calculator is used to perform mathematical operations on raster dataset, here it is used for selecting streams having flow accumulation greater than 30000 cells. The criteria for selection of 30000 cells is based on quality of the DEM and extent of the basin. Baganza is a small catchment of 188 km^2 but the resolution of DEM is high. This number is chosen after having several attempts and finding suitable representation of streams at that value.
8. Stream order command is used afterwards to categorize streams on the hierarchical position within Baganza River network.

To find morphometric parameters such as stream order, bifurcation ratio, drainage density, shape factor, form factor and dimensionless ratios etc., a specific morphometric toolbox by Beg (2015) has been used as shown in flowchart.

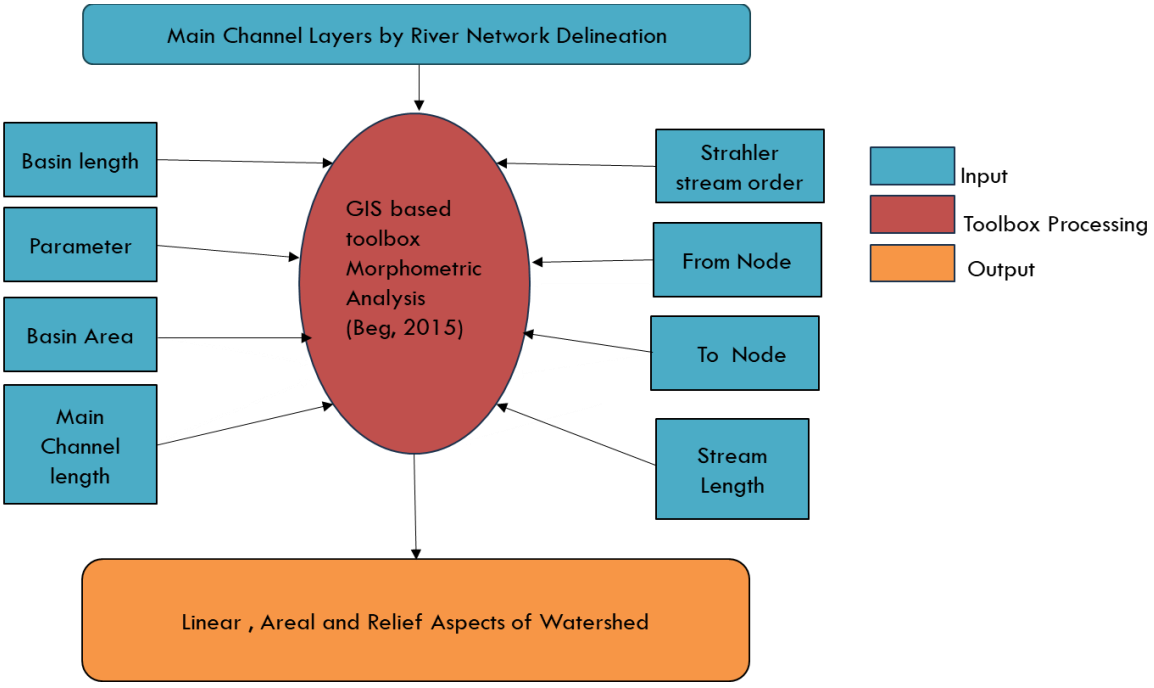

Figure 2.4 Flow chart showing input, processing and output related to morphometric toolbox.

The toolbox is supported by ArcGIS and the files obtained in the above step are utilized to obtain result in the form of text file. The results were cross checked with the help of manual calculation in excel by using different formulas provided in the literature review.

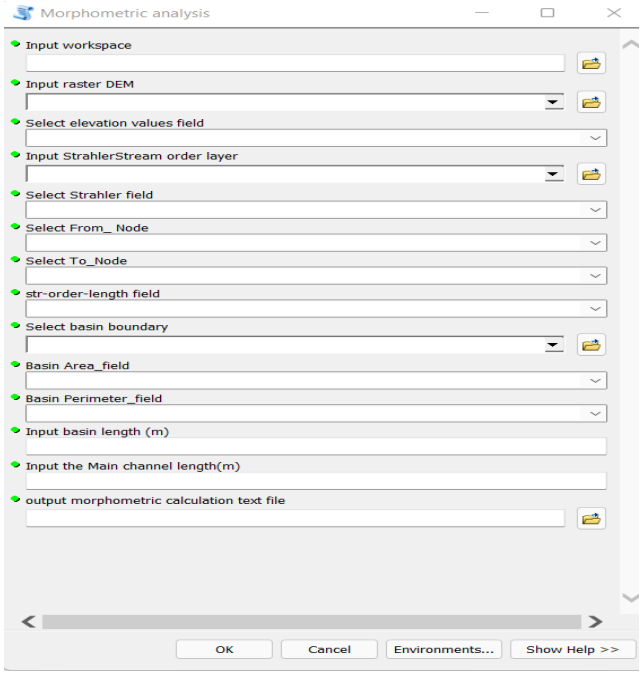

Figure 2.5 Morphometric toolbox file panel.

Only those variables that are important and needed further for this research are included in the tabulated form for further analysis as provided in Table 2.1

Table 2.1 Formulae for computation of Morphometric parameters and corresponding results

No.	Basin Parameter	Symbology	Formulae	Result Value	Method
1	Stream order	U	Rank of streams	1-4	Strahler (1952)
2	Stream length ratio	RL	RL=Lu/Lu-1	0.29-3.10	Horton (1945)
3	Mean bifurcation ratio	Rbm	Rbm= Nu/Nu+1	4.77	Strahler (1964)
4	Stream frequency	Fs	$Fs = \sum Nu/A$	0.66	Horton(1932)
5	Drainage density	Dd	$Dd = \sum Lu/A$	1.22	Horton(1945)
6	Length of overland flow	Lg	Lg=1/2*Dd	0.61	Horton(1945)
7	Form factor	Rf	$Ff = A/Lb^2$	0.06	Horton (1945)
8	Shape factor	Bs	$Bs = Lb^2/A$	17.82	Horton (1945)
9	Elongation ratio	Re	$Re = 2/Lb * (A/pi)(0.5)$	0.27	Schumm (1956)
10	Drainage texture	Rt	$Rt = \sum Nu/P$	1.02	Horton (1945)
11	Circulatory ratio	Rc	$Rc = 4piA/P^2$	0.16	Strahler (1964)
12	Basin Relief	R	$R = H - h$	1432	Schumm (1956)
13	Relief ratio	Rh	$Rh = H/Lh$	0.026	Schumm (1956)
14	Slope	S	$S = H - H'/L$	$0^0 - 63^0$	Mesa (2006)
15	Milton Ruggedness number	MRN	$MRN = (Hmax - Hmin)/A(0.5)$	0.104	Strahler (1958)

2.2.4 Results and Discussions

The stream order is the arrangement of rivers from headwaters to plain areas. The stream order of Baganza catchment suggest it is a fourth order basin with an area of 188 km². An increasing trend in the stream length

ratio from lower order to higher order indicates mature geomorphic stage of basin. Mean bifurcation ratio less than 5 indicates that the drainage pattern is affected by the geologic structures and both stream erosional tendency and fluvial risk are associated to it. The result value shows a poorly drained basin with a slow hydrologic response. Surface runoff is not rapidly removed from the watershed making it highly susceptible to flooding and gully erosion. Besides, low value of Drainage density (Dd) denotes a permeable subsoil material, dense vegetation, and low relief. The value greater than 0.3 in Length of overland flow (Lg) is considered as high value which means gentle slopes and long flow paths, more infiltration, and reduced runoff.

The significance of geomorphological characterization of the Baganza River basin lies in its ability to identify key morphometric parameters essential for understanding and managing the river system. By studying the morphology of the basin, including features such as river channels, slopes, and landforms, researchers can gain insights into the underlying processes shaping the landscape. This information is crucial for various applications, including flood risk assessment, river management, and environmental conservation. Identifying key morphometric parameters allows researchers to assess the vulnerability of the Baganza River basin to natural hazards such as floods, landslides, and erosion. By understanding the geomorphological characteristics of the basin, authorities can develop effective mitigation strategies and infrastructure planning to minimize the

impact of these hazards on communities and ecosystems. The graphical representation of some of the key morphometric parameters are shown below as:

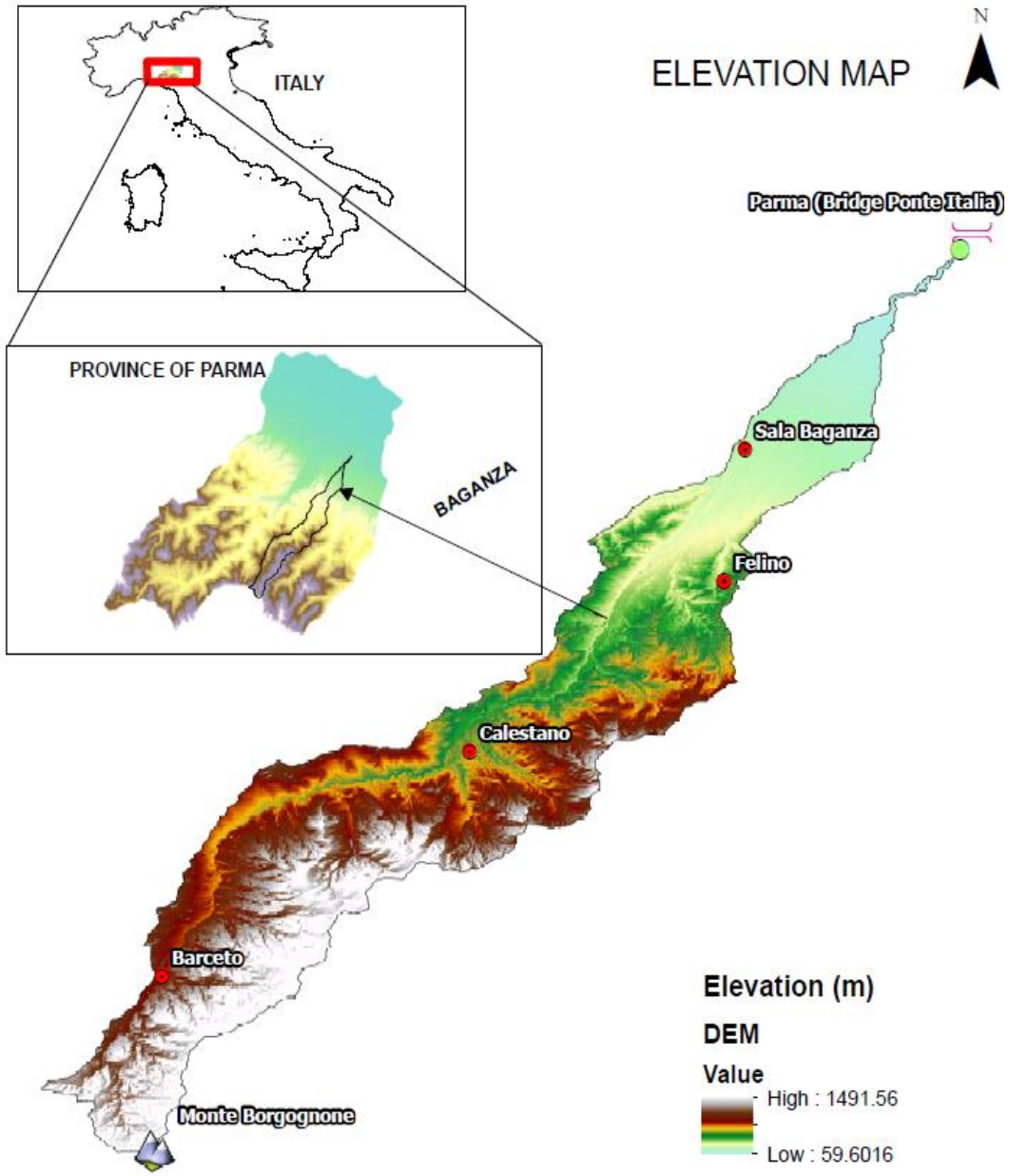

Figure 2.6 Map showing the basin relief in terms of high elevations in white color whereas low altitude in dull green color.

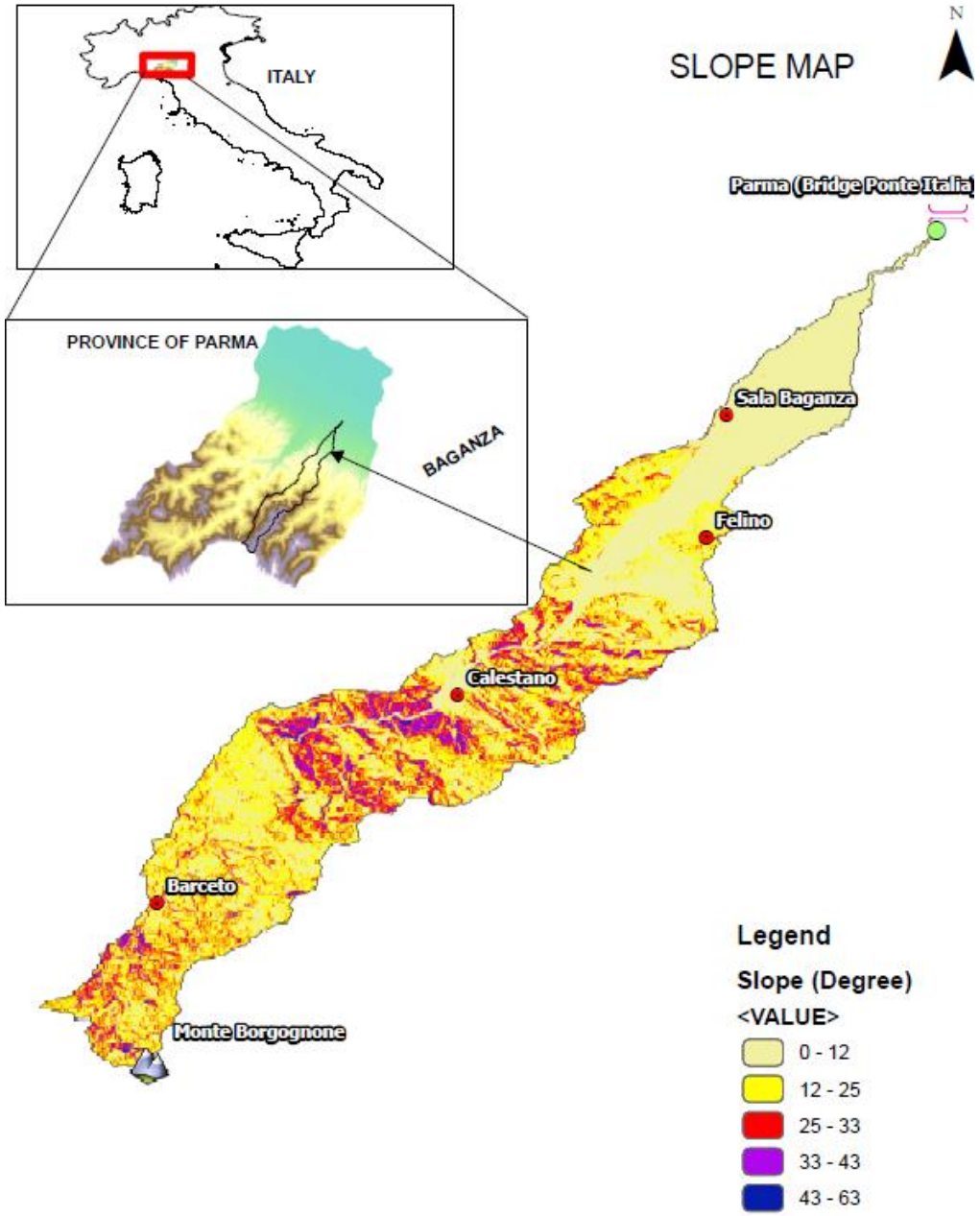

Figure 2.7 Slope map for Baganza catchment showing the increase in slope from light yellow being flat to dark blue steepest slope

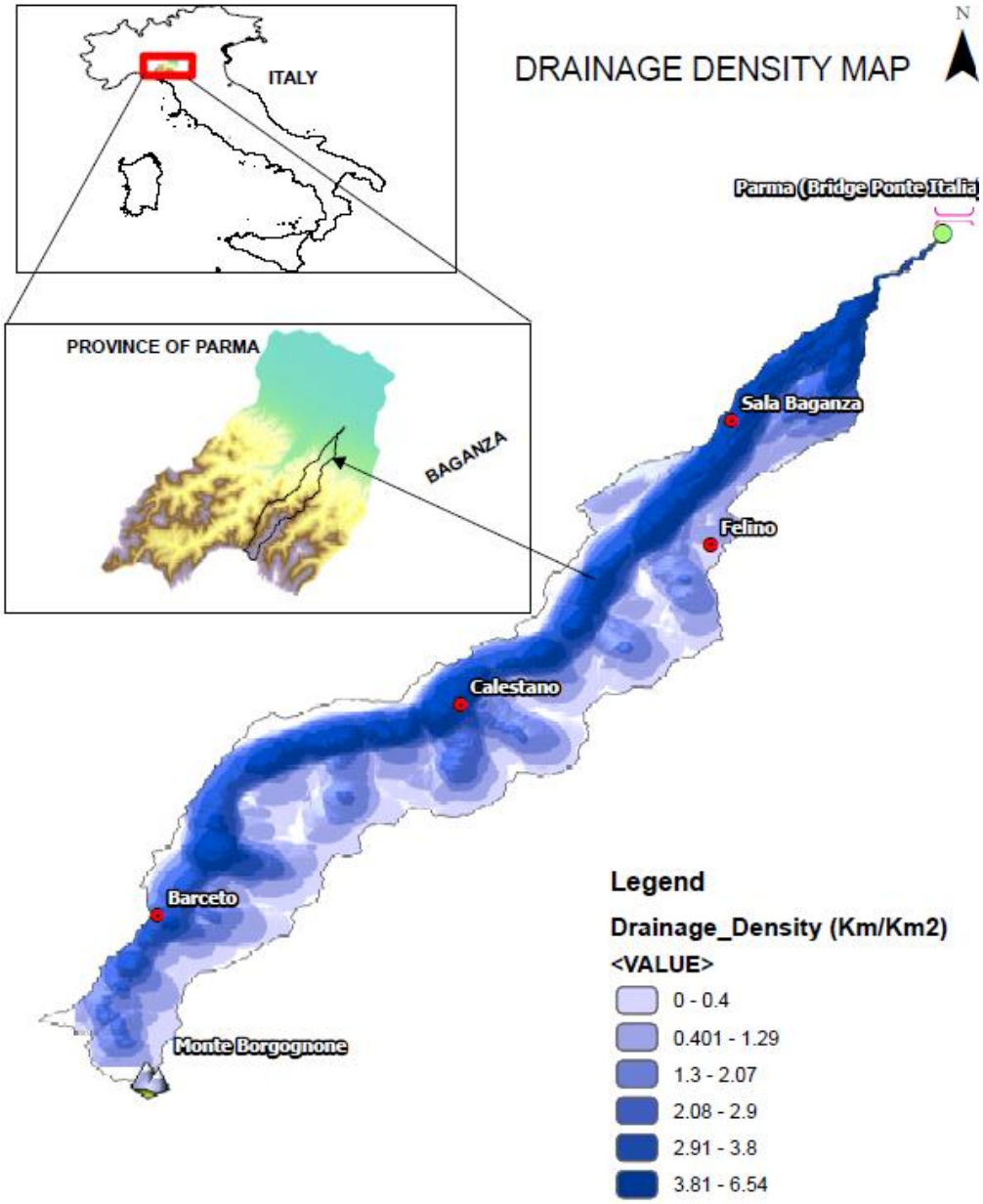

Figure 2.8 Drainage Density of baganza catchment

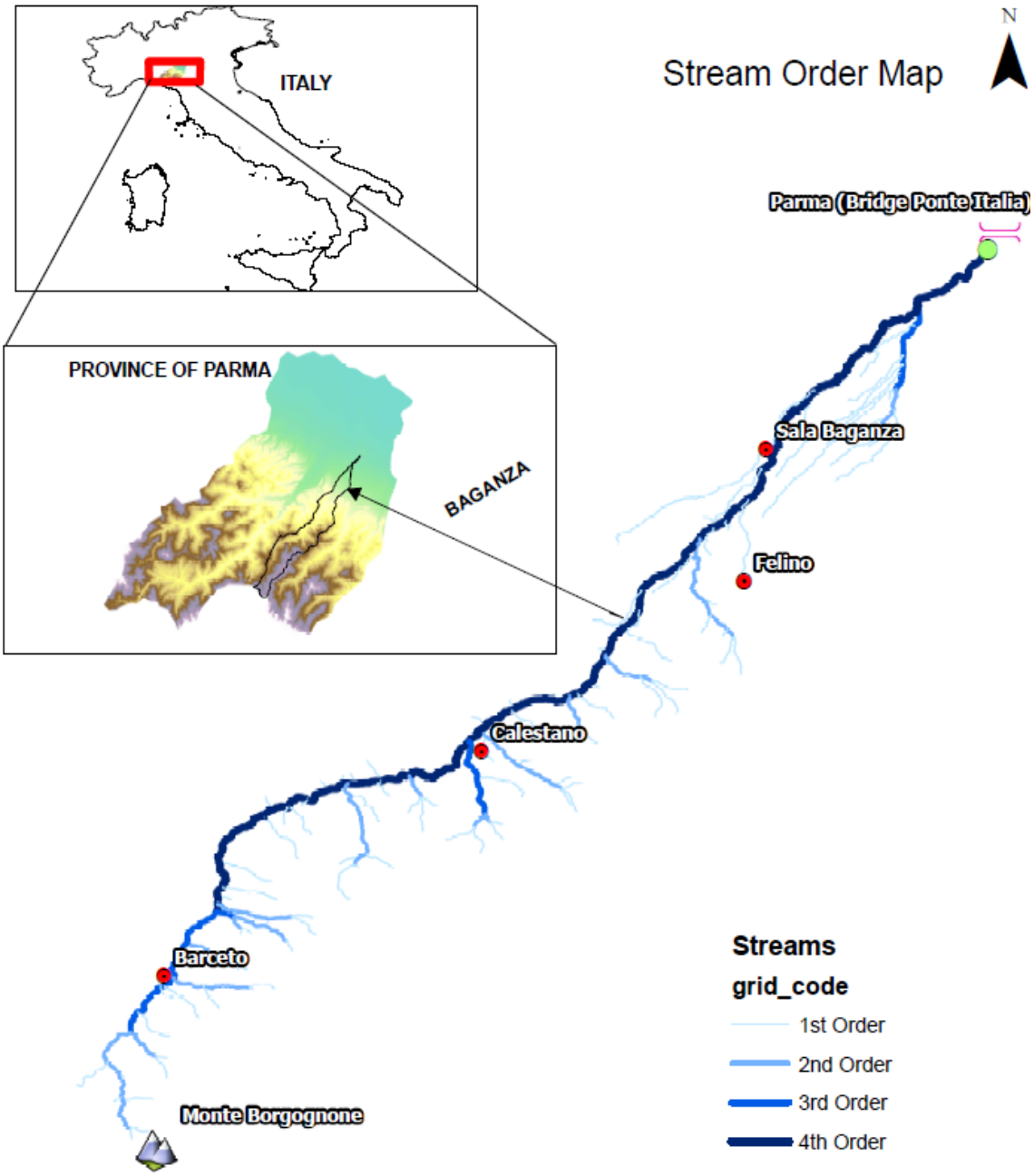

Figure 2.9 Stream order of baganza catchment showing drainage contributing directly to main stream.

Chapter 3: GRANULOMETRIC CHARACTERIZATION

This chapter includes the part of research published in MDPI Water: Khan, U.A.; Valentino, R. Investigating the Granulometric Distribution of Fluvial Sediments through the Hybrid Technique: Case Study of the Baganza River (Italy). ***Water*** **2022,** ***14*****, 1511. https://doi.org/10.3390/w14091511.**

3.1 Introduction

Grain size distribution (GSD) is one of the basic parameters that allows to describe the properties of soils and rock fragments and determine the conditions of their deposition inside a catchment. GSD is also of crucial importance to understand the physics of sediment transport and sediment fluxes in natural systems, to model many problems in the fields of river engineering, hazard assessment, and food plain and coastal management (Dade, 2000; Dade & Friend, 1998; Hassan & Church, 2000; Wilcock, 2001; Le Roux & Rojas, 2007; Venditti et al., 2010; Su et al., 2016). To obtain these distributions, grain size analysis is performed using different methods. The criteria for opting suitability of such methods depend on different conditions, such as purpose of the trial, the type of work in-hand and spatial scale of interest. One of the most famous and widespread method among researchers related to direct computing of the grain size was presented by Wolman (1954) in the middle of the 20th century. More recently, Syvitski (1991) proposed a method for quantifying particle sizes using planimetric technique. In the beginning of 21st century, concept of direct measurement of grain sizes faded away and transformed into digital measurement methods. One of the main reasons of this shift was tiresome efforts that were required to conduct field sampling of sediments, for instance justifying the criteria weight of sample must be 20 times the weight of D_{max} particle size, as reported by (Roberts & Church, 1986; Smart, 2003; Aberle & Nikora, 2006). As informed by Kondolf et al. (2007), analysing grain size distribution using digital photographs was firstly mentioned in 1971. In that case grid was placed over surficial sediments before taking photographs and then results where compared with the bulk samples. Earlier technique focuses on measurement of grain sizes in three different forms, which include methods such as percentage by volume, percentage by weight and quantitative assessment. Automated grain size analysis using image processing is an emerging technique since last decade. This is a rapid and accurate method to obtain grain size distribution of sediments present on the surface of riverbed. Some issues pertaining to the identification of the grain boundary has been also discussed by Kondolf et al.(2007). These issues are caused by grains sharing due to surface roughness such as large grains hide the actual size of nearby grains, bad segmentation of large grains and fusion of neighbouring grains with each other. The errors generated are not random and can be removed by setting truncation limits for instance, discarding all particles having size less than 8 mm.

The benefits when compared with the minor issues of automated grain size analysis are much higher. They comprise protection of the bed surface composition and opportunity to collect data by the operators with no training, small field struggle and laboratory time. Processing of digital images for obtaining grain size distribution can be performed in any of the two following ways: based on pixel counting and based on edge detection (Graham et al., 2005a, 2005b). An important consideration for getting an accurate result through this

process is by taking a snapshot perpendicular to the surface, establishing four controls points on the snapshot and determining the distance between these points under good lighting conditions. Sediment sampling based on digital photographs has been successfully employed by some researchers to characterize a flood event through sediment analysis Di Francesco et al. (2016). As already discussed, various methods are available for quick examination of particle sizes, but for coarse grain deposits there are some restrictions on their use, due to possible anomaly and limitation posed by the detection algorithm working behind the scene.

This research compares the results obtained from sieve analysis based on physical sampling and photogrammetric method, by using Digital Gravelometer software (Sedimetrics®) (Graham et al., 2005a, 2005b). It considers advance image-processing procedure to detect grain sizes present in digital photographs. Digital Gravelometer has been tested on a variety of gravel bed rivers and its algorithm captures all sort of sediment shapes including round, angular and spherical comfortably (Di Francesco et al., 2016; Reid et al., 2010). Software interface is user friendly and doesn't require any expert user understanding prior to its use. The main objective of this part of research is assessing the reliability of the photogrammetric technique and shed light on both advantages and limitations of this technique with respect to the more traditional sieving analysis.

3.2 Study Area

3.2.1 Location

The study area known as Baganza River is in Emilia Romagna region, northern part of Italy. The source of this river catchment is situated in the Tuscan-Emilian Apennines near Mount Borgognone, with a basin area of 228 km^2. The total river length is 55 km, and it ends up intersecting Parma River, close to "Ponte Italia" bridge. The Baganza River, which flows in the direction from south to north, presents a significant variability of characteristics along its spatial advancement: from the stretches of the mountain valley, which are very narrow and often confined by the slopes, to the crossing of important inhabited centers such as Sala Baganza and Parma, up to the stretch of the Parma stream meandering and completely embanked in the low plain Figure 3.1.

3.2.2 Geology

The valley develops in a SW–NE direction. A noteworthy feature of the valley is the V-shaped cross profile, with a noticeable asymmetry: the eastern slope is much more extended than the left slope, which is steeper with lower peaks. This asymmetry, uncommon in the Emilian Apennine basins, is conditioned by the structural setting. The mountain territory is essentially made up of flyschoid, clayey and arenaceous units structured in a complex structure, controlled by tectonics. From these characteristics derives the predisposition of the hilly and mountainous territory to the formation of large landslides. The strong tectonic action to which the arenaceous-marl and calcareous-marl formations have been subjected and the widespread presence of clayey

soils determines a general condition of instability of the slopes and an accentuated susceptibility to surface erosion ("Variante al Piano per l'assetto idrogeologico del bacino del fiume Po (PAI): Torrente Baganza da Calestano a Confluenza Parma e torrente Parma da Parma a confluenza Po," 2015, p. 12).

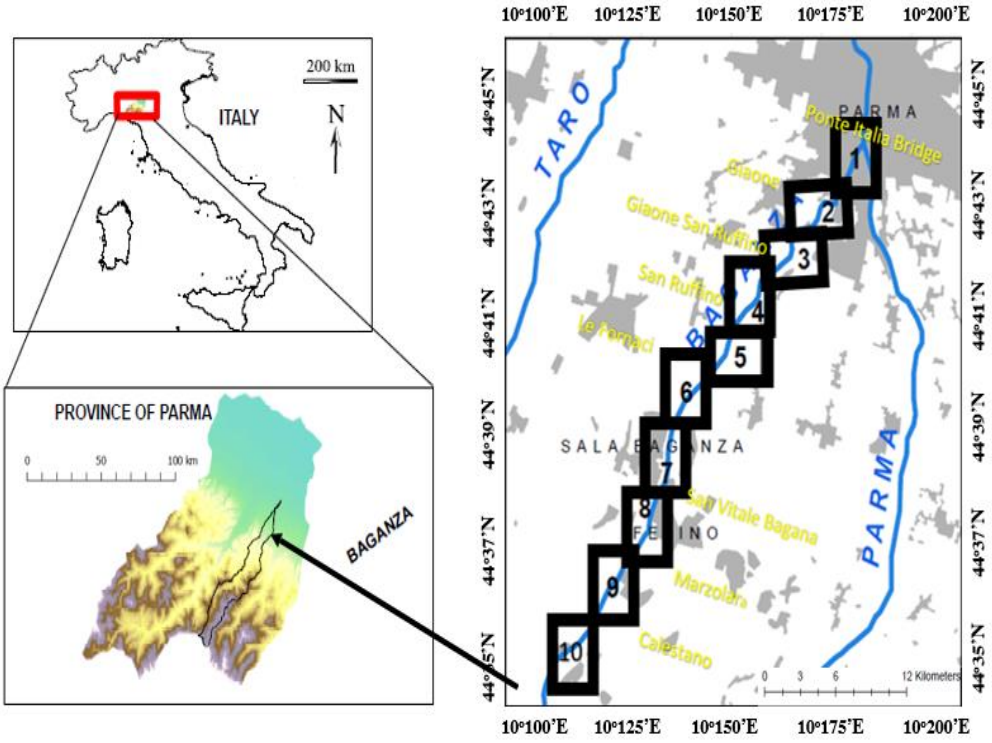

Figure 3.1 Geographical location map of sediment sampling points along Baganza River.

The study area extends from Calestano (upstream) to Ponte Italia Bridge (downstream, at confluence point of Parma and Baganza Rivers) and is randomly distributed into 10 cross sections, whereas length of selected reach is 28.68 km as given in Table 3.1

3.2.3 Morphology

From the morphological point of view, river stretch from Calestano to Marzolara presents riverbed type having intertwined channels pattern. Whereas, from Marzolara to Sala Baganza the tendency of narrowing is evident as the width of river is reduced in this section. Moving further downstream, high mobility of the riverbed found together with the reactivation of bars can be seen due to possible previous floods in the area. When passing through the valley area up to confluence with Parma River, the Baganza River shows sinuous single pattern along with incised bed and alternating side bars. This river segment is intensely regulated, and many hydraulic structures have been found.

Table 3.1 Salient features of the sections and reference coordinates of location

Section No.	Distance from Confluence (km)	Avg. River Width (m)	Place	Longitude	Latitude
1	0.15	40	Near Ponte Italia Bridge	10°19'22.24"E	44°47'35.99"N
2	3.186	55	Giaone	10°18'5.96"E	44°46'22.23"N
3	5.894	66	Giaone - San Ruffino	10°16'41.83"E	44°45'32.24"N
4	7.465	150	San Ruffino	10°15'58.07"E	44°44'53.28"N
5	10.88	90	Le-Fornaci	10°14'27.46"E	44°43'28.53"N
6	12.422	90	Sala Baganza	10°14'9.86"E	44°42'39.68"N
7	16.081	160	Sala Baganza - San Vitale Baganza	10°12'46.58"E	44°41'0.37"N
8	18.766	150	San Vitale Baganza	10°11'33.58"E	44°39'53.31"N
9	23.007	85	Marzolara	10°10'9.07"E	44°37'53.71"N
10	28.688	150	Calestano	10° 7'6.64"E	44°36'6.13"N

3.2.4 Hydrometry

The historical hydrometric measurement stations of the catchment area of the Baganza River are in Marzolara and Ponte Nuovo. For these stations, no digital discharge records are available since long. Whereas, in 2003 ARPA Emilia Romagna (Hydrographic Service) installed tele-hydrometers for measurement of discharge. Previously, only the water levels were measured and recorded manually since 1954. The significant flood event in recent history was recorded on 13 October 2014. This flood affected roads, infrastructures, and settlements closest to the engraved riverbed.

3.2.5 Site Selection

This reach of Baganza River for sediment sampling was selected based on following aspects:

- The morphological characteristics of the riverbed;
- The presence of defense works and their impact on longitudinal and lateral continuity;
- The main effects of the October 2014 flood on the areas in the vicinity.

To gain insights of the sediment grading, distribution and composition river stretch from Calestano up to confluence of Parma and Baganza River was divided into ten cross sections. At each cross section three points along the transect hydraulic on the right, middle, and left were selected, which holds the morphological features such as bars, pools, and riffles to accommodate the sediment variability. To include all sediment characteristics of the river, sample locations were managed to be both on left and right flood plains, central bars, and alternate bars. Sediment samples were collected at those locations which were sufficiently upstream or downstream of a hydraulic structure such as bridges, culverts, and weirs to remove bias. Representativeness of the sample points from the whole cross section was also determined by observation and judgement. Mainly, the boulders and cobbles were found near the main channel of the river, and fines were sorted further to the bank. The

sample points selected in the field practice were in such a way that they could be assumed as an average of the whole cross section. Recording the GPS location of each sample and coding the sample was carefully conducting in the field.

3.3 Experimental Procedure

By performing field reconnaissance of the area, at each of the ten selected cross sections Figure 3.1, three suitable spots were identified and marked as right (R), middle (M), and left (L), to account for the wide range of sediment sizes and shapes. It should be noticed that before sampling, it was observed that mainly the large grains such as boulders and cobbles were found near the main course of the riverbed, and fines were sorted further to the floodplain and bank. The sample points in the field practice are selected in such a way that they were the average of the whole cross section, to account for sediment sample representativeness. After performing the site selection and necessary demarcation, sediment samples were collected performing an excavation to a depth of 0.3 m. In total, 30 samples were collected form the 10 cross sections (3 for each section) and they were sieved using mesh sizes ranging from 63 μm to 100 mm. Sieve analyses were performed at the geotechnical laboratory of Interregional Agency for the Po River (AIPO). At the same sampling points (3 points per cross section), an alternative method was used to determine the grain size of the stream bed material. The idea was to take photographs of exposed layer of riverbed comprising sediments of distinct shapes and sizes. These photographs were pre-requisites for deriving GSDs through image processing software (Digital Gravelometer). Simple mobile device model Infinix X680, 720 x 1600 pixels, 20:9 ratio (~266 ppi density) equipped with camera of 16 Mega pixel was used for this purpose. To maintain coherent methodology for sampling, a temporary frame with the size of 1m x 1m was constructed and checked precisely with measuring tape. Later, this technique also helped in the image analysis by locating four corner points at each edge of the grid. The sediment sampling frame size (1m x 1m) was directly proportional to the pixel density of the camera, meaning that greater the pixel resolution of the photographic camera, larger the sample area can be selected for a given least grain size.

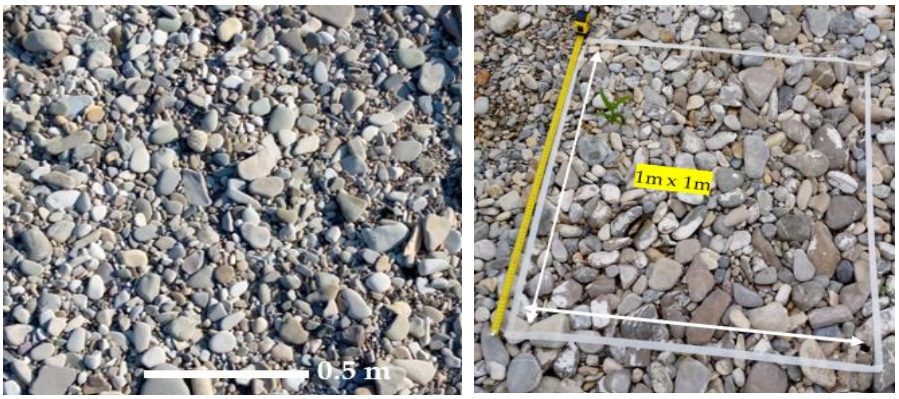

Figure 3.2 Digital photographs of Baganza stream bed, taken for grain size analysis using Digital gravelometer.

In total, 30 locations were identified (3 per cross section) to collect sediment samples. Images were taken in daylight and camera was kept at sufficient height to obtain clear results avoiding casting shadows (Figure 3.2). These digital photographs were then carefully numbered with alphanumeric characters i.e., 3M, is taken at 3rd cross-section and in the middle portion. Cross-sections were numbered in the increasing order from downstream to upstream, opposite to the direction of the flow (Figure 3.1). All images were geo-tagged with the location, date, name, and coordinates using mobile application (GPS mobile camera). The described campaign, which included both sieve analysis and photogrammetric technique, was carried out between July and September 2021.

3.4 Data Collection

3.4.1 Data Input Representation

After obtaining digital photographs in preprocessing step, the next stage is to supply the required input data to the software, to obtain required grain size distribution of the area. The idea is to enable the software to identify the different particles in the image efficiently. Digital Gravelometer software computes the grain size distribution by counting the individual grains in the digital photographs or frequency by the number method. This technique is different from the traditional sieving method, which uses weights of grains to calculate the size distribution. The frequency by number is further classified into two methods, i.e. area by number (areal sample) or grid by number (grid sample). Areal samples consider measurement of all grains present in the photograph, whereas grid samples measure sediment sizes only on the predetermined grid point intersections. The area by number method is also known as the paint by pick method whereas the grid by number method is known as the Wolman grid count. It is worth noting that the Digital Gravelometer was unable to identify smaller particles (silt and clay) and often grouped these much smaller particles into one much larger clast, probably because the particles were all the same colour. Therefore, to exclude fines such as sand and silt, lower truncation was set to 2mm whereas the upper truncation for particles was set to 256 mm, so that the very large particles avoided touching the boundary of 1m x 1m frame.

3.4.2 Sieve Correction Factor for the GSD Comparison

To compare the particle size distributions obtained from sieving conducted in the laboratory with results obtained from Digital Gravelometer, it is imperative to include sieve correction factor. Sieve holes are square in shape and thus correction is needed as the shape of grain is not symmetrical. A typical grain consists of three axes, as shown in Figure 3.3 The b-axis of the particle is mostly used by sedimentologists as reference scale for measuring grain sizes. While performing sediment sampling, the pebble count method was also opted for computing a-, b-, and c-axis of 40 random particles in 1m x 1m grid (one grid at each sample point). In total 120, particles per cross section were counted.

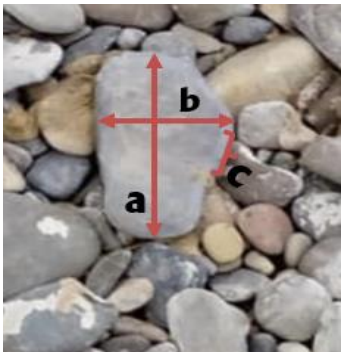

Figure 3.3 Typical grain measurement axis (a=long, b=intermediate and c=short axis).

In fact, the sieve on which a grain is retained is a function not only of its b-axis, but also of its a and c-axis. This is because a grain with a large b-axis and small c-axis may present itself to the sieve hole diagonally and pass through a hole that is nominally smaller than the true b-axis of the grain. In this study, a correction factor for individual grain flatness (c/b) ratio was also applied based on a-, b- and c-axis obtained from pebble counting method at each sample location, to compare the results directly with conventional sieve analysis method. Ds/b is the ratio of the square whole sieve size with true b-axis, which is related to the flatness ratio of the grain (c/b) presented by Church et al. (1987) as *equation 3.1;*

$$\frac{D_s}{b} = \frac{1}{\sqrt{2}}\sqrt{1+\left(\frac{c}{b}\right)^2} \qquad 3.1$$

3.5 Data Processing

3.5.1 Grain Size Identification and Quantification Mechanism

The different stages of the grain size measurement and identification procedures employed by Digital Gravelometer software can be summarized as follows:

1. The conversion of the digital photograph into grey scale image and correction for radial lens distortion.
2. The projection transformation of the photograph to adjust the camera angle.
3. The mechanism for the identification of particles in the image (i.e., grains selection).
4. The grain separation algorithm.
5. The mask overlay.
6. The measurement of the grains and extraction of the relevant information in the form of pixels.
7. The conversion of grain sizes in mm.

Some of the main steps involved in determining the GSD are reported in Figure 3.4 Briefly, the colored images obtained in the field are converted into greyscale images and radial lens distortion is applied to the photographs. In this manner, the greyscale images were modified. After that images were checked for verticality right above the center of 1m x 1m frame. This transformation requires the number of pixels per mm. Although the software automatically computes this value, it can also be provided manually by the user. Initially, the noise present inside the images is reduced with the help of (5m x 5m) pixels default filter. The image was then enhanced for gaps in between the grains. The identification of grains was fulfilled by converting greyscale image into binary black and white image by placing a two threshold values: threshold one was used for identifying all the gaps having intra-grain noise whereas threshold two was used to identify further dark points. Two binary images are afterwards combined to obtained third binary image, which contained only the gaps of the first image that were linked to second binary image.

Afterward, the binary image was subjected to smoothing, which was controlled by the suppression parameter with a default value of one. Lowering this default value will cause an increase in the over segmentation of particles whereas increasing this value may cause failure to separate the grains that are touching each other. Four control points (top left, top right, bottom left, and bottom right) that were initially set to mark the boundary of 1m x 1m frame were utilized to measure the number of grains inside the frame. An ellipse shape was fitted to the particles in the image for the b-axis measurement whereas the grain sizes were specified from pixels to mm in this step. The selected grains were measured afterward.

It is evident from the photographs that only the area inside the square frame (1m x 1m) was taken for the computation of grain sizes. As some of the grains were large and touched the frame boundary, these grains must be ruled out, as there is a chance that the software will detect frame boundary as part of these grains and compute the wrong grain sizes. Therefore, a suitable window size inside this frame boundary should be dictated to the software (i.e., 0.8 m x 0.8 m or similar, as per the available site condition).

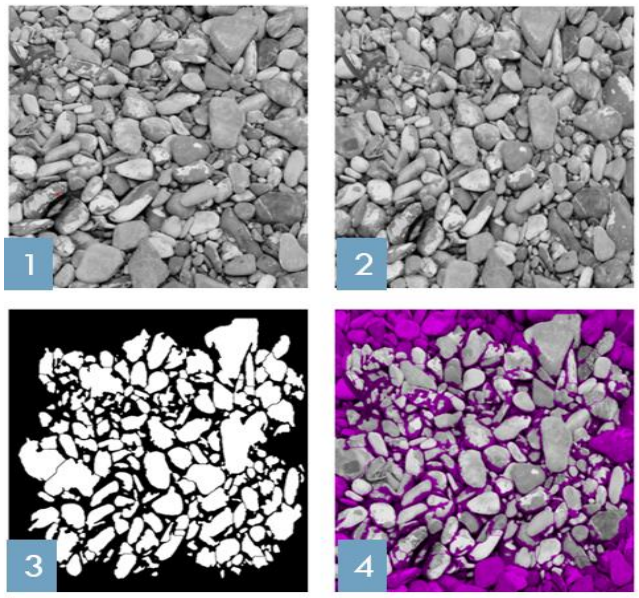

Figure 3.4 Graphical illustration of key steps performed in Digital Gravelometer software for identification and measurement of different grain sizes 1) Grey-scaling 2) Projection transformation for camera adjustment 3) Grains selection 4) Grey scale image mask overlay on the selected grains in previous step.

3.6 Results and Discussion

3.6.1 Spatial Comparison

A comparison was made between the results obtained from the sieve analysis and the photogrammetric method. The processed data revealed that the gravel content (2–64 mm) is one of the dominant classes of sediments in the Baganza catchment among other classes including boulders, cobbles, gravel, and sand. On one hand, the sieve analysis showed that the gravel class range varied between 75% and 80 %, and sand from 20% to 25%. On the other hand, the Digital Gravelometer (area by number) methods showed that the gravels ranged from 95 to 98% and cobbles ranged from 2 to 5%. The exposed fluvial sediments were made of large fractions, among which small grains resided and Digital Gravelometer could not access grain fractions smaller than 2 mm, thus the finer fractions were ignored by this method. Therefore, it is not unusual that the GSD trend obtained from the manual sieve analysis resulted in a finer fraction that was much higher than the evaluations of the surface sediments by Digital Gravelometer. It is significant to note that when considering the grain size analysis, the sample size is of key importance. In this case, each sediment sample had an average weight of 3–5 kg. This is because our main objective was to introduce an efficient mechanism for grain size analysis by combining both the conventional and modern methods to significantly reduce the sampling time and effort. The grain size distribution above and below the exposed surface was unlike each other, so cannot be comparable in the actual as per suggested by Bunte et al. (2001).

Sediment photographs processed in Digital Gravelometer were able to identify and measure the grains exposed on the surface. However, in order to compare these results with the conventional sieving method, the pebble

count was performed at each observation point and the ratio of the c/b axis was calculated and marked in the software to allow us to compare both results. In order to compare the results of the laboratory sieve analysis with those of the photogrammetric method (both "grid by number" and "area by number"), three reference sizes, namely D10, D50, and D90, as defined in, have been considered.

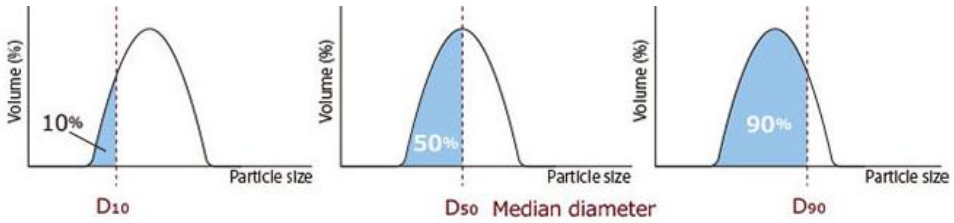

Figure 3.5 D10, D50 and D90 percentiles with graphical representation

Table 3.2 summarizes the obtained results in terms of D10, D50 and D90. The reported values are the average calculated at each cross section, based on the three observations points (Left, Middle, Right).

Table 3.2 Quantiles comparison of different methods and grain size statistics of Baganza River.

Sr.No	Sections	Sieve Analysis D (mm)			Photogrammetry Method D (mm)						Grain Size Statistics (Folk and Ward, 1987)			
					Grid by Number			Area by Number			Mean	Sorting	Skewness	Kurtosis
		D_{10}	D_{50}	D_{90}	D_{10}	D_{50}	D_{90}	D_{10}	D_{50}	D_{90}				
1	Ponte Italia Bridge	3.62	27.79	59.5	12.32	38.71	78.17	2.68	6.66	27.25	7.43	2.44	−0.22	0.88
2	Giaone	0.16	15.85	36.9	8.11	28.5	74.46	2.53	5.8	19.47	6.28	2.19	−0.19	0.93
3	Giaone - San Ruffino	2.24	13.95	30.1	16.08	43.15	102.8	4.52	13.1	39.89	13.36	2.31	−0.1	0.88
4	San Ruffino	0.72	8.47	30.5	13.92	33.93	72.19	5.03	13.5	35.19	12.41	2.21	−0.1	0.92
5	Le Fornaci	0.34	9.33	26.9	13.92	35.71	81.19	4.36	12.7	33.6	10.43	2.05	−0.1	0.93
6	Sala Baganza	0.35	7.05	21.4	10.95	27.36	66.27	4.18	10.3	26.18	10.44	2.23	−0.1	0.95
7	Sala Baganza - San Vitale Baganza	0.37	9.14	23.6	14.86	40.84	91.88	4.53	12.7	34.65	12.22	2.22	−0.1	1
8	San Vitale Baganza	0.18	9.54	23	12.02	32.34	64.16	3.69	10.5	29.65	10.43	2.21	−0.1	0.95
9	Marzolara	0.25	12.47	31.1	11.49	36.91	92.43	3.65	9.33	27.6	9.63	2.2	−0.1	0.96
10	Calestano	0.29	5.55	32.7	10.6	34.72	85.86	3.68	8.7	24.74	9.04	2.11	−0.1	0.96
	Average	**0.85**	**11.91**	**31.56**	**12.43**	**35.22**	**80.94**	**3.89**	**10.33**	**29.82**	**10.17**	**2.22**	**−0.12**	**0.94**

Quantile comparison at each cross section revealed that the average particle diameter present in 50% (D50) and 90% (D90) of the cumulative distribution were pretty much analogous to each other in the case of the area by number method when compared with the sieve analysis method, as shown in Table 3.2

However, the grain size stats showed that the sediments inside the catchment were coarsely skewed and extremely poorly sorted. Moreover, in all sections, except for the "Ponte Italia Bridge", the skewness value was −0.1, and it corresponded to a nearly symmetric appearance, as per the criteria defined by Folk & Ward (1957).

It is pertinent to mention that the negative sign of skewness moved toward the fine side and suggests that the river presents dynamic features such as high energy, turbulent flow, coarse sediments, upstream meandering patterns, and deficiency in the straight approach, as discussed by Awasthi (1970). Figure 3.6 shows how the cross-sectional average values of specific grain sizes (D10, D50 and D90) obtained from in situ sampling (sieve analysis) followed a power relationship when compared with the longitudinal profile of the Baganza River, as depicted by R^2 values of 0.86, 0.86 and 0.73 respectively.

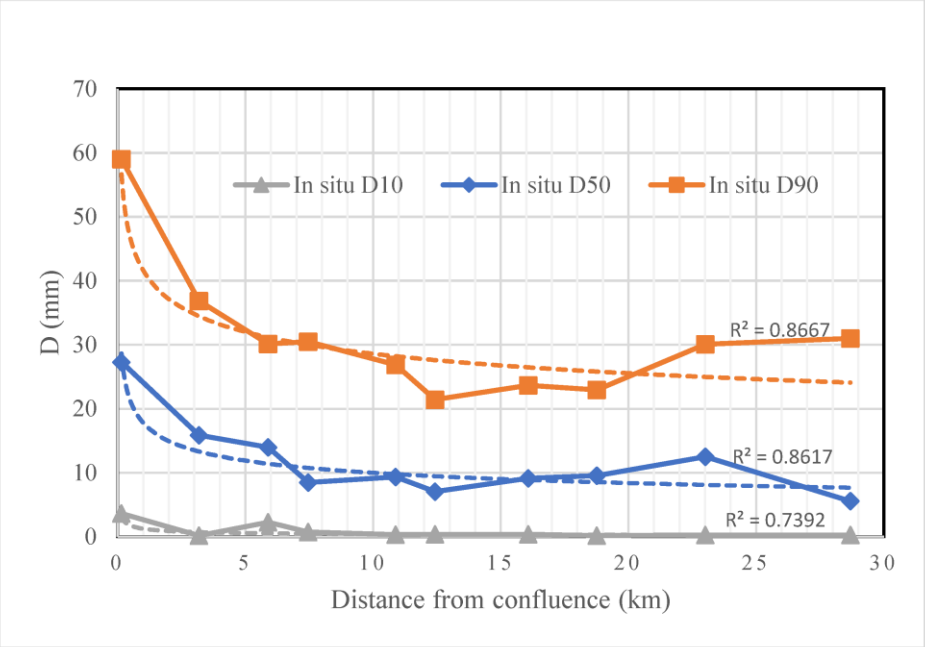

Figure 3.6 Power relationship of average values of specific grain sizes (D10, D50 and D90) along the longitudinal profile of Baganza River.

A comparison between the photogrammetry method and sieve analysis was made at each cross section, as shown in Figure 3.7 . The Wentworth classification allocates the sediment sizes in different categories such as sand (<2 mm), gravel (2–4 mm), pebble (4–64 mm), cobble (64–26 mm), and boulder (>256 mm). The gravel and pebble classes in the present study was further divided into sets of five (2–4 mm, 4–8 mm, 8–16 mm, 16–32 mm, and 32–64 mm). From Figure 3.7 it can be seen that the amount of sand content was the maximum in Section 8, which was up to 35%, whereas the minimum was in Section 1 where the value was 3% for the in situ sample. The sand content was invisible in the photogrammetry technique because of the restriction applied on the measurement of content smaller than 2 mm. On the upper side, the restriction was applied for the measurement of grain sizes larger than 256 mm. This restriction was applied in order to avoid the errors caused by splitting the large grain size particles into smaller ones, commonly referred to as over-segmentation. The amount of gravel content measured by both techniques in all sections showed comparable results, except in Sections 3 and 5, where no gravel content was found in Section 3 and only 0.5% in Section 5 by the photogrammetry method.

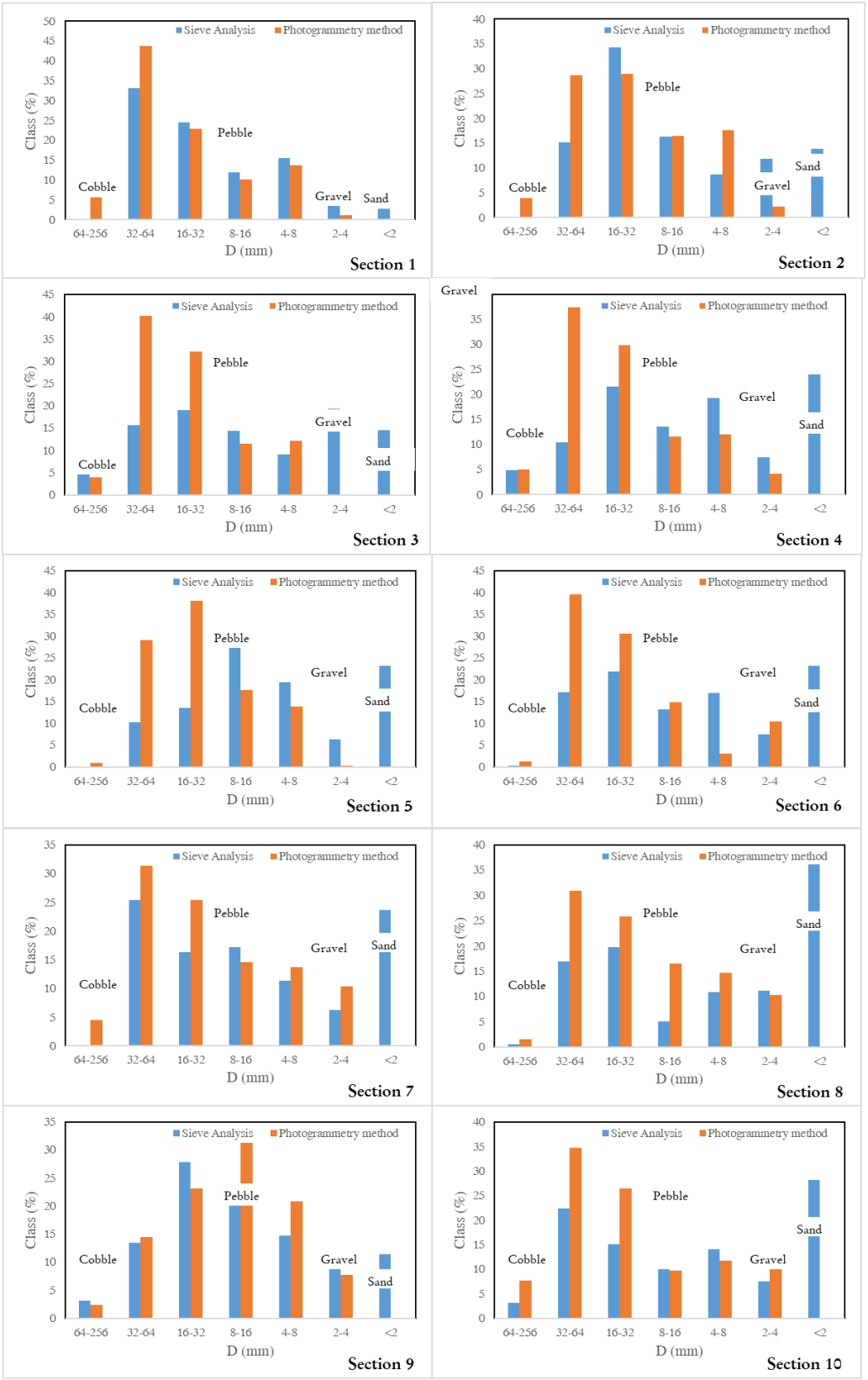

Figure 3.7 Comparison between photogrammetry method and sieve analysis at each cross sections.

Furthermore, the content measured by the photogrammetry method in the pebble class size of 32–64 mm was always greater than that measured by the sieve analysis. This difference was the maximum in Section 4, where the value measured by the sieve analysis was only 10% against the 38% computed through the photogrammetric method. The variation between the photogrammetry and sieving methods varied from site to site. For instance, at Section 2, both methods closely matched each other in the gravel and pebble classes. Overall, the comparison suggests that based on both methods, the maximum class ranged from 16 to 64 mm, which fell into the category of pebbles, and was present in all sections, except in Section 9, where the dominant class was 8–16 mm.

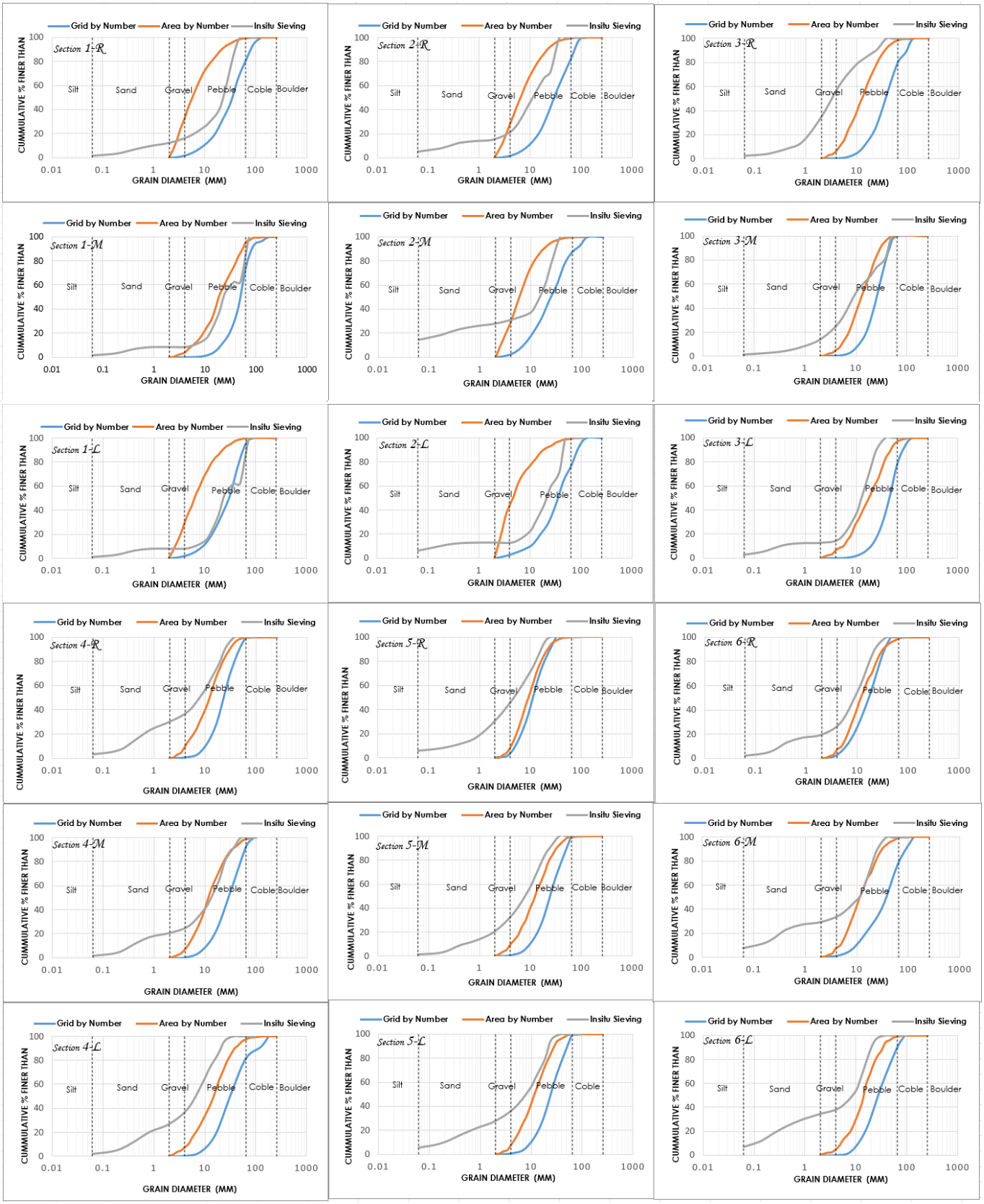

Figure 3.8 Grain size distribution curves acquired at observation points (Right, Middle and Left) at each cross sections through photogrammetric technique (area by number, grid by number) and through sieve analysis method.

In total, 90 individual granulometric curves were acquired through the "area by number" and "grid by number" methods and sieve analysis Figure 3.8. For each method, the reference particle equivalent diameters (D10, D50, and D90) were obtained. The results from the photogrammetric methods (areal and grid) were compared with the sieve analysis, and both of them gave distinct outcomes because the probability of finding the grains in these methods was different from each other. In the "area by number" method (areal), the probability is the same for measuring an individual grain size across the whole of the sampling area. On the other hand, in the grid based approach, the probability of finding a grain in a sample of a given size is proportional to its cross-sectional area. Another important consideration is that the traditional sieving method takes into account both the surface and subsurface samples. Initially, the image processing technique takes into account the surface sample only, unless frequency distributions obtained through both methods (photogrammetric and sieving) are adjusted to make a single combined frequency distribution representative of both, as mentioned in the following 3.6.4. This implies that the percentage of fines from the sieve analysis is much higher with respect to that obtained from the photogrammetric technique. It could also be observed that the grid by number method showed coarser GSDs, providing large grain sizes than normal at all cross sections, however, the area by number method showed better agreement with the manual sieving results in the context of surface grains (size >2 mm) Figure 3.8. Moreover, Figure 3.8 shows how granulometric analysis through standard sieving in the laboratory revealed that sediment samples contained a good percentage of gravel, mostly having particle size ranges between 2 and 64 mm. One of the reasons could be that the surface layer of the gravel riverbed is sort of an armored layer, and small sized particles are underneath bigger particles, which require effort to collect. While taking samples, it was possible to dig at least as much as 0.3 m.

3.6.2 Temporal Comparison using photogrammetric technique

The same photogrammetric technique had been used during a past experimental campaign in 2019 (AIPO, 2019) at four out of ten cross sections investigated more recently in 2021. In fact, digital photographs for surficial sediments were obtained inside Baganza River at Ponte Marzolara, San Vitale Baganza, Ponte Sala Baganza and San Ruffino. In order to ascertain the temporal variation of sediment sizes along the profile of the river with past data of 2019 (AIPo, 2019) and also with the intention of building a reference point for comparison, current samples were collected and processed using photogrammetric technique at these four cross sections, even in the 2021 campaign. Past data related to sampling points (i.e., GSDs and location coordinates) were obtained for the year 2019 from AIPO. Looking at first glance at the comparison of the exposed sediments is pretty much in correlation with each other from both years (2019 and 2021) as reported in Figure 3.10

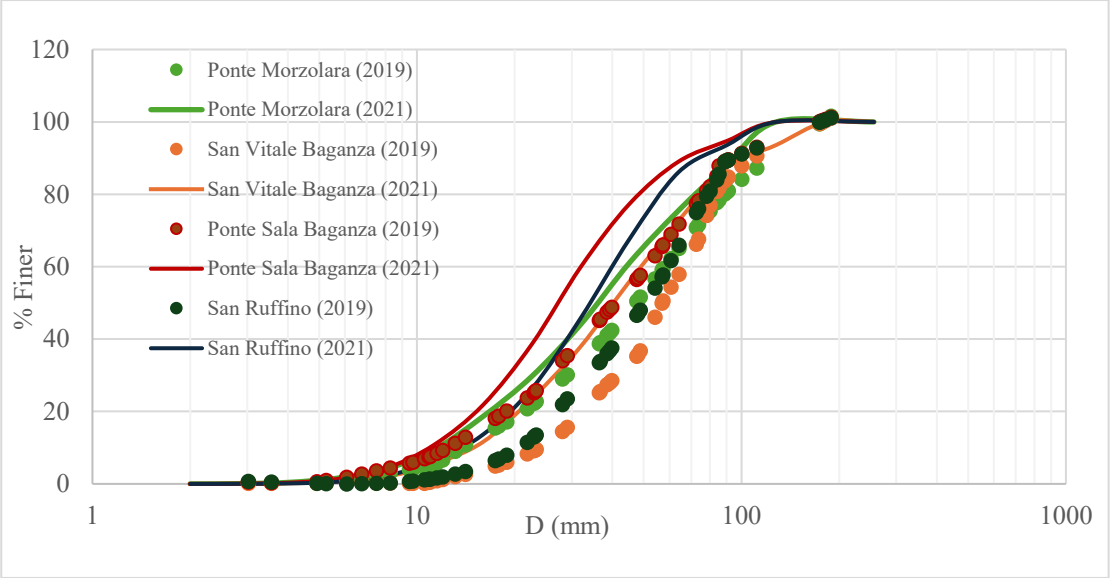

Figure 3.10 The comparison of the exposed fluvial sediments in the superficial layer from 2019 and 2021 (photogrammetric technique) at all sections.

By looking at each section Figure 3.10, it can be noted that the cumulative distributions (from year 2019 and 2021) overlapped each other. D_{10} and D_{90} at these sections were almost similar, whereas there was a little variation in D_{50} that is within permissible limits.

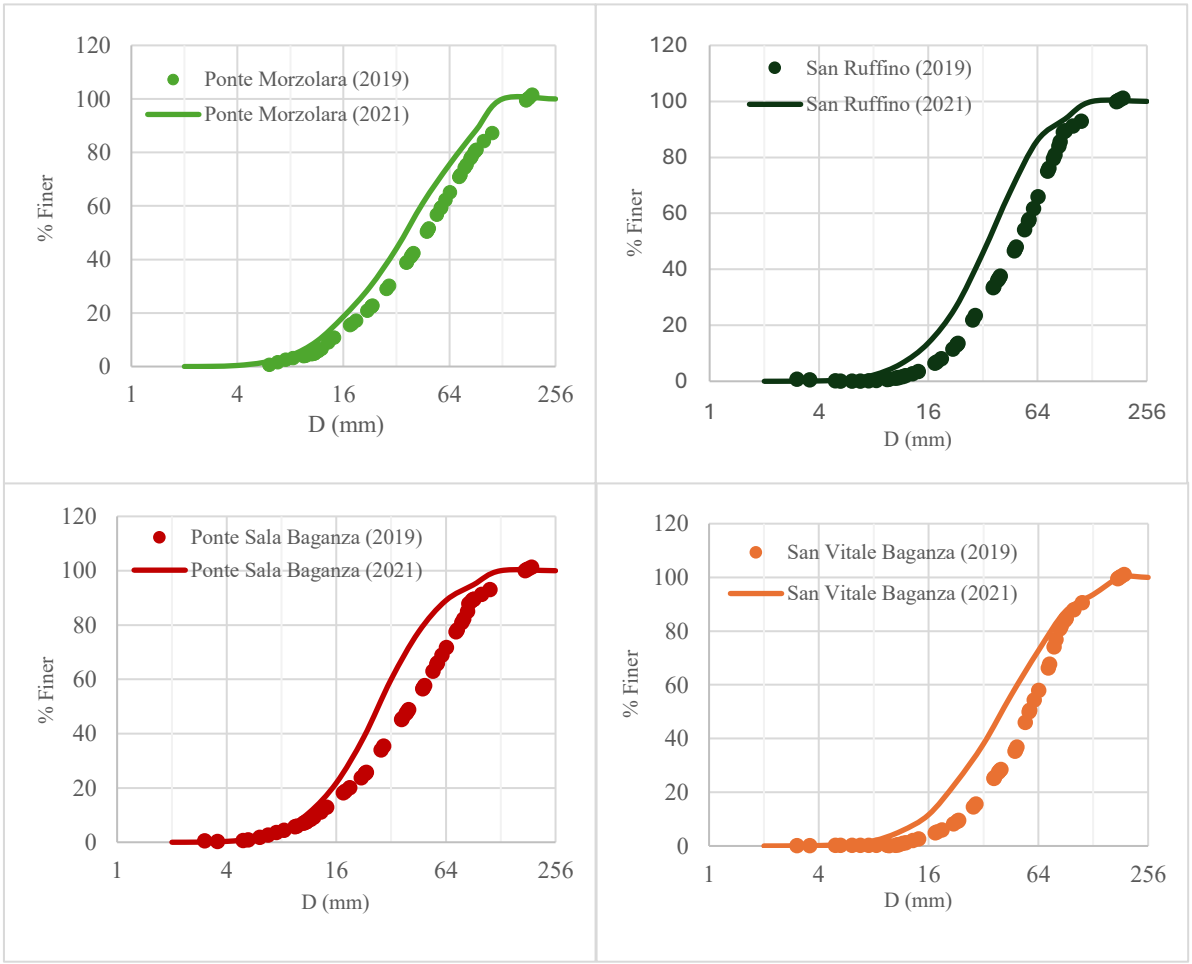

Figure 3.9 The individual grain size distribution of the surface sediments at each investigated section (the photogrammetric technique)

3.6.3 Temporal Comparison using Sieve Analysis

Similar to the surface sampling as described in 3.6.2, sub-surface sampling was also performed at these locations after removing the top layer by an excavator machine in 2019 AIPO (2019). In this case, almost 200 kg of sediments were collected at each sample site, but 60% of the amount was utilized due to the difficulty in transportation, and sieve analysis was applied after a quartering process. The current samples for sieve analysis in 2021 were collected using the procedure described in 3.3. Both the results are reported in Figure 3.11. Bifurcating results and comparing individual samples at the respective section as per Figure 3.12 showed that GSDs in 2019 were coarser than those of 2021, which may be due to an increase in the number of sediment count from a surface area of 4 m^2 (2 m × 2 m), which was larger than the 1 m^2 (1 m × 1 m) area used in 2021. This caused significant bias due to the contribution of a large amount of heavy coarse grains. One of the ideas behind the present study was to introduce an efficient hybrid technique and verify the results reliability by reducing the sediment sample collection time in the field. The results obtained by sampling different volumes at the same investigated location appeared to be quite reasonable. In particular, D10 was similar for both years, however, D50 and D90 were different and samples collected in 2021 seemed to be finer than those collected in 2019.

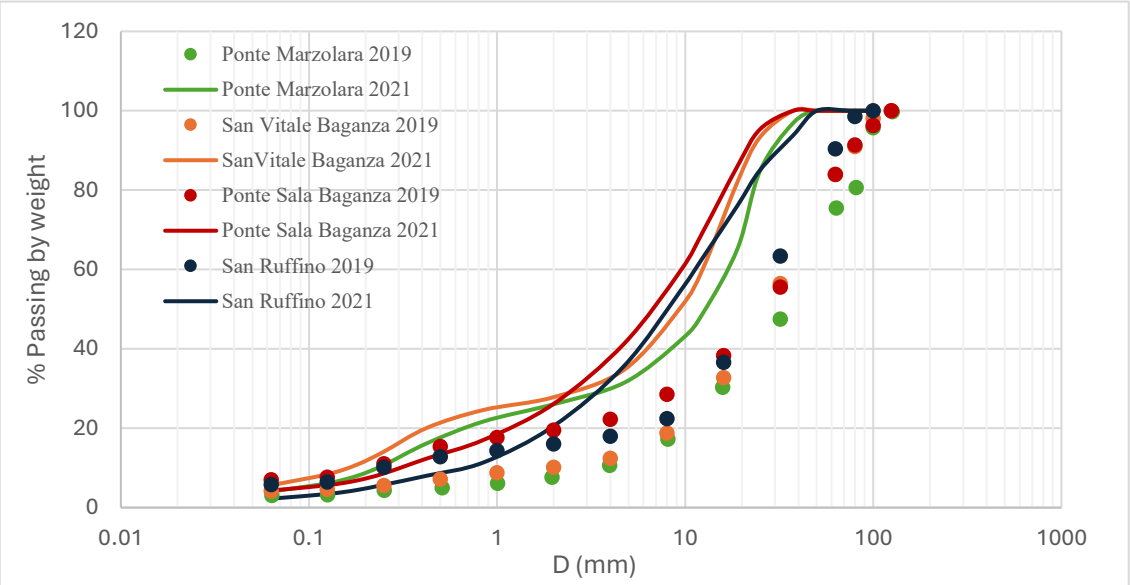

Figure 3.11 Combined comparison of sediments in subsurface layer from year 2019 and 2021 (sieve analysis)

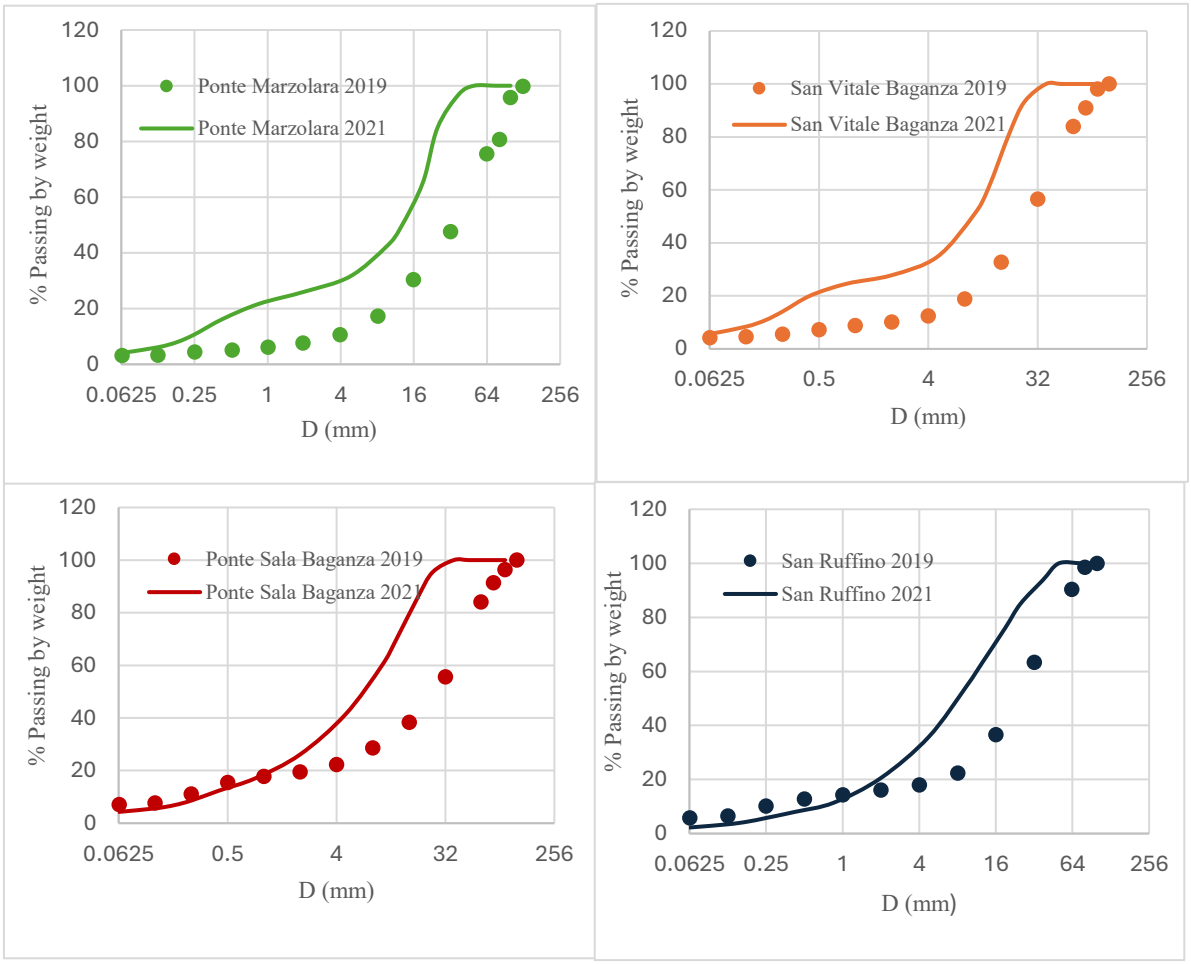

Figure 3.12 Individual grain size distribution of sub surface sediments at respective sections (sieve analysis).

3.6.4 Combination of the Photogrammetric Technique and Sieve Analysis

Different methods are available in the literature for combining the frequency distribution of two samples such as "rigid combination" and "flexible combination" (Bunte et al., 2001; Fripp & Diplas, 1993), or by combining two original percent frequency distributions (e.g., from an areal sample converted to a grid by number distribution beforehand and from a pebble count) Fripp & Diplas (1993). However, for this study, the frequency distributions obtained through both methods (photogrammetric and sieving) were adjusted to make a single combined frequency distribution that was representative of both. This task was accomplished by taking the average values of the surface and subsurface samples. The two samples contained the same grain size distribution frequencies for all size classes D (mm) in the coarser fraction. For the finer fraction of <2 mm, the values for the surface sample (distribution generated from photogrammetric technique) were taken as zero, due to the incapability of the photogrammetric technique to measure the sizes less than the selected value. In order to compare the GSDs of 2019 and 2021, the same procedure was repeated on the 2019 dataset and a

comparison was made afterward, as shown in Figure 3.13. The grain size distribution curves were in good agreement in both the finer and coarser parts. The differences in both the 2019 and 2021 GSDs were small and can be explained by the fact that the high river flows remain inactive to alter the grain size distribution and channel morphology in a significant manner in this period. Such a comparison is suitable for riverbeds that remain dry for some time, so the phenomenon that alters the grain size distribution can be easily traced.

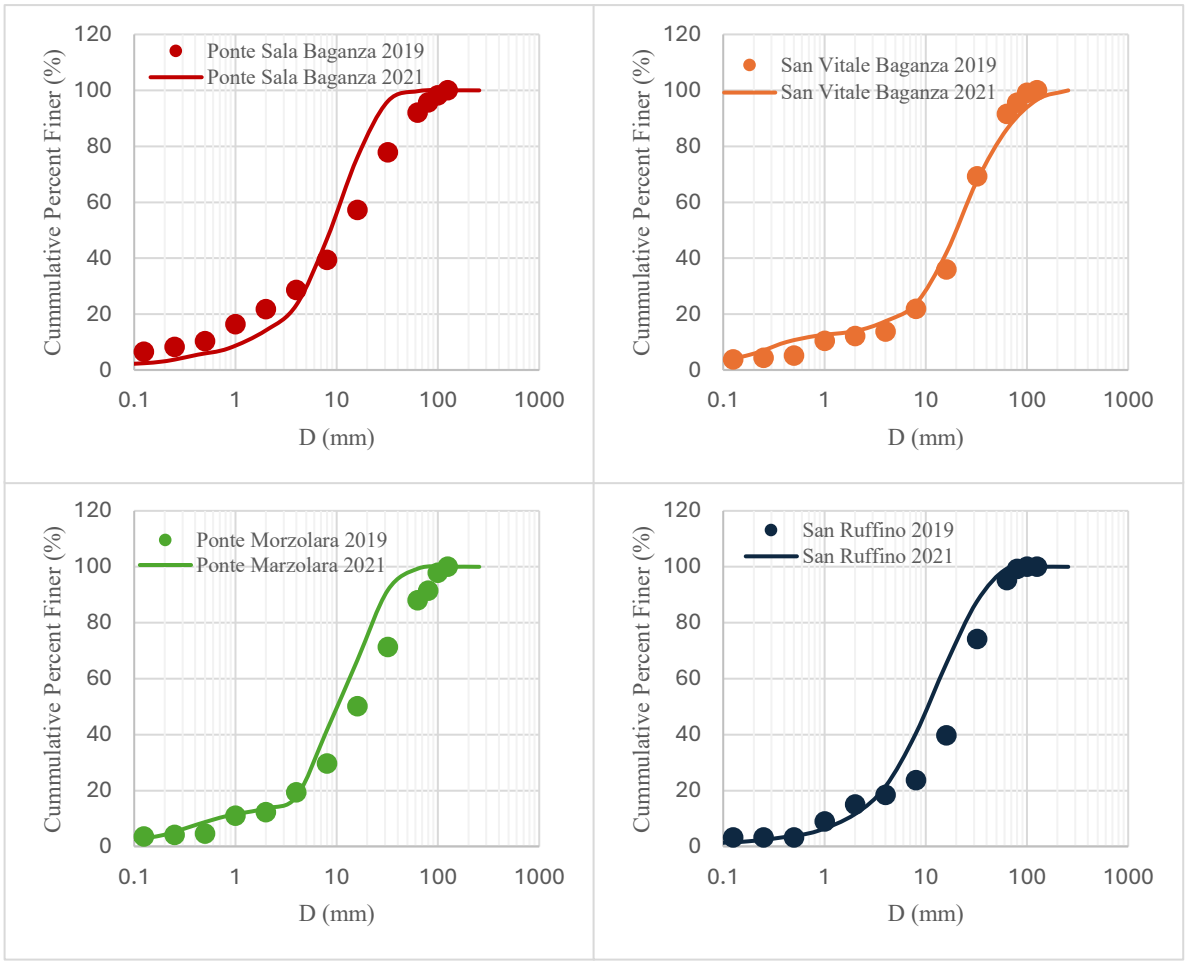

Figure 3.13 The GSD yield from the fusion of both the photogrammetry and in situ sieving temporal.

It is important to note that the quantity of material collected at these four sites in 2021 was very small compared to 2019 as shown in Table 3.3, due to which the amount of time for collecting a sample was reduced considerably, which can be harnessed in featuring various aspects of the photogrammetric technique.

Table 3.3 A comparison between the quantities of material collected in two years.

Section	Sample Weight in kg (2019)	Sample Weight in kg (2021)
San Ruffino	90	2.5
Ponte Sala Baganza	95	2.1
Ponte Marzolara	85	3.2
San Vitale Baganza	90	2.3

3.7 Conclusion and Recommendations

This research presents a hybrid technique that takes into account the photogrammetric technique and traditional sieving method applied to sediments forming the bed of the 3 km long reach of the Baganza River, Italy. For the photogrammetric part, the grain size distribution was generated through the analysis of digital pictures of the sediments taken on the riverbed in dry conditions. An open source software, namely Digital Gravelometer, was adopted by applying two methods (i.e., "grid by number" and "area by number"). The sieving part was carried out at 10 accessible locations along the length of the Baganza River. The spatial comparison revealed that the gravel and pebbles ranging between 2 and 64 mm were one of the dominant classes of sediments in the Baganza catchment among other classes including boulders, cobbles, gravel, and sand. For greater detail, the values ranging from 2 to 64 mm containing gravels and pebbles were divided into five sets (2–4 mm, 4–8 mm, 8–16 mm, 16–32 mm, 32–64 mm). This detail further clarifies that the maximum class present in the samples ranged from 16 to 64 mm, except in Section 9, where the dominant class was 8–16 mm. Grain size stats showed that the fluvial sediments present inside the Baganza catchment were coarsely skewed and extremely poorly sorted. This corresponds to dynamic features such as high energy, turbulent flow, coarse sediments, upstream meandering patterns, and deficiency in the straight approach of the Baganza River. Regarding the "grid by number" and "area by number" methods, the GSDs based on the "area by number" method appeared to be much more comparable with the GSDs obtained with sieve analysis in the coarser part of the fraction. In fact, the photogrammetric method was obviously missing in the finer part as the lower truncation value was set to 2 mm due to the limitation offered by the Digital Gravelometer software. A temporal comparison was made on the dataset for the years 2019 and 2021 with respect to the photogrammetric technique, sieve analysis, and the combination of both by adjusting the frequency distribution to obtain a single grain size distribution. The hybrid technique appears to be quite efficient and promising in determining the GSD by reducing the sediment sample quantity, and consequently, less time in the field. The results obtained by sampling different volumes at the same investigated location appeared quite reasonable in comparison. In particular, the case study of the Baganza River showed that the different techniques are complementary and help in acquiring data referring to two main levels: the surface stream bed and the soil beneath. The surface streambed can be satisfactorily characterized by using the photogrammetric technique. With regard to the material below the surface streambed, this needs to be characterized by classical

sieve analysis. For sieve analysis, it was shown that it is sufficient to collect a relatively small sample (from 2 to 5 kg) at a depth of 0.3 m instead of collecting a huge amount of material at higher depths, since the results were comparable. These aspects imply a certain cost reduction and the fast applicability of these techniques with a satisfactory precision. The resulting information of various grain sizes is accurate and can be transferable to other channels with minimal time needed for sample collection, within specified locations. Using the hybrid technique, it is also possible to address the need for repeated surveys, especially in catchments where the river morphology has changed drastically due to the flooding that takes place with short return intervals (under two years).

Due to the non-disturbing nature of the photogrammetric method, this approach is also beneficial from an ecological perspective. With regard to practical tricks, it is advised that image quality can be compromised if the images are repeatedly saved after editing. Therefore, in order to avoid such incidents from happening, saving the file in the jpeg format for one, is recommended. Another vital point is to get rid of the vegetation and avoid casting shadows at the sampling location, since it can create problems in the processing of the images and may produce flawed results by indicating non-sediment areas as sediments. The spatial scale of interest can be increased by adjusting the height of the camera, but the quality of the image should be excellent in order to obtain accurate results. One of the major limitations of the photogrammetric technique is that it does not measure the fine fraction of the particle size distribution inside the riverbed, which could affect the sediment transport process (i.e., grain size distribution fluctuates during this process as a result of interplay (feedback) between the flow discharge and grain size). However, the results obtained through different techniques can vary substantially due to the reason that generally, a gravel riverbed is characterized by a fixed armored layer, so that exposed sediments are much coarser than the subsurface layer, which contains finer particles. Therefore, it is advisable to use different sampling techniques at different depths to obtain the sediment samples, since each method includes a different percentage of small particles that are partially hidden between the large clasts.

Chapter 4: SEDIMENT TRANSPORT MODEL

4.1 Introduction

The field of numerical modelling encompasses a wide range of approaches, these approaches differ in their underlying principles and methodologies. First, it is important to discuss the equations utilized to represent fluid movement within these numerical models. At the forefront are models that employ the 2D shallow water equations. These equations embody critical aspects such as mass conservation, gravity representation, frictional forces, and momentum conservation. Some models adopt simplified versions, neglecting inertia and struggling with supercritical flows or shock waves. Instead, other models extend these equations to 3D, allowing for detailed modelling of structures, although their scalability for larger scenarios is limited.

Numerical models operate on discretized domains. For instance, the Digital Elevation Model (DEM), which provides elevation data, needs to be discretized to align with the computational grid of the numerical model. This trial enables the translation of real-world topography into a format suitable to be processed by the numerical model. The process of discretizing topography into computational grids can follow either a fixed grid or a flexible mesh approach. Fixed grids are known for their computational efficiency and control over cell sizes, providing stability in post-processing analysis. On the other hand, flexible meshes, although geometrically adaptable, require time-consuming mesh generation and may incur potential run-time overheads.

Different numerical discretization methods, such as finite volume, and finite element approaches, dictate how the equations are processed through space. These methods vary in complexity, computational requirements, and applicability within 2D numerical solvers. Temporal calculations in numerical models are driven by implicit and explicit schemes. Implicit schemes offer accuracy but require computations for the entire domain, while explicit schemes, offer parallelization benefits but have limitations in timestep selection.

The order of solution schemes, whether first-order or second order, determines the accuracy of numerical approximations. First-order schemes are simpler, but their accuracy diminishes during transient flows, often resulting in substantial numerical diffusion. On the contrary, second-order schemes, though more complex, ensure heightened accuracy, especially in complex flow scenarios.

Selecting the appropriate 2D numerical model entails consideration of various aspects, including equation representation, solution order, grid flexibility, and topographic reliability. Rigorous testing during model development phases, focusing on convergence, sensitivity to cell sizes, and maintaining mass balance, is indispensable for validating the suitability of a numerical model for specific objective.

4.2 Parflood Model

In this study, the hydrodynamic model employed is the Parflood code developed by Vacondio et al. (2014, 2017), at the University of Parma (Italy). This code utilizes an explicit Finite Volume (FV) scheme to solve the

conservative form of the two-dimensional shallow water equations (2D-SWE), mathematically presented in Equation 4.1 by Toro (2001).

$$\frac{\partial U}{\partial t} + \frac{\partial F}{\partial x} + \frac{\partial G}{\partial y} = S_o + S_f \qquad 4.1$$

In Equation 4.1 the vector U signifies the vector of conserved quantities. The terms F and G denote the fluxes of conserved variables in their respective x and y directions. Additionally, the source terms S_o and S_f account for bed slope and frictional effects, respectively present on the right-hand side. The Equation 4.1 ensures the preservation of still water, irrespective of how the slope term is discretized. This modification, adapted for wet-dry interfaces, builds upon the algebraic adjustments made by Rogers et al. (2003). The Equation 4.1 encapsulates the conservation of these quantities in a control volume. The left hand side represents the change of these quantities in time and space due to advection (the movement of the quantities in space). The right-hand side represents sources or sinks that contribute or take away from the system. Moreover, in Equation 4.2 vector of conserved variable U encompassing the water depth h and the unit discharge components (hu and hv) along the x and y directions.

$$U = [h; hu; hv]^T \qquad 4.2$$

Furthermore, the velocity field components (u, v) are expressed in depth-averaged form, and are given by Equations 4.3 and 4.4, respectively. In this context, $\eta = h + z$ represents the water surface elevation, whereas z is the bed elevation.

$$G = \left[hv; hv^2 + \frac{1}{2}g(\eta^2 - 2\eta z); uvh\right]^T \qquad 4.3$$

$$F = \left[hu; hu^2 + \frac{1}{2}g(\eta^2 - 2\eta z); uvh\right]^T \qquad 4.4$$

Similarly, Liang & Borthwick (2009) expressed bed S_o and S_f and friction slope terms using balanced formulation as shown in Equation 4.5

$$S_o = [0; -g\eta\frac{\partial z}{\partial x}; -g\eta\frac{\partial z}{\partial y}]^T \qquad S_f = [0; -gh\frac{n^2\, u\sqrt{u^2+v^2}}{h^{4/3}};\ -gh\frac{n^2\, v\sqrt{u^2+v^2}}{h^{4/3}}]^T \qquad 4.5$$

In Equation 4.5 g is the acceleration due to gravity (m/s^2) and n is the Manning's roughness coefficient. Recent applications evaluating real flood scenarios have underscored the robust computational efficacy of the Parflood code, even when compared with vast domains comprising millions of computational cells (Dazzi et al., 2018), (Ferrari et al., 2019). Extensive investigations by Vacondio et al. (2016), Dazzi et al. (2018), and Dazzi et al. (2019) have rigorously assessed its performance across varied scenarios. The computational framework adopts

the HLLC (Harten-Lax-van Leer contact) Riemann solver (Toro, 2001) to compute intercell fluxes, coupled with a corrective technique devised by Kurganov & Petrova (2007) to mitigate unrealistic velocities near wet/dry interfaces. For discretization, a centered approximation handles the slope source term (Vacondio et al., 2014), while an implicit formulation proposed by Caleffi et al. (2003) addresses the friction source term. Adherence to the CFL (Courant–Friedrichs–Lewy) stability condition guides the determination of the smallest allowable time step (Toro, 2001). Leveraging CUDA/C++ code for GPU parallelization significantly enhances computational efficiency compared to sequential implementations.

4.3 Introducing Sediment Effects into Parflood Model

It is important to note that for the hydrodynamic part, the model used in this research followed the methodology as per section 4.2 and domain discretization following as per section 4.3.1. Regarding the sediment part, the implementation of Juez et al. (2014) is adopted. They introduced a model where the hydrodynamic equations are dissociated from the Exner equation, which characterizes the changes in bed morphology over time known as decoupled or asynchronous model. Asynchronous techniques, inherent in weak coupling, operate under the assumption that morphodynamic changes occur slowly relative to hydrodynamics, thus allowing fluid mass and momentum equations to be solved separately from the Exner equation. While fully coupled methods provide comprehensive treatment of morphodynamic, weakly coupled approaches remain popular for their modularity, reduce complexity and computational efficiency. Two main approaches have been used in this research, namely the approach suggested by Meyer-Peter and Müller (1948) (henceforth identified as MPM) and that proposed by Smart (1984) (henceforth identified as SMART), The 2D Exner equation governs the sediment transport mechanism, which is used as the closure equation is expressed as follows:

$$\frac{\partial z}{\partial t} + \left(\frac{1}{1-p}\right)\left(\frac{\partial q_{s,x}}{\partial x} + \frac{\partial q_{s,y}}{\partial y}\right) = 0 \qquad 4.6$$

In Equation 4.6, z represents the bed elevation, $q_{s,x}$ and $q_{s,y}$ signify the sediment discharge in x and y direction, respectively, and are represented by MPM (Meyer-Peter and Müller, 1948) and SMART (Smart, 1984) bedload transport formula in this work. Furthermore, p is the porosity of the bed material. The dimensionless parameter ϕ in Equation 4.7 assumes a pivotal role in both MPM and SMART approaches. It is computed differently for each method. The bedload discharge is calculated in a dimensionless manner using the SMART approach, as outlined below.

$$\phi = 4\,(D_{90}/D_{30})^{0.2} F S^{0.1} \theta^{0.5} (\theta - \theta_c{}^{s}) \qquad 4.7$$

Furthermore, in Equation 4.7 D_{90} & D_{30} are characteristic grain sizes for which 90% and 30% by weight of the material is finer, respectively. Similarly, S is the friction slope with a value between 0.0004 to 0.02. F represents the Froude number, θ signifies the dimensionless shear stress, also referred to as Shield's parameter, which is function of shear stress ($\theta = \frac{\tau}{g(\rho_s - \rho)D50}$), ${\theta_c}^s$ is critical shield parameter. It is important to highlight from Equation 4.7 that sediment transport will occur only when the $\theta > {\theta_c}^s$ otherwise $\phi = 0$. The bedload discharge is calculated in a dimensionless manner using the MPM approach, as follows:

$$\phi = 8\,(\theta - \theta_c)^{1.5} \tag{4.8}$$

Also,

$$\phi = \frac{|q_s|}{\sqrt{(g(s-1)\,{D_{50}}^3}} \tag{4.9}$$

$s = \frac{\rho_s}{\rho_w}$ is the ratio between solid material and water density. Furthermore, for MPM approach, D_{50} median grain size diameter ranges between 0.4 mm to 29 mm. For SMART approach ($D_{90}/D_{30} \leq 10$) and for uniform sediments (D_{90}/D_{30}=1.05).

These parameterizations enable the accurate modeling of sediment transport dynamics. As already discussed, the model is a weakly coupled sediment transport model as the term "weakly coupled" characterizes the weak interaction between water flow and sediment transport components in the model. This implies that while sediment transport is influenced by water flow, the reciprocal feedback from sediment movement on water flow is limited. This pragmatic approach strikes a balance between capturing the essential interactions between these processes and maintaining numerical stability. To solve the governing equations numerically, the model employs a finite volume scheme. This method discretizes the domain into finite volumes known as cells and calculates the fluxes of conserved quantities across the cell interfaces. The finite volume approach provides a robust framework for simulating fluid dynamics and sediment transport in complex geometries.

4.3.1 Domain Discretization and Flux Computations

In Parflood hydrodynamic model, the evolution of flux at each time step (and at the subsequent time step) involves updating the conserved variables (water depth and discharge components) as shown in Equation 4.10. The fluxes (F and G) of conserved variables are calculated across the cell interfaces in the x and y directions as shown in Figure 4.1, considering bed slope S_o and frictional effects S_f. For the i^{th} cell having length Δx, the following equation allows to update the solution in time Δt

$$U_{i,j}^{n+1} = U_{i,j}^{n} - \frac{\Delta t^n}{\Delta x}(F_{i+1/2,j} - F_{i-1/2,j}) - \frac{\Delta t^n}{\Delta y}(G_{i,j+1/2} - G_{i,j-1/2}) + \Delta t^n(S_o + S_f) \quad 4.10$$

Equation 4.10 can be discretized on rectangular mesh. The superscript n in Equation 4.10 represents the time level, i, j and $\Delta x, \Delta y$ represent the cell position and size of grid in the x and y directions, respectively. To mitigate the occurrence of high velocities and instabilities, a precautionary measure is implemented. If the water depth falls below a predefined fixed threshold the corresponding cell is designated as dried.

This adjustment aims to stabilize the system and prevent undesirable outcomes. Here it is also important to note that the timestep Δt is controlled by CFL (Courant-Friedrichs-Lewy) condition as given in equation 4.11 by Dazzi et. al (2014) where $C_r \leq 1$

$$\Delta t = 0.5 C_r \min\left(\frac{\Delta x}{|u| + \sqrt{gh}}, \frac{\Delta y}{|v| + \sqrt{gh}}\right), \Delta t = \min(\Delta t) \quad 4.11$$

4.3.2 Bed Level Updating

Increase and decrease in bed elevation z depends upon the solid discharge q_s^* coming in and out of the cell as per Equation 4.12

$$z_{i,j}^{n+1} = z_{i,j}^{n} - \frac{\Delta t}{\Delta x}(q_{s,i+1/2,j}^{*} - q_{s,i-1/2,j}^{*}) - \frac{\Delta t}{\Delta y}(q_{s,i,j+1/2}^{*} - q_{s,i,j-1/2}^{*}) \quad 4.12$$

Bed elevation z is then updated accordingly, considering sediment discharge and its wave speed estimation. Bed level at next timestep $z_{i,j}^{n+1}$ is equal to bed level at previous timestep z_i^n minus the difference of the sediment fluxes coming in and going out of the cell. The term q_s^* represents the bedload flux at each intercell. and the term λ_s represents the bedload celerity. In particular, if $\lambda_s > 0$, $q_{s,x,i,j}^{*} = \left(\frac{1}{1-p}\right) q_{s,x,i,j}$ and if $\lambda_s \leq 0$, $q_{s,x,i,j}^{*} = \left(\frac{1}{1-p}\right) q_{s,x,i+1,j}$. Moreover, the bedload celerity is computed as $\lambda_s = \frac{\delta q_{sn}}{\delta z}$ and flux is computed as $\delta qs_x = \delta qs_{x,i+1,j} - \delta qs_{x,i,j}$ and $\delta z = \delta qz_{i+1,j} - \delta qz_{i,j}$

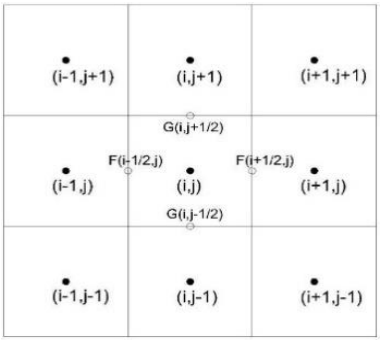

Figure 4.1 2D finite volume mesh.

4.3.3 Model Limitations

The bedload transport model has the following limitations:

- the model neglects vertical velocities, assuming that vertical movement within the water column is negligible;
- the model assumes hydrostatic pressure conditions;
- the model assumes that the slope of the river is small enough so that the sine of the slope can be approximated with the value of the slope angle;
- the model employs a friction approach based on uniform flow conditions;
- the sediment model does not account for changes in grain size distribution over time due to bedload transport.

4.4 Benchmark Testing

Numerical benchmark testing for sediment transport model involves comparing the prediction of a model with observed data from laboratory experiment under controlled conditions. The purpose of this testing is to evaluate the performance of the model in predicting sediment transport process. The benchmark tests typically involve a set of standard laboratory tests, which are designed to simulate specific sediment transport phenomena, such as bedload transport, suspended load transport, or incipient motion of sediment particles. The experiments are conducted using a variety of sediment sizes and flow conditions, and the resulting data are used to evaluate the model's ability to predict sediment transport rates, bedform evolution, and other relevant parameters.

The results of the benchmark testing can be used to identify areas where the model needs improvement, such as its ability to predict the onset of sediment motion, the effect of turbulence on sediment transport, or the interaction between sediment transport and bedform evolution. The testing can also be used to compare the

performance of different sediment transport models and to identify the most effective approaches for simulating sediment transport processes.

Overall, experimental benchmark testing is an important tool for evaluating and improving sediment transport models, and it plays a critical role in advancing our understanding of these complex natural processes. 1D and 2D benchmark tests discussed in sediment transport literature, such as the dam break tests and evolving profiles with migrating knickpoints, have proven to be effective for evaluating the performance of sediment transport models. These tests allow researchers to isolate and understand the physical mechanisms underlying sediment transport and provide a simplified representation of real-world phenomena.

4.4.1 1D Dam Break Test Case by Spinewine and Zech (2007)

The 1D dam break test case conducted by Spinewine & Zech (2007) is a widely used benchmark test case for evaluating the performance of 1D numerical models in simulating the propagation of flood waves, resulting from a dam break. The test case is useful because it provides a controlled laboratory setting, in which the bahaviour of the flood wave can be observed and measured under different conditions. The results of these simulations could be used to better understand the dynamics of dam breaks and to improve the accuracy of numerical models for predicting the impacts of dam failures

4.4.1.1 Experimental Setup

The channel had a total length of 6 m, and in the middle at x = 3 m a central gate was operated for simulating a dam break. The sand used for the bed of the channel was coarse uniform sand with size of 1.82 mm, a solid density of 2683 kgm^{-3}, a friction angle $\phi = 30^{o}$, porosity = 0.47 and Manning's coefficient n= 0.0165 $sm^{-1/3}$. The regions on the left (L) and on the right (R) of the central gate were filled with different water and sand depths. Table 4.1 summarizes the set of experiments selected in this work. From the numerical simulation point of view, the cell size (Δx= 0.01m) and the CFL = 0.4 are used in both Tests A and B. Test A describes a situation where morphological changes are produced in presence of a dry bed and a flat bottom. Test B allows checking the numerical assessment against the different types of waves that may arise in a dam break case over a wet bed and a bottom step.

Table 4.1 Initial Condition of test cases

Test	h_L	h_R	Z_L	Z_R
A	0.35	0.00	0.00	0.00
B	0.25	0.10	0.10	0.00

4.4.1.2 Test A

In test A the flow evolves in time generating a left rarefaction wave upstream the gate ending in a flooding front dominated by friction. The simulated results computed through both SMART and MPM formulae are close to experimental results, over dry and fixed bed Figure 4.2 to Figure 4.9 display numerical results and experimental data for times ranging from 0 to 1 s, in terms of dry bed case with h in (m) is the water depth, z in (m) the bed elevation, h + z in (m) the water surface elevation. The front wave is numerically well reproduced both in case of SMART and MPM and the production of a little scour is also provided by the computed results.

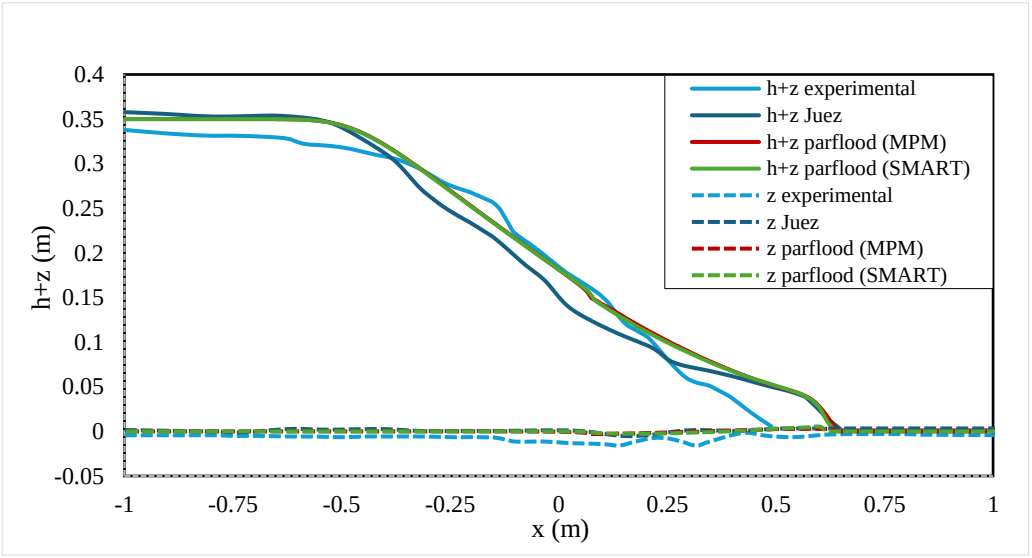

Figure 4.2 Dam break profile on dry bed at T=0.25 secs

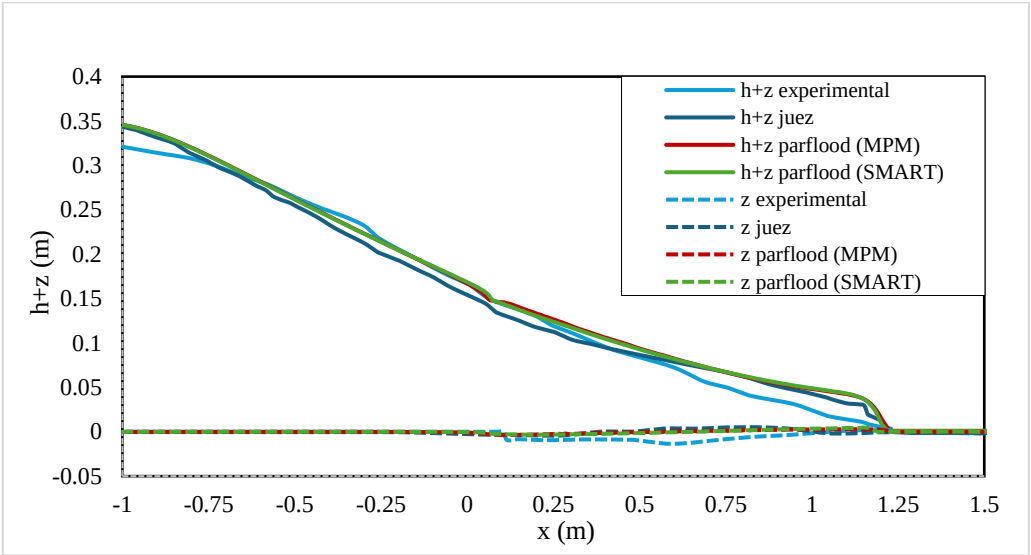

Figure 4.3 Dam break profile on dry bed at T=0.5 secs

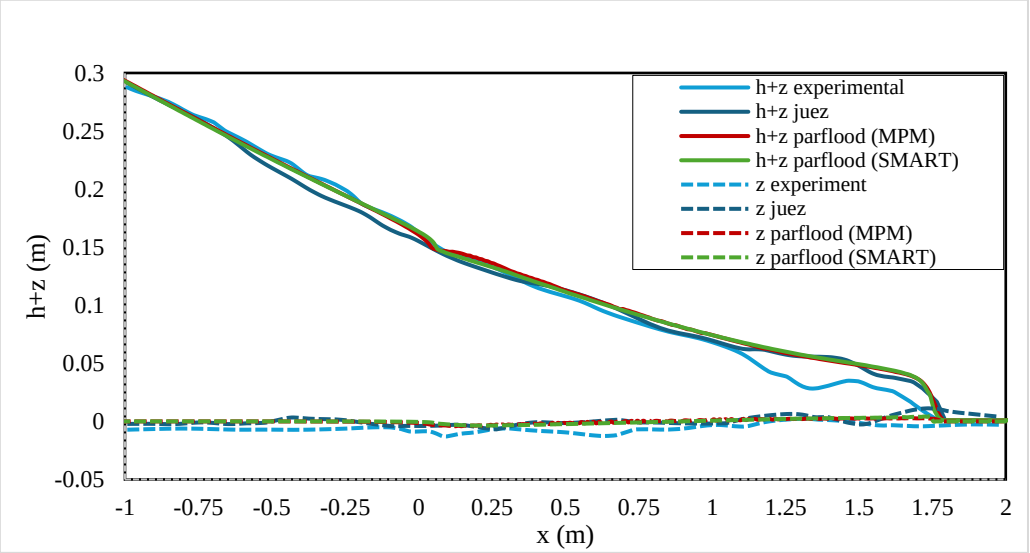

Figure 4.4 Dam break profile on dry bed at T=0.75 secs

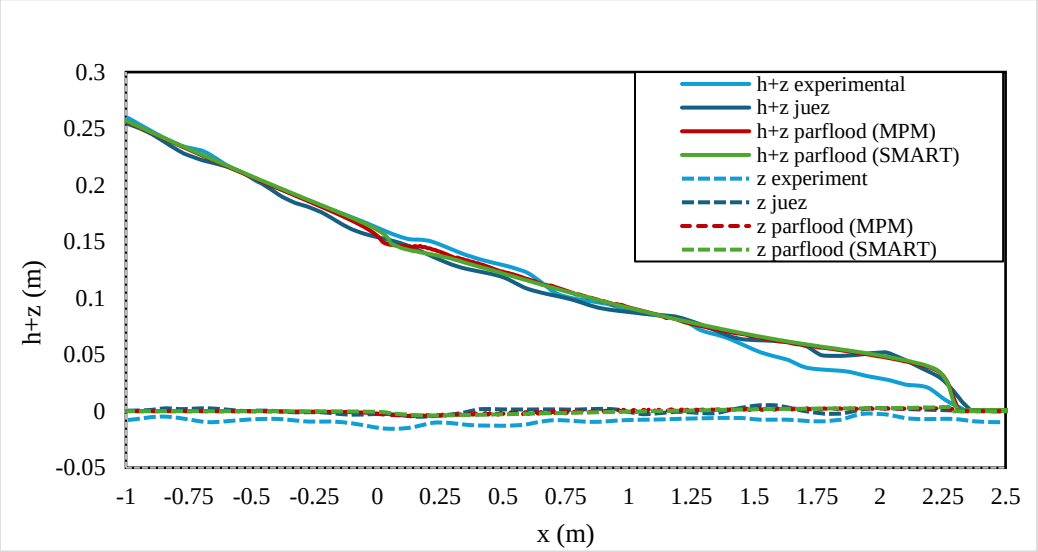

Figure 4.5 Dam break profile on dry bed at T=1.0 secs

4.4.1.3 Test B

Test B of the 1D dam break test case represents a scenario where a bed step is present with a water level below the gate. Over time, the flow evolves, resulting in a left-moving rarefaction wave upstream of the gate, followed by a steady hydraulic jump downstream of the gate and a shock wave that advances to the right side. The hydraulic jump is a phenomenon that occurs when the flow is subjected to transition from supercritical to subcritical state, resulting in a sudden rise in the water surface elevation and a decrease in flow velocity. The formation of a hydraulic jump downstream of the bed step causes the flood wave to slow down and increase in height, leading to the formation of a high-water mark. Figure 4.6 to Figure 4.9compare the computed and experimental data for the free surface and bed level profiles at different times (0.25, 0.5, 0.75, and 1.0 seconds),

in terms of wet bed case. The shock wave celerity is well captured by both the SMART and MPM approaches, although minor differences are observed due to fast transient energy variations, associated with the existence of a hydraulic jump, and density variations in the vertical column, associated with sediment concentration. The test provides a valuable benchmark to assess the ability of numerical models to accurately simulate the complex bahaviour of flood waves resulting from dam breaks over bed steps. The test case highlights the importance of considering factors such as hydraulic jumps and sediment concentration to accurately predict the bahaviour of flood waves in dam break scenarios.

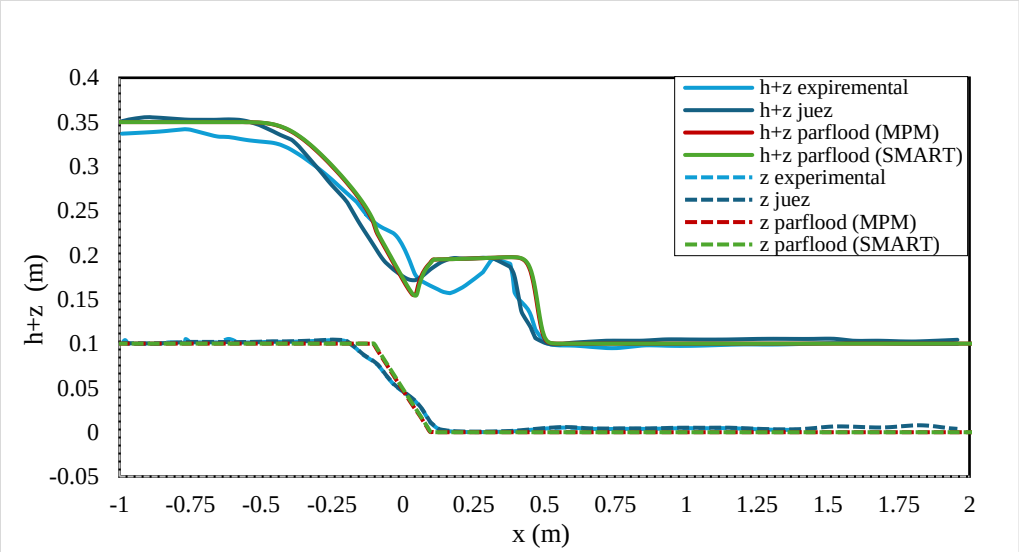

Figure 4.6 Dam break profile with bottom step on wet bed T=0.25 secs

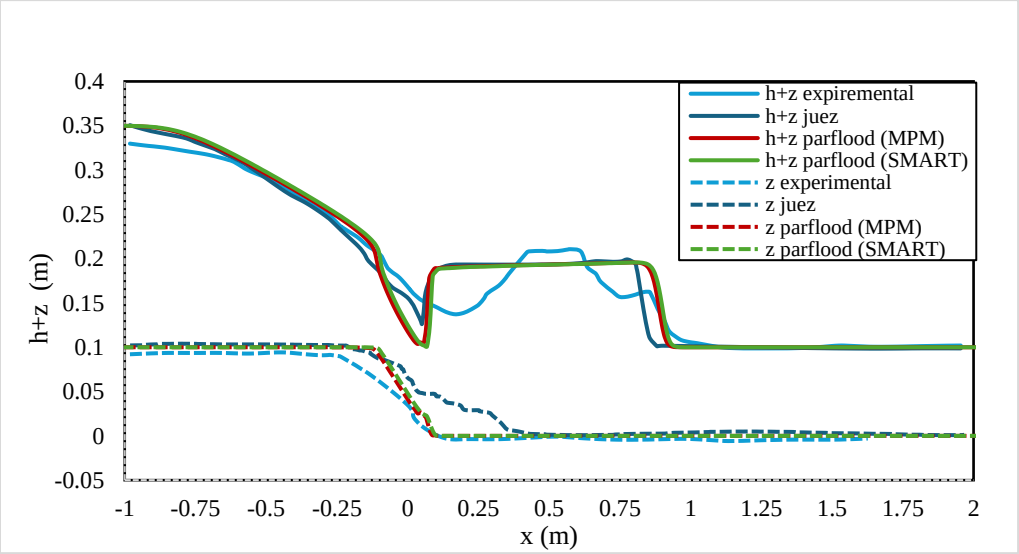

Figure 4.7 Dam break profile with bottom step on wet bed T=0.5 secs

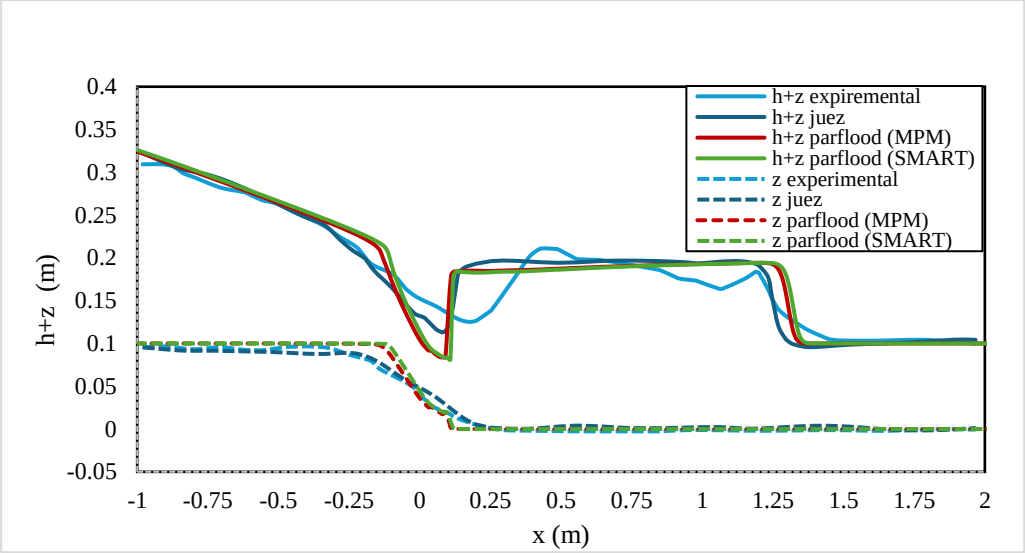

Figure 4.8 Dam break profile with bottom step on wet bed T=0.75 secs

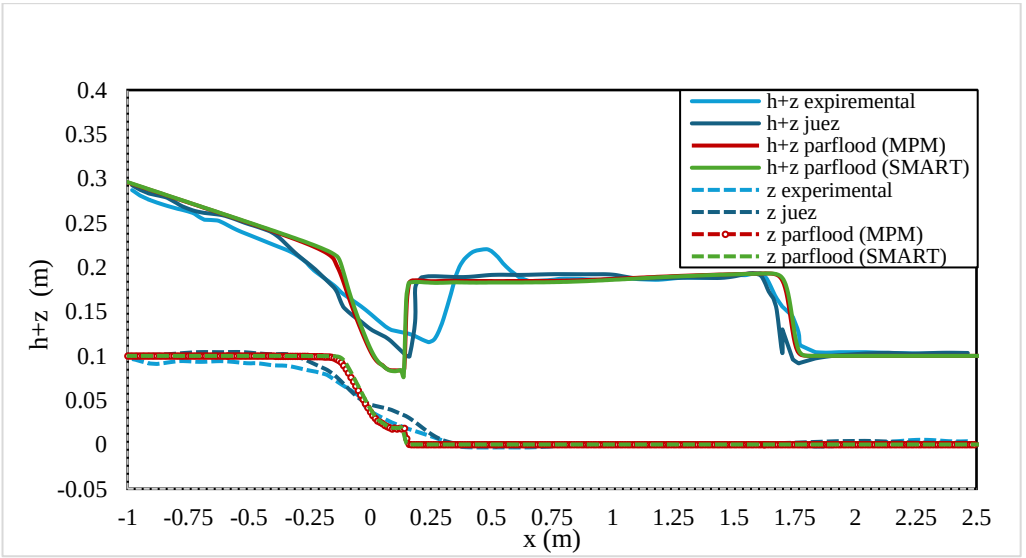

Figure 4.9 Dam break profile with bottom step on wet bed T=1.0 secs

4.4.2 Knickpoint Evolution Test Case

The knickpoint evolution experiment was conducted by Bellal et al. (2004) to investigate the ability of numerical models to manage a sudden flow transition from subcritical regime over a mild slope (M2 water profile) to supercritical regime over a steep slope (S2 water profile). The symbol S stands for steep slope and M stands for mild slope and 2 means the profile is in zone 2. It is pertinent to note that the normal flow is supercritical on steep slope and subcritical on mild slope. In M2 profile the normal depth of water is greater than actual depth of water which itself is greater than critical depth mathematically can be expressed as hn >

h > hc. On the contrary, for S2 hc > h > hn. The practical example of S2 could be flow from a reservoir on steep slope and M2 could be free overfall over mild slope.

This type of flow transition can cause significant morphological changes in the bed of a channel, and accurate simulation of these changes is important for predicting the evolution of natural rivers and streams. Field observations and laboratory experiments suggest that these sharp slope breaks can preserve their identity even as they migrate upstream under retrogressive erosion. The experiment was conducted by measuring morphological changes in an erodible bed with different slopes.

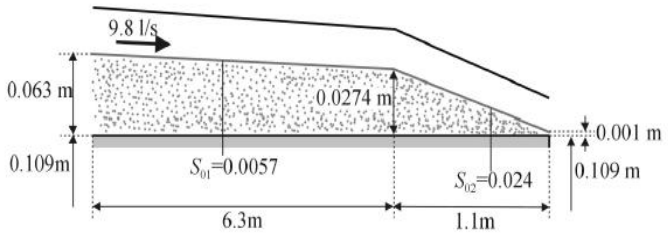

Figure 4.10 Typical configuration of a knickpoint test case by Bellal et al. (2004).

4.4.2.1 Experimental Setup

The initial conditions of bed slope were set up as shown in Figure 4.10. The experiment was conducted in a flume, and a flow with a constant discharge was introduced into the channel. The flow started over a mild slope and then encountered a sudden change in the slope at the knickpoint. During the experiment, the bed elevation was measured using a laser scanner at different times. The morphological changes in the bed were very useful for comparisons to evaluate the accuracy of the numerical models in simulating the flow transition and its effects on the bed. The original experiment was carried out using a coarse and uniform size sand with negligible cohesion, porosity equal to 0.42., and a Manning's coefficient n = 0.0165 $sm^{-1/3}$. The initial condition is a water level surface equal to 0.028 m. The boundary conditions imposed are, upstream, a water discharge equal to 9.8 l/s and, downstream, a water surface level equal to 0.11 m. The domain, 7.4 m long, is divided using cell size dx = 0.05 m, CFL = 0.9. The initial position is located about 100 cm from downstream.

4.4.2.2 Results

The simulation results were compared with the experimental data to assess the performance of the numerical model. The knickpoint propagation may be clearly observed in Figures 4.11 to 4.14. Progressive degradation wave described previously extends in the upstream direction, causing further decrease of the bed levels in the supercritical reach, while the average upstream bed slope is still unaffected. As this degradation develops, the slope of the channel in this region is reduced and tends to an equilibrium value at the end of the test. The erosion at the knickpoint is predicted at the same rate as in the experiment and the final evolution can be seen

on the graph in Figure 4.14 the final bottom level is also well achieved especially with SMART approach, since it appears to be more stable than MPM.

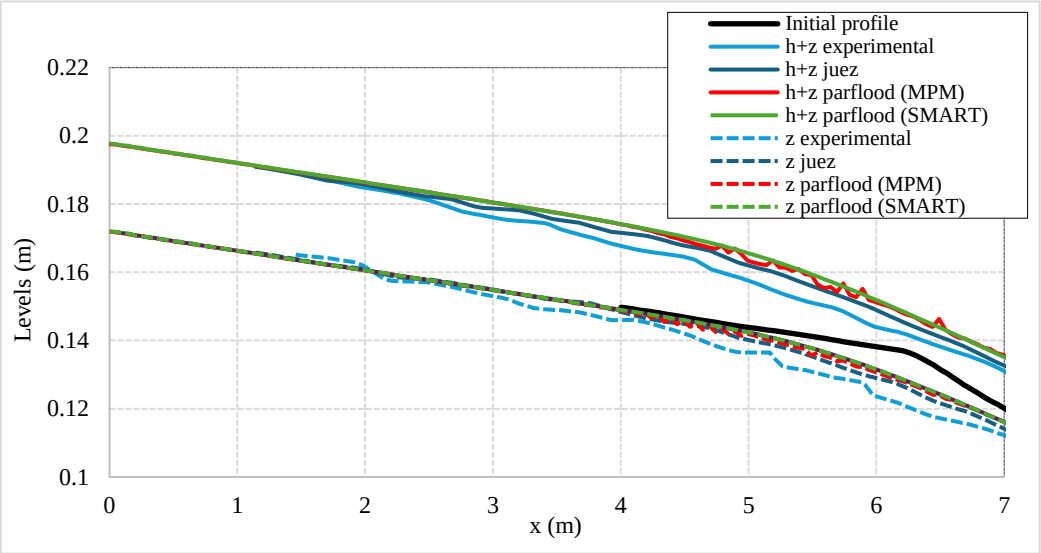

Figure 4.11 Knickpoint profile comparison at T=165 secs

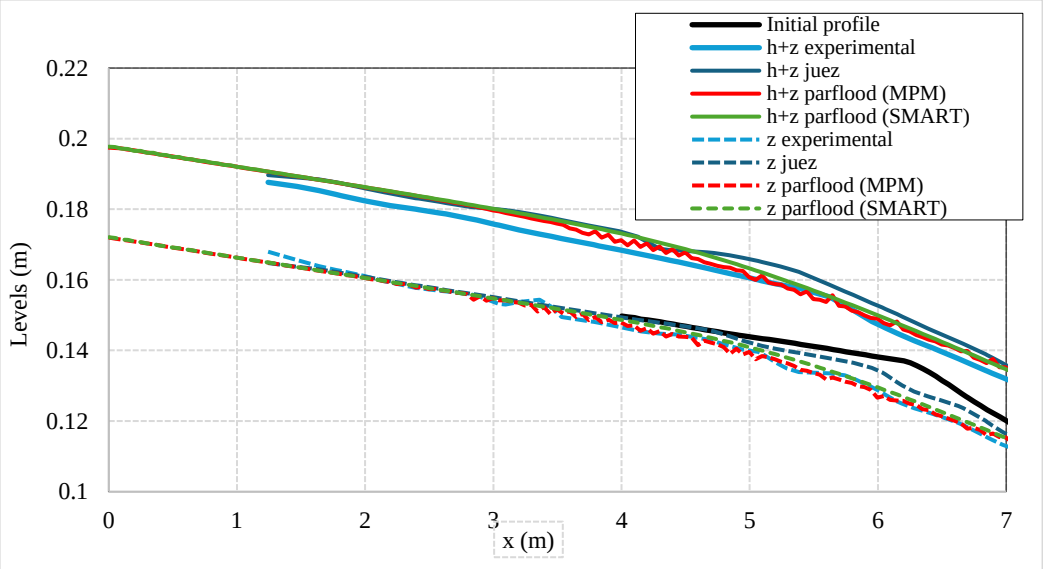

Figure 4.12 Knickpoint profile comparison at T=345 secs

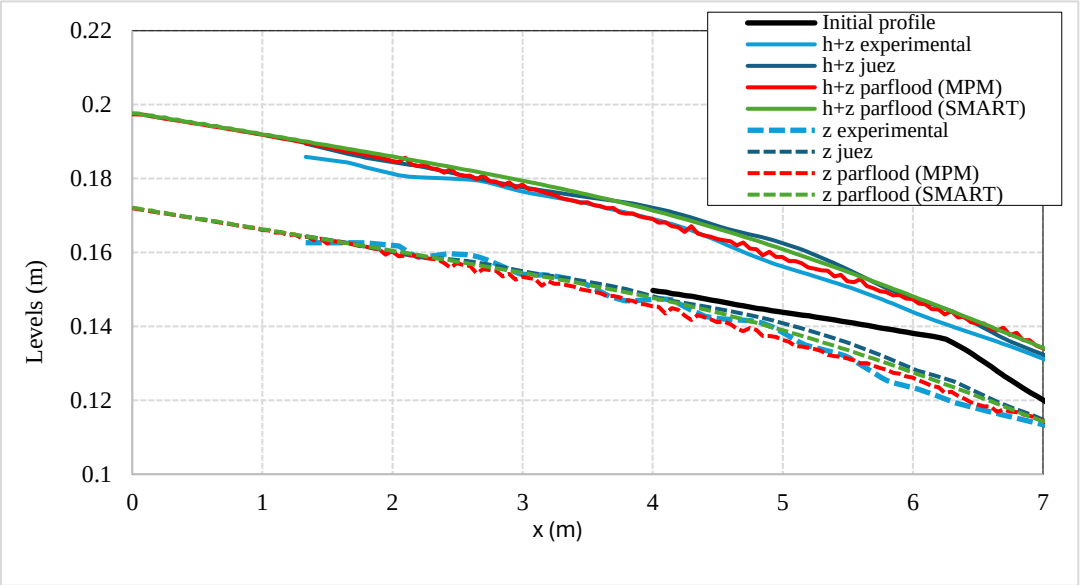

Figure 4.13 Knickpoint profile comparison at T=589 secs

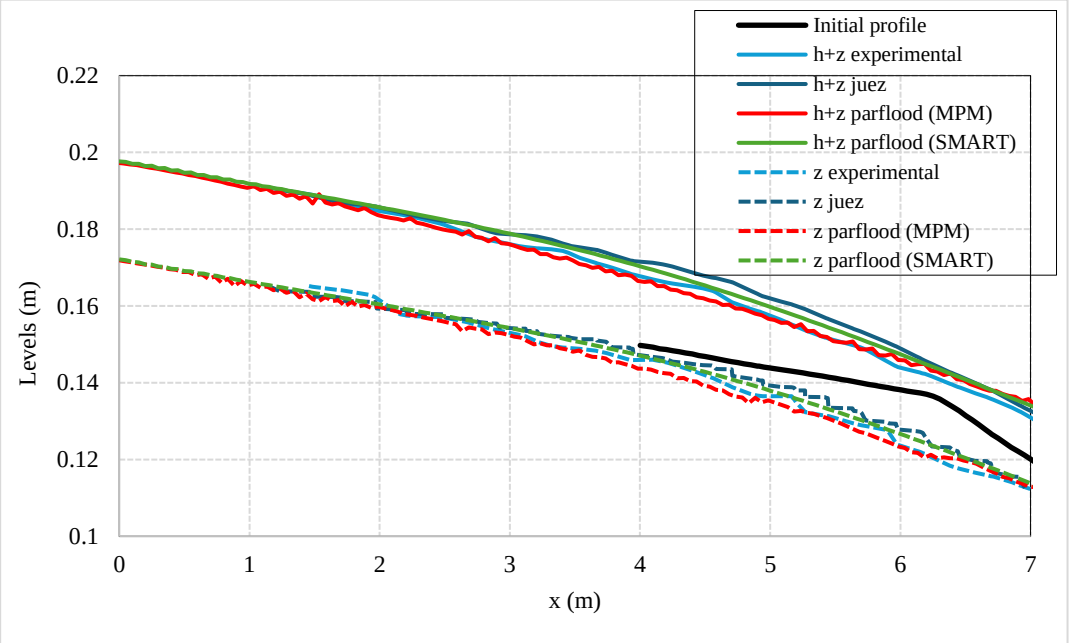

Figure 4.14 Knickpoint profile comparison at T=851 secs

The time progression delineates three distinct zones along the flow:

1. Upstream area (distance < 2 m),

2. Middle zone (2 m < ~ distance < ~ 6 m) characterized by escalating sediment discharge towards the knickpoint, resulting in gradual slope steepening,

3. Downstream section past the knickpoint, where the flow becomes supercritical, leading to a decline in bed slope due to regressive erosion.

The model predictions closely mirror experimental outcomes, accurately replicating erosion rates at the knickpoint and final bottom levels.

4.4.3 2D Dam Break Test by Soares Frazão et al. (2011)

In this 2D test, numerical simulations were performed using cell size dx = 0.01 m and CFL = 0.4. No outlet condition is considered downward the channel. The simulated results were obtained using two different approaches, namely, MPM and SMART approach, and both were compared to experimental (measured) results. This benchmark test case involves the simulation of a dam break scenario in a 2D rectangular domain. This experiment was conducted at the University of Liège (Belgium) using a hydraulic flume and the experimental setup was designed to mimic the conditions of a dam break in a natural setting. The purpose of the 2D dam break test cases was to investigate the morphological changes and characteristics of the shock and rarefaction waves that are generated when a dam breaks over mobile bed, and to study how these waves propagate and interact with the surrounding terrain.

4.4.3.1 Experimental Setup

The experimental set up consists of a flume 3.6 m in width and approximately 36 m in length. The flume was bounded by a solid wall at its upstream end and featured a sediment trapping disposal system at its downstream, detail can be seen in Figure 4.15. The gate, located at x = 0 m, was connected to an upstream reservoir, and was 1 m wide. In experimental setup by Soares Frazão et al. (2011) the gate was rapidly raised using a mechanical counterweight system to simulate a dam break. The precise opening time, measured at 0.23 seconds, marked the instant when the gate no longer touched the water, signifying an instantaneous dam break. The experiment lasted 20 seconds, during which morphological changes were observed to be minimal after the gate closure. The sand was extended over 9 m downstream of the gate and 1 m upstream of the gate, with a thickness of 0.085 m. A complete sketch of the experiment can be seen in Figure 4.15. The properties of the sand were: solid density ρ = 2,630 kgm-3, mean diameter equal to 1.61 mm, $\phi = 30^{o}$, negligible cohesion, porosity p = 0.40. The roughness was characterized by a manning factor n = 0.0165 s/m1/3. Initially, the water level at upstream side in the flume is at 0.47 m and at the downstream side the condition is dry.

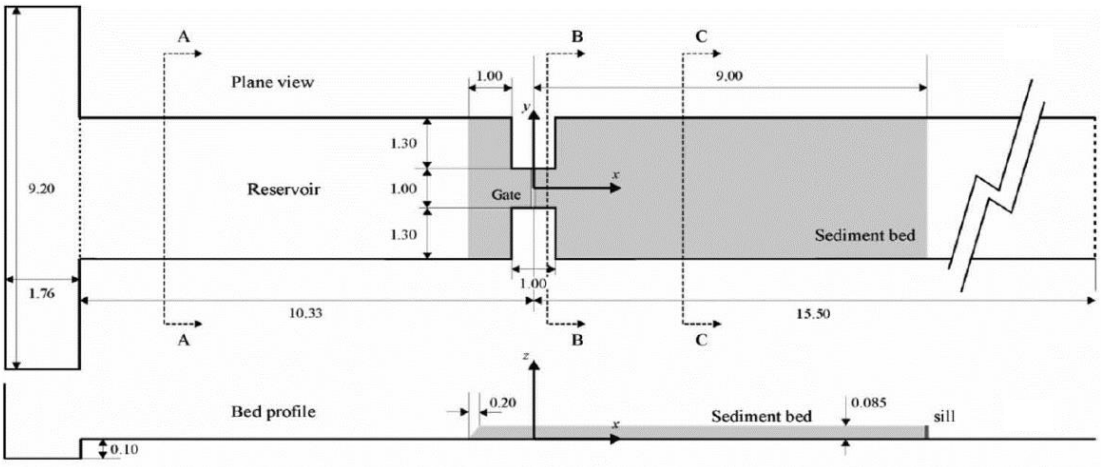

Figure 4.15 Schematization of 2D test proposed by Soares Frazão et al. 2011

4.4.3.2 Results

The measured final bed topography at the end of simulation is given in Figure 4.16. The color convention used by Soares Frazao et. al (2011) depicts blue as erosion and red as deposition. The visible scour due to erosive action can be seen immediately after the enlargement. Furthermore, the increased depositional tendency can be seen near the edges in curved portion where the color changes from yellow towards red.

When compared with measured data the numerical simulation with MPM and SMART predicted the results rather accurately, as it can be observe in Figure 4.17 and Figure 4.18, respectively. Furthermore, the tongue shape pattern is visible and can be seen both in measured and simulated data respectively, although with a different shape. This distinctive pattern ends at around 6 m downstream of the gate position. Also, it can be seen in the centre there is some anomaly where the scheme shows needle like pattern and that is missing in the actual experiment which is more visible in the MPM approach than in the SMART approach. As already discussed, the dam break simulation time was stopped at 20 seconds and for downstream boundary condition the closed wall (sill) was used. Therefore, the time was not sufficient for downstream boundary condition, and it does not have any impact on the concerned area under investigation due to back flow.

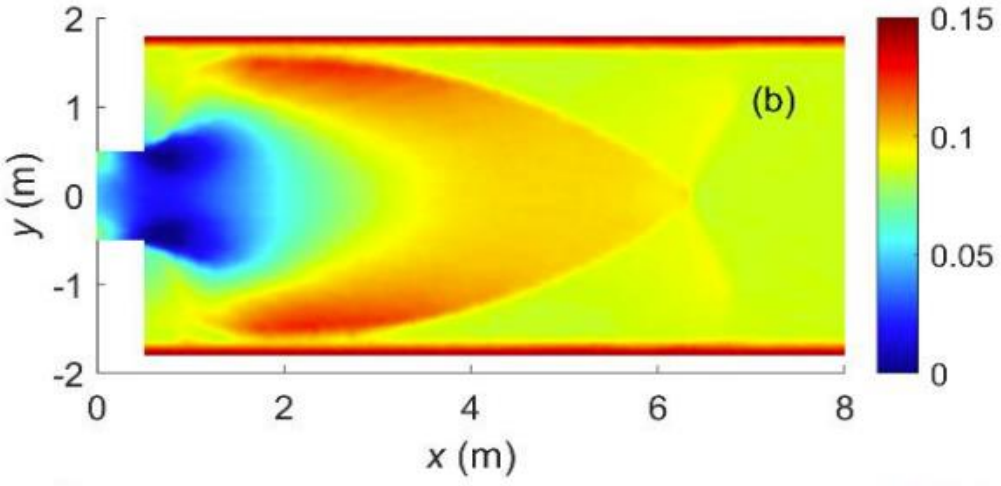

Figure 4.16 Bed level (m) measured after 20 secs using Soares Frazão et al. (2011)

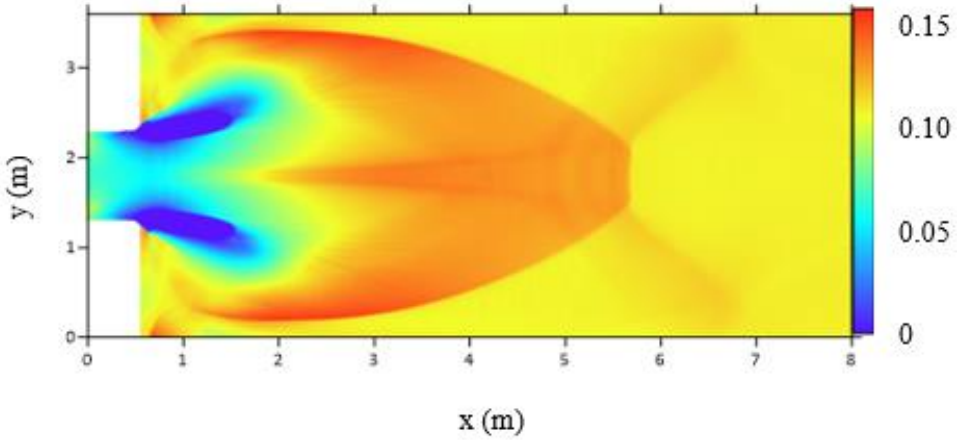

Figure 4.17 Bed level (m) measured after 20 secs using Parflood (MPM)

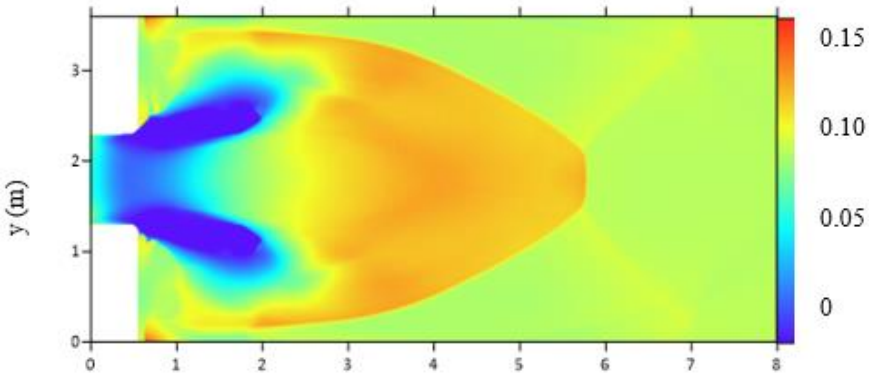

Figure 4.18 Bed level (m) measured after 20 secs using Parflood (SMART)

Figure 4.19 shows the timestep progression of the 2D Dam Break Test by Soares Frazão et al. (2011). Considering erosion, the advancement after each 4 secs is more evident in SMART approach then the MPM approach. Similarly, the curved deposition pattern around the edges is more pronounced in the SMART approach over time. While the numerical simulation effectively anticipated scouring near the dam and sediment deposition downstream, no variations were evident in the shape and extent of the deposited area, as well as in the magnitude of both scouring and deposition.

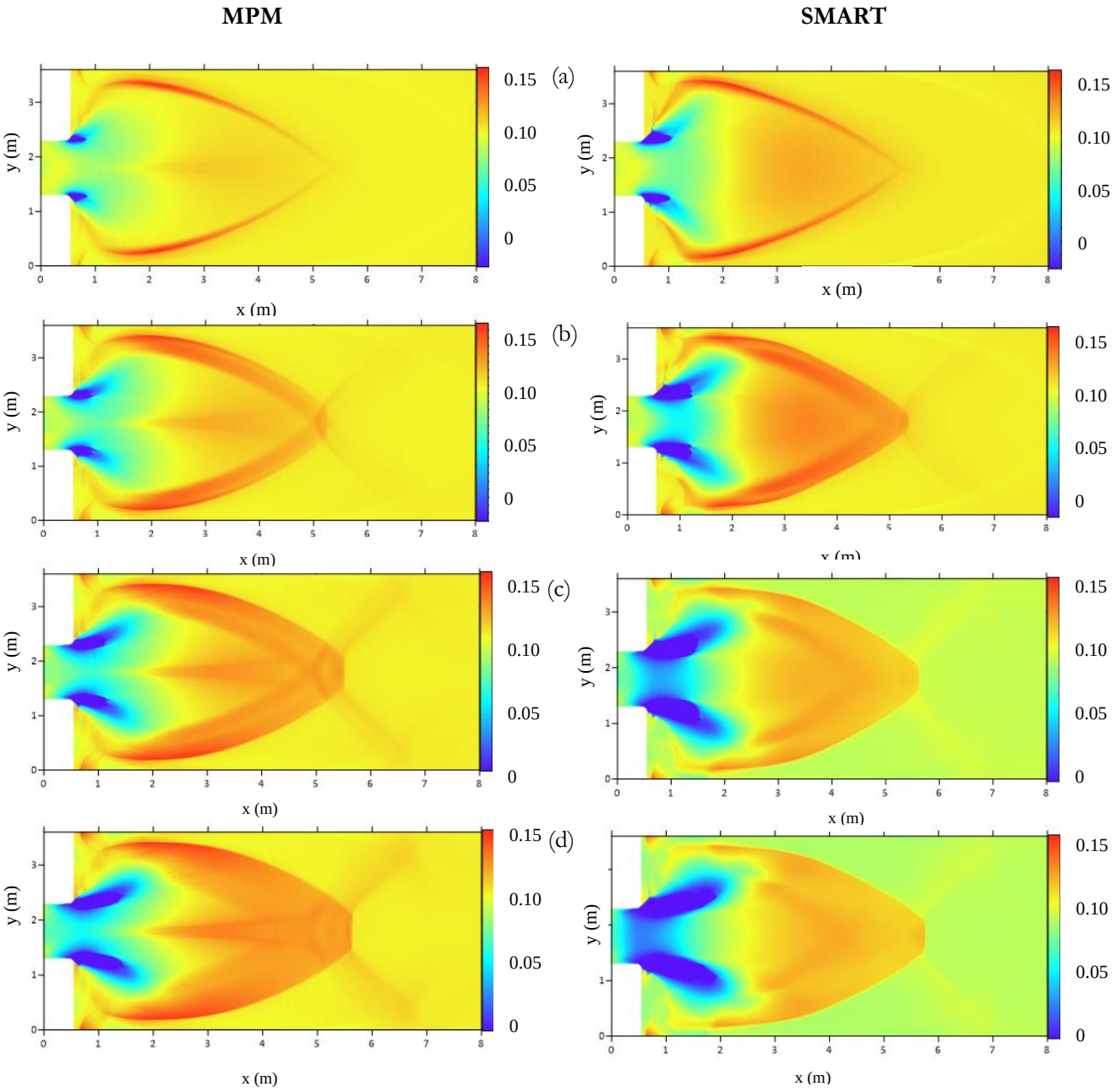

Figure 4.19 Bed evolution of sediment profiles at instants a) 4s, b) 8s, c) 12s, and d) 16s, expressed in meters.

The maximum deposits occurring in the initial part along the flume edges. These deposits subsequently formed a distinctive "W" shape until merging at both deposition fronts.

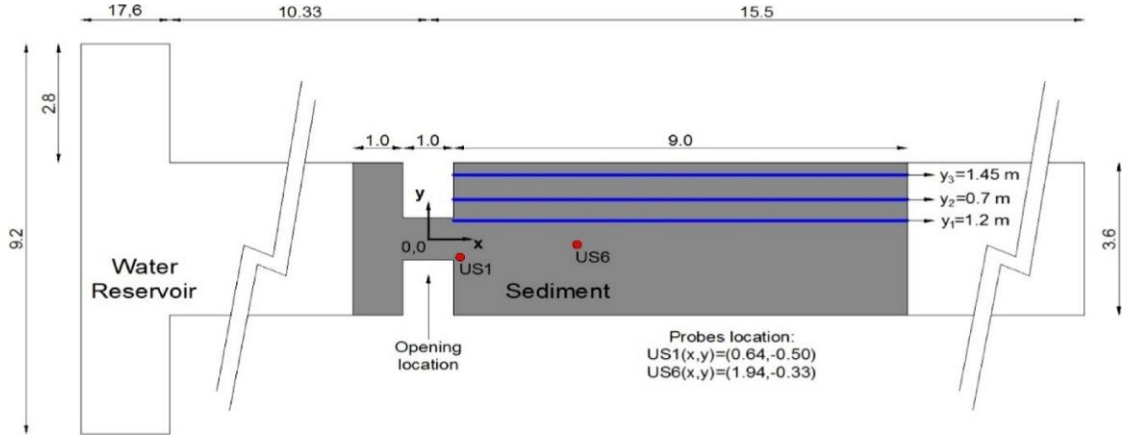

Figure 4.20 Schematics of the 2D test proposed by Soares-Frazão et al. (2011), illustrating the placement of gauges and demarcation of long sections.

Variation in bed levels were observed at three locations marked as y1, y2 and y3 as shown in Figure 4.20. All the three longitudinal profile shows good agreement in terms of comparison between the numerical simulated data and experimental data as can be seen in Figure 4.21 andFigure 4.22 respectively. The bed level changes are visible in both MPM and SMART approaches.

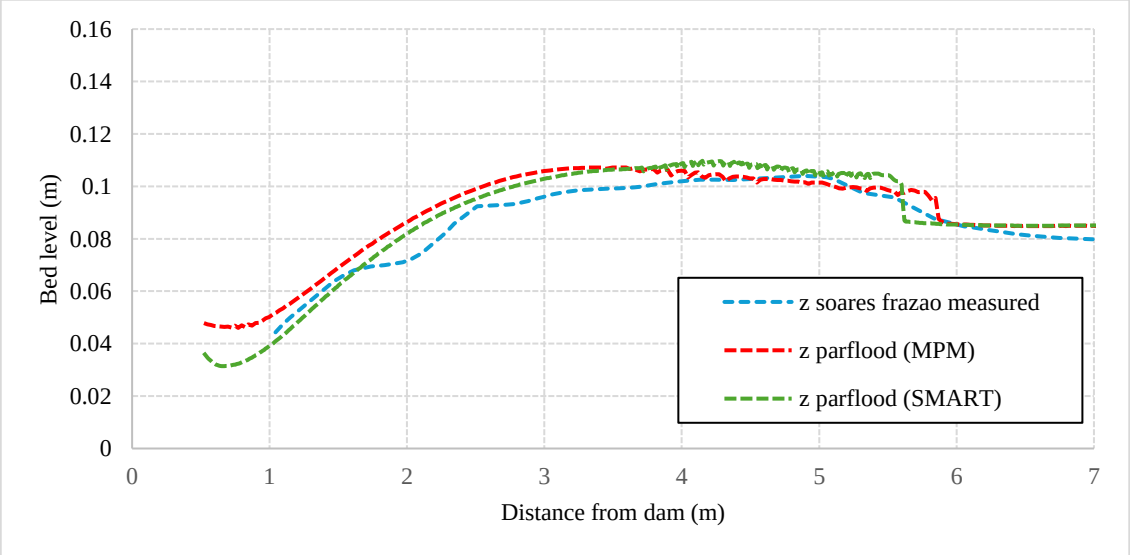

Figure 4.21 Final longitudinal bed profiles at y1=1.2m

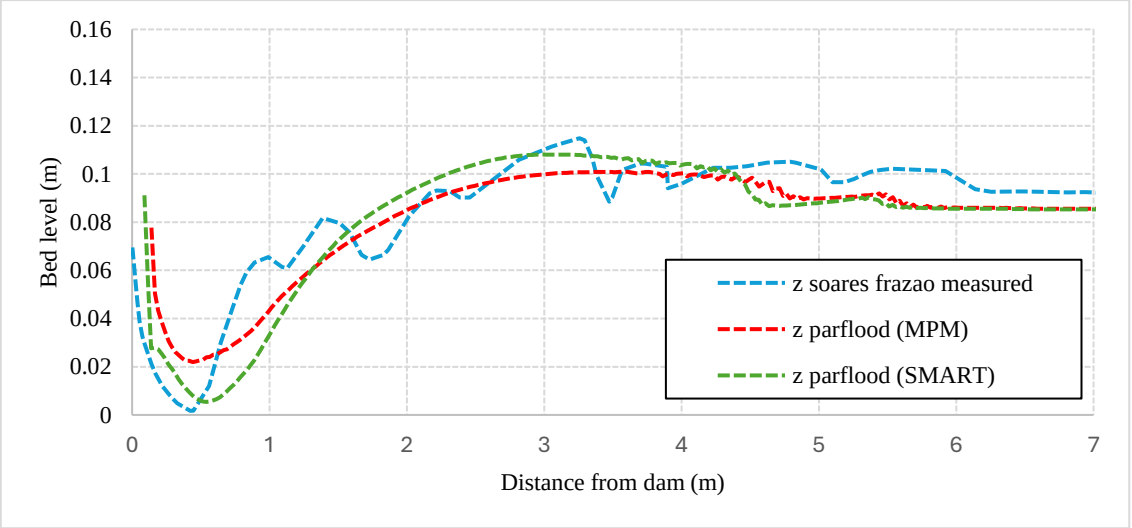

Figure 4.22 Final longitudinal bed profiles at y2=0.7m

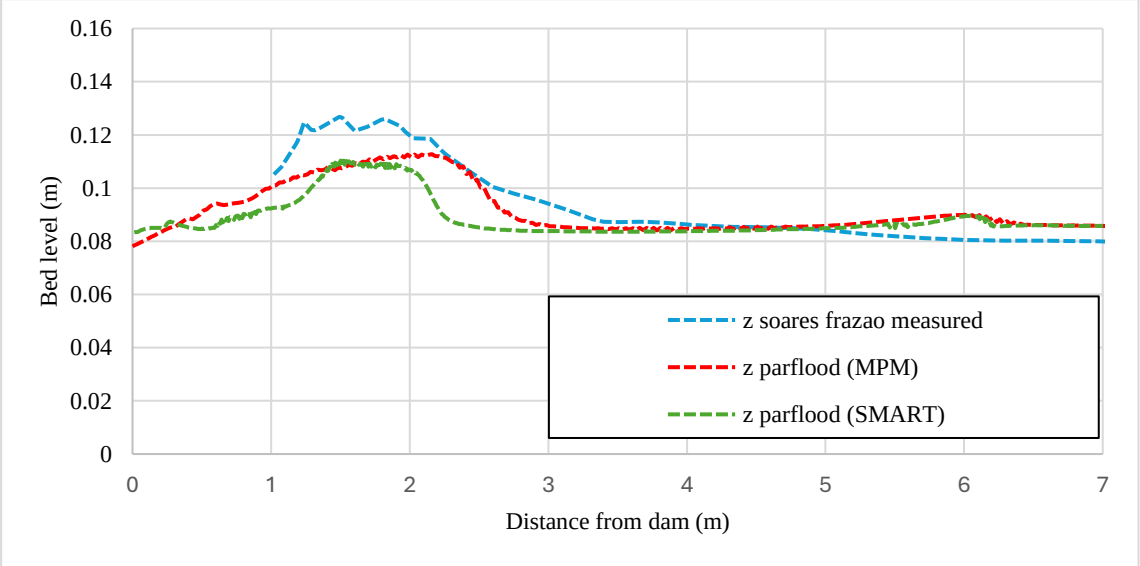

Figure 4.23 Final longitudinal bed profile at y3=1.45m

Figure 4.24 and Figure 4.25 present the water surface elevation at gauging points 1 (US1) and 6 (US6), respectively. The US1 is positioned near the dam abutment, as illustrated in Figure 4.20, while US6 is located further downstream. It is important to highlight that due to the spreading effects of waves, the impact on the area where US1 is installed within the experimental setup is more noticeable. Both runs were included from the measured data to see in comparison with SMART and MPM approach. At the US1, water surface elevation for MPM approach is more in agreement with both the experimental runs, as can be clearly seen in Figure 4.24. Similarly, for the gauge 6, the SMART approach outperforms the MPM approach for both runs. In

particular, in the first 6 seconds and last 12 seconds the SMART approach is in full agreement with the 2nd run, as it can be seen in Figure 4.25

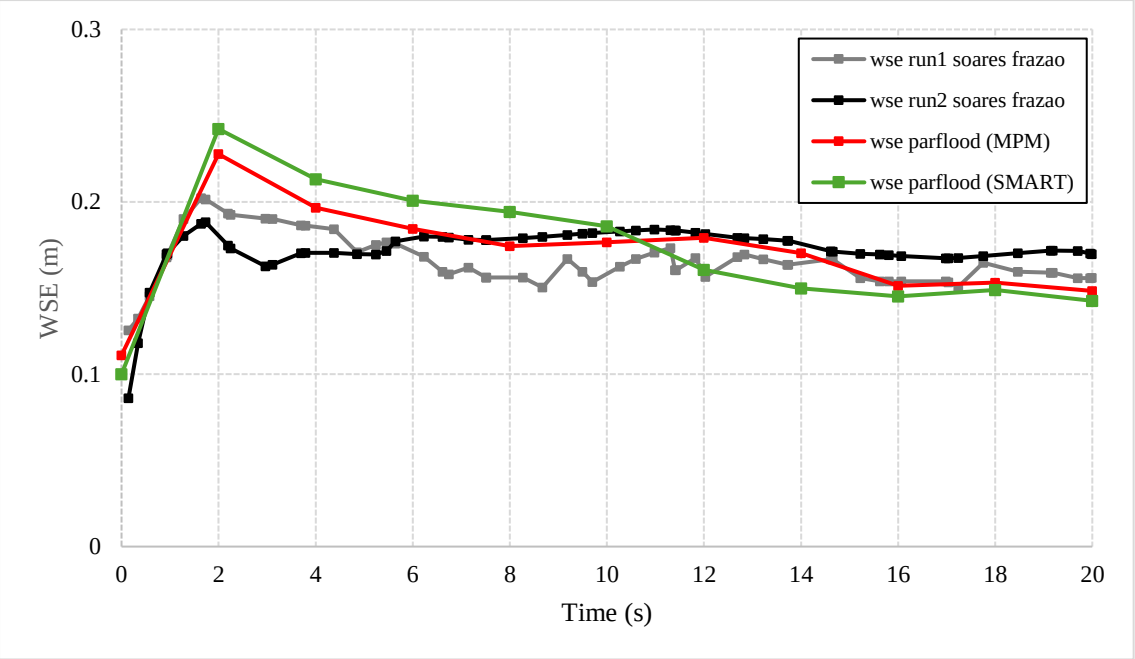

Figure 4.24 Water level comparison at US 1

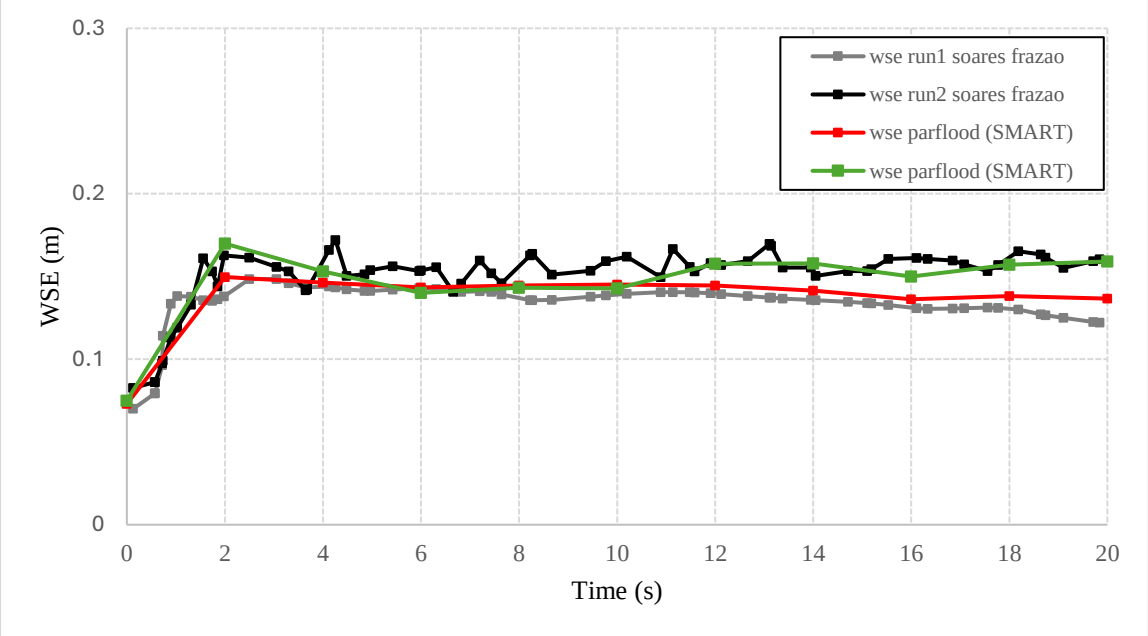

Figure 4.25 Water level comparison at US 6

4.4.4 Dam Break Flow Over Erodible Channel with a Sudden Enlargement

4.4.4.1 Experimental Setup

This study, documented by Palumbo et al. (2008), was conducted at the Université Catholique de Louvain (UCL) in Belgium and is presented in this section with numerical data. The objective is to investigate the morphological bahaviour in a two-dimensional context under specific test conditions. The experiment involved a 3-meter-long reservoir and a total channel length of 6 meters as shown in Figure 4.26. Initially, the water depth upstream was set at 0.25 meters, with a sediment layer of 0.1 meters depth fully saturating the flume. Downstream, 1 meter from the reservoir's end, a change in width was introduced, varying from 0.25 to 0.5 meters. The sediment employed was uniform coarse sand, characterized by a mean diameter of 1.65 mm, a density of 2630 kg/m3, friction angle 15^0 and a porosity of 0.42. A free outflow boundary condition was applied at the downstream outlet, while a manning coefficient of 0.0185 s·m-1/3 was established. Notably, the initial water depth at the upstream side of the dam was 0.25 m, but downstream, there was no water depth, and the condition was dry.

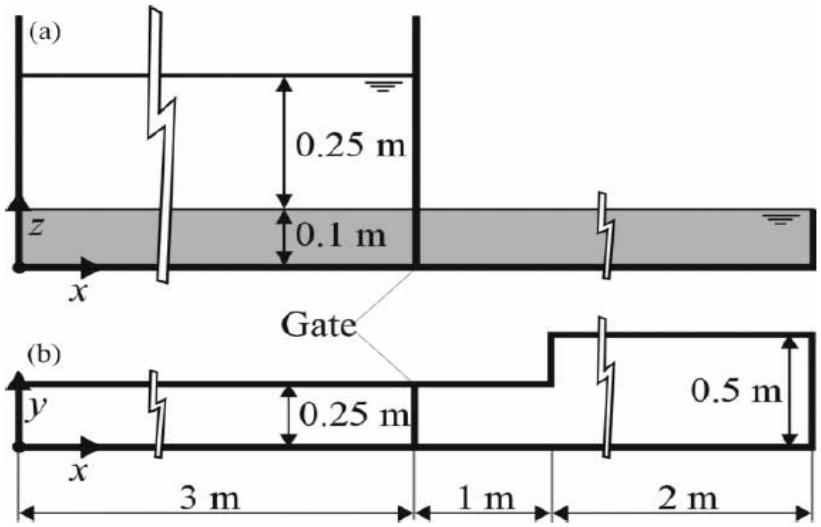

Figure 4.26 Schematic sketch of Sudden Enlargement Experiment

4.4.4.2 Results

In the 2D model simulation, a cell size of $\Delta x=\Delta y=0.025$ was utilized. Figure 4.27, Figure 4.28, and Figure 4.29 show the final bed topography as measured, simulated with Parflood MPM and with Parflood SMART approach, respectively. It is possible to notice how the erosion occurs near the corner of the expansion after 4 m and can be seen in Figure 4.27, Figure 4.28, and Figure 4.29, respectively. The eroded sediment deposits mostly occur at the expansion zone because of the nature of sudden dam-break flow. The increase in flow velocity occurs due to abrupt expansion of the area from a narrower one to wider one.

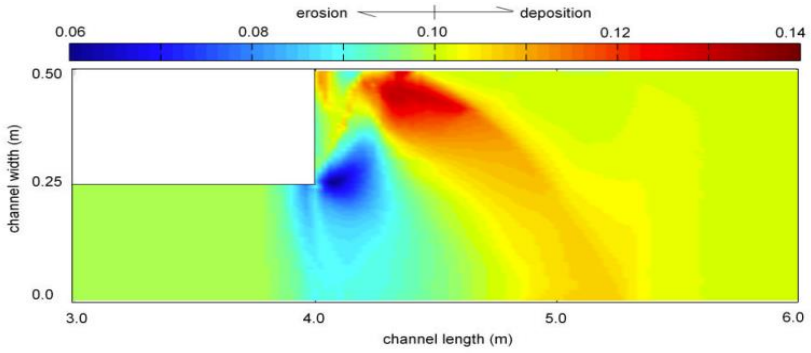

Figure 4.27 Measured final bed topography

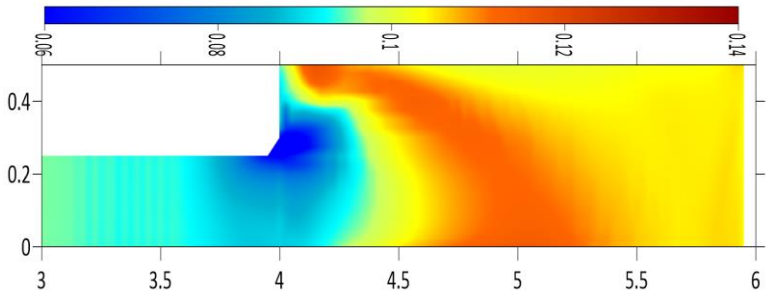

Figure 4.28 Simulated final bed topography Parflood (MPM)

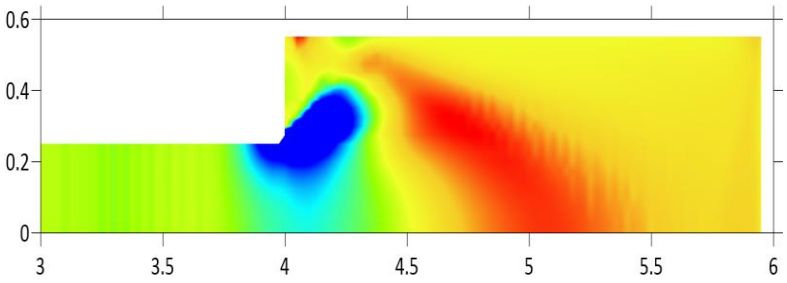

Figure 4.29 Simulated final bed topography Parflood (SMART).

The accurate simulation of sediment transport induced by dam break flow requires accounting for spatial and temporal lag effects between transport capacity and local hydrodynamic conditions. Specifically, it's crucial to understand how the movement of sediment lags changes in flow dynamics over both space and time.

Regarding the experiment involving dam-break flow in an erodible channel with a sudden enlargement, it is generally be replicated with reasonable precision. This successful replication showcases the model's adeptness in addressing the complexities of dam-break flow over a movable bed.

Figure 4.30 and Figure 4.31 show the comparisons between the predicted and observed bed level (z) profiles at two measured cross-sections, P1 (x = 4.15 m) and P2 (x = 4.3 m). At section P1 the simulated maximum

bed scouring depth slightly over-estimates the measured data with both Parflood (MPM) and Parflood (SMART) approaches. On section P2 the lateral bed profile is predicted correctly especially for the maximum bed scouring depth. Moreover, the evolution of bed shapes towards general erosion on the left side and a deposition on the right side is well reproduced at this section. Figure 4.30 and Figure 4.31 differences are due to the non-inclusion of vertical acceleration in the sediment transport model.

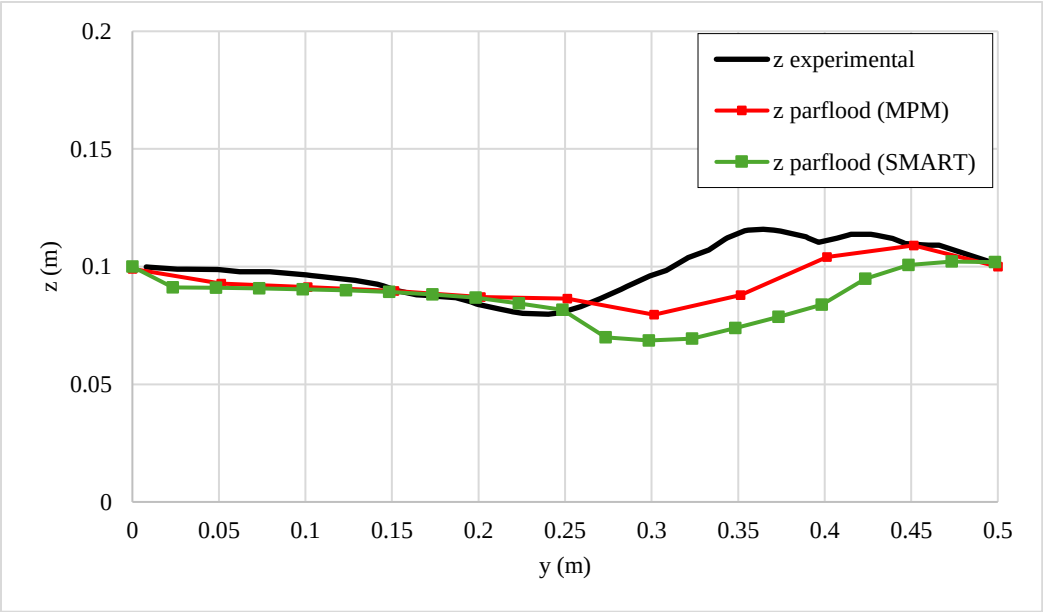

Figure 4.30 Comparison of simulated and experimental final bed profile at x=4.15

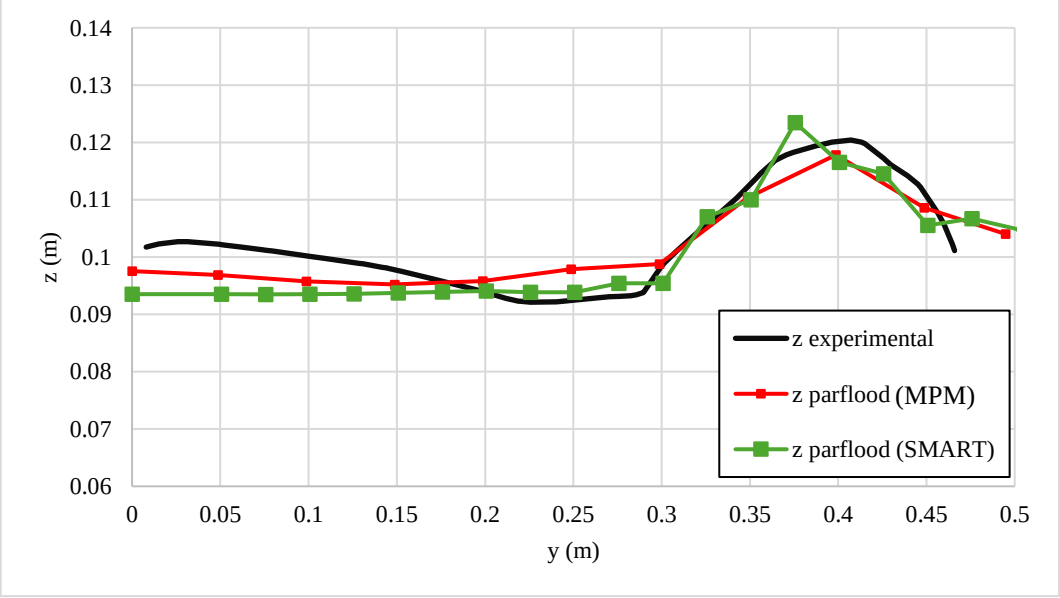

Figure 4.31 Comparison of simulated and experimental final bed profile at x=4.30

4.4.5 Benchmark Results Summary

In sections 4.4.1 to 4.4.4, the model was validated through benchmark 1D and 2D testing for both the Parflood (MPM) and Parflood (SMART) approaches. Key findings, which include precise replication of dam break scenarios, capturing hydraulic jumps, erosion, and deposition, are summarized below:

- 1D Test Cases:

1D dam break tests served as controlled experiments to explore the behaviour of water flow and sediment transport during dam breaks. In the dry bed scenario (Test A), both the SMART and MPM approaches closely matched experimental results. The numerical model accurately reproduced the front wave, and minor scour was observed. In the wet bed scenario (Test B), the hydraulic jump downstream of the bed step was well-captured by both approaches. Particularly, the wet bed scenario (Test B) results underscore the importance of considering hydraulic jumps and sediment concentration in dam break simulations. The knickpoint evolution test case aimed to understand flow transitions from subcritical to supercritical regimes. By accurately simulating morphological changes in the bed, including knickpoint propagation, the model provides valuable insights for predicting natural river and stream evolution, especially in managing river channels and mitigating erosion.

- 2D Test Cases:

In the context of 2D dam break scenario, the model accurately reproduced experimental results, specifically identifying location of erosion and deposition through both MPM and SMART approaches. For instance, visible scour due to erosive action was captured, and a tongue-shaped pattern downstream of the gate was observed. An anomaly near the centre in the MPM approach highlighted the need for further refinement. This test successfully replicated morphological behaviour in a 2D context. The model adeptly addressed 2D dam-break complexities, demonstrating its reliability by comparing predicted and observed bed level profiles. The non-inclusion of vertical acceleration in the sediment transport model informs future refinements.

Chapter 5: CASE STUDY OF BAGANZA RIVER (ITALY)

5.1 Historical Flooding Events

Baganza River is tributary of the Parma River and has recently become known due to its frequent floods (Figure 5.1 a) and significant role in sediment supply. The urgency of studying Baganza River becomes clear when we see its history of floods i.e., 2014 floods, which shaped the landscape over time. Local communities around the Baganza River, like Felino, Marzolara, and Calestano, face real challenges from these floods.

Figure 5.1 a) Flooding due to heavy rainfall on October 13, 2014, which also affected road infrastructures and settlements closest to the engraved Baganza River.b) Cassa di espansione sul torrente Baganza project capable of making the parma city safe. c) Closer look of the cassa di espansione work under progress July 2023.

While in this study the modelling approach focuses solely on the development and application of a bedload transport model for the targeted river reach, its application lays a foundation for potential future assessments regarding the impacts of infrastructure projects like a new lamination dam ("Cassa di Espansione del Baganza") (Figure 5.1 b and c) on river dynamics. This proactive approach ensures that this research lays the groundwork

for informed decision-making regarding flood resilience and sustainable river management practices in the region.

5.2 Data Preprocessing

5.2.1 Hydrodynamic

The domain for simulating the entirety of Baganza River can be seen in grey in Figure 5.4. Further, detail of which is given in Section 5.5 (Simulation Complete Domain), extending from upstream of Calestano to the Ponte Italia bridge. Similarly, the region marked in pink is designated for modelling the morphological evolution and conducting sensitivity analyses detail of which is given in Sections 5.3 and 5.4 respectively.

5.2.2 Riverbed Fixation

The purpose of riverbed fixation in the start and end of a reach is to identify regions within the domain where bedload transport cannot alter the bottom elevation. This is crucial for model stability and reliability of results. In such areas, values are assigned either as the no-data value or a value exceeding 1e10. Conversely, in the remaining portion of the domain, the model facilitates the specification of a local minimum bottom elevation, establishing a threshold below which bed erosion is prohibited. By default, the riverbed fixation assumes the entire domain is erodible, without constraints on the maximum bottom erosion. For simulation, file is created to keep the areas near the upstream and downstream boundary conditions as non-erodible, while elsewhere the riverbed can be eroded up to 3 m. This is because 3 m threshold provides realistic representation of sediment transport model while maintaining computational efficiency. For this purpose, first 1600 m and last 2000 m are fixed in the domain (randomly). In these two portions only, deposition can take place whereas no erosion is allowed, as depicted in Figure 5.2a and 5.2b, respectively.

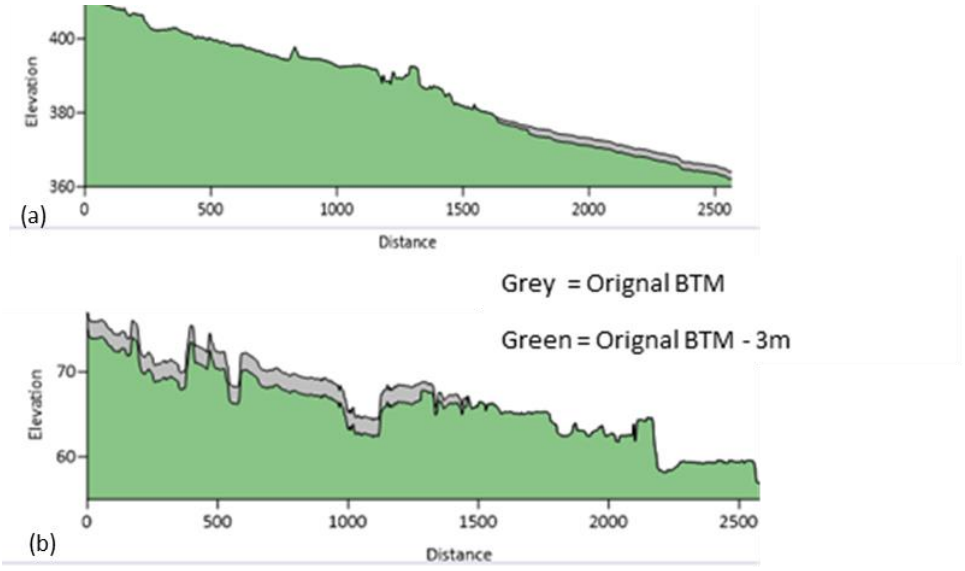

Figure 5.2 a) Upstream section near Calestano b) Downstream section near Ponte Italia bridge.

5.2.2.1 Interface between erodible and non-erodible regions

If the riverbed fixation value matches (same levels) the bathymetry value in certain parts of the domain, only sediment deposition occurs in those cells, with no erosion permitted as discussed in section 5.2.2. This is particularly beneficial near open boundary conditions to prevent significant modifications that could lead to model instability as discussed already in section 5.2.2. Conversely, when fixed bed contains no data values, neither erosion nor deposition occurs locally. This can be advantageous outside the river region, where sediment transport is typically not simulated.

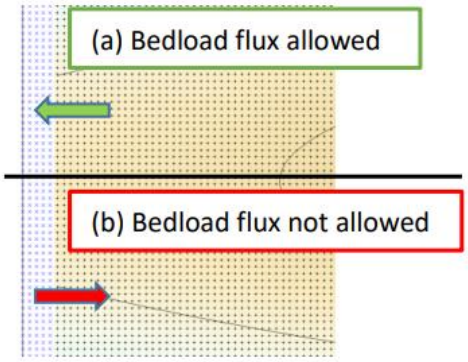

Figure 5.3 Example of .FXB no data values near the left border of the grid (blue crosses), and actual values elsewhere (e.g. 3m below the initial .BTM)

5.2.3 Spatial Distribution of D50 Raster

Bed-material from the entire reach affects bedload transport. As first attempt, using the reach averaged bed-material size distribution for bedload transport modelling within a given cross-section seemed appropriate. For this reason, the spatial distribution using D50 raster file was produced. It is also a raster map (with same size of bathymetry and roughness map) that contains the spatial distribution of mean grain size, based on available information from the field as detailed in Chapter 3:. The distribution is assumed constant in time, e.g. it is assumed that the bedload transport does not modify the grain size distribution in the domain. If the D50 file is absent, the default condition is that a constant value can be used in the whole domain. The average value is used to estimate the sediment flux at the interface. The description of the D50 values used for simulation purpose is shown in Figure 5.5.

5.2.4 Bed Material

The bed material file serves as a vital repository of bed material parameters and additional parameters. This file contains information related to both MPM and SMART approaches. It also contains shield's criterion for incipient motion. It is imperative to note that a small variability of the D90/D30 ratio ranging from 3.5 to 5.7 (with an average of 4.43) has been observed. Considering this variability and its influence in the SMART approach where the parameter (D90/D30) is raised to the power of 0.2. As shown in Equation 4.7, resultant values range from 1.28 to 1.41 (averaging 1.34). Thus, adopting a constant average value instead of spatially

variable values may lead to a maximum 5% difference in sediment discharge, which, given the several uncertainties, remains within an acceptable range.

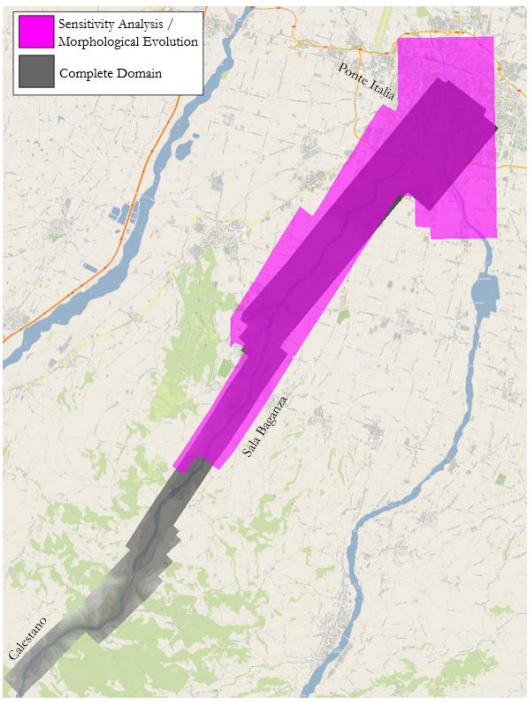

Figure 5.4 Bathymetry of Baganza River utilized for simulation purposes.

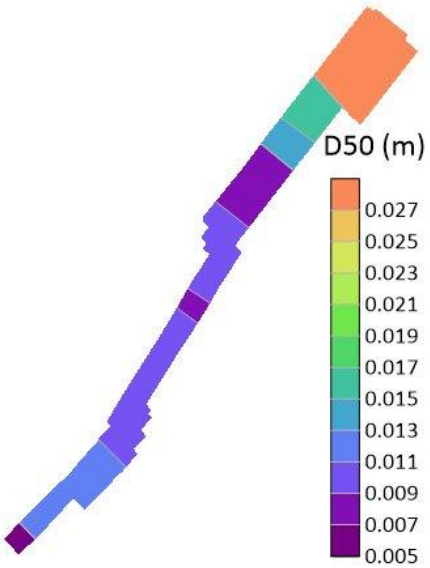

Figure 5.5 spatial distribution of the D50 value, based on available information from the field data.

5.3 Modelling Morphological Evolution: 2008-2014 Flooding Period

In this section, the sediment transport model simulates the morphological evolution of a specific stretch of the Baganza River, shown in pink in Figure 5.4. It is worth noting that the pre-flood DTM from 2008 shares the same resolution as the post-flood DTM conducted after the 2014 flood i.e. (4 m x 4m). The 2008 DTM border is just upstream of Sala Baganza, resulting in a visible overlap of approximately 50% with 2014 DTM. It is pertinent to highlight that in this part the focus is on modelling the series of floods occurring between 2008 and 2014. The most significant flooding events within the 2008-2014 timeframe on the Baganza River were identified. Subsequently, discharge hydrographs were computed for these events and arranged in series as shown in Figure 5.6, which spans total of 450 hours of simulation. The simulation focus is primarily on high flow conditions summarising flood events during 2008-2014 period. However, it is essential to recognize that. in reality rivers also experience non-flood conditions, which play a significant role. For instance, vegetation growth in the riverbed and sedimentation of fine material altering morphology. The hydrograph serves as the inflow boundary condition for the simulations. For downstream boundary condition, a constant water level is applied just upstream of Ponte Italia bridge on Parma River (confluence point of Baganza River and Parma River).

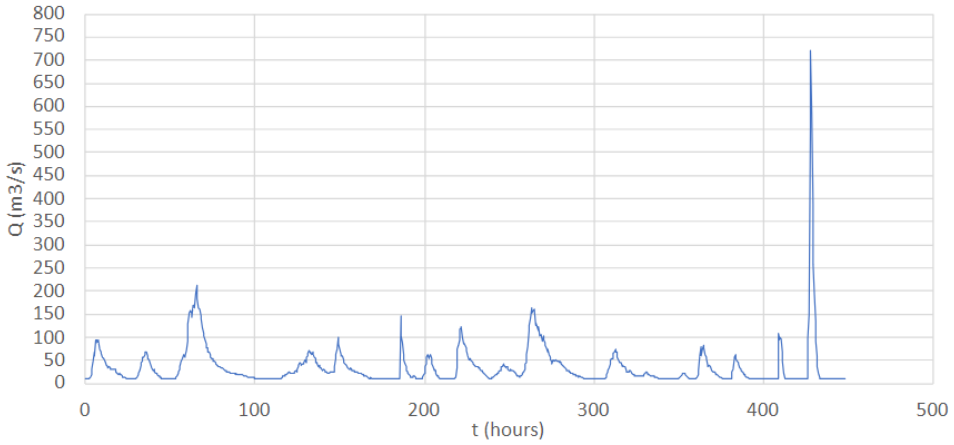

Figure 5.6 Hydrograph used as upstream boundary condition for 2008-2014 flooding case.

5.3.1 Results

Analysis of the simulated results for the morphological evolution during the 2008-2014 flooding period involved dividing the domain into upstream, middle, and downstream sections based on more focused analysis of localised changes in bed elevation and sediment erosion, deposition patterns. This segmentation provides valuable insights into the spatial distribution of morphological evolution over the studied period. The stretch starting just upstream of Sala Baganza as shown in Figure 5.7. Comparisons between the riverbed topography resulting from numerical simulation, based on 2008 DTM and the measured 2014 DTM were conducted see Table 5.1. Changes

in the bed elevation were assessed, and the maps illustrating the intensity of net erosion and deposition were generated for each of the three river sections.

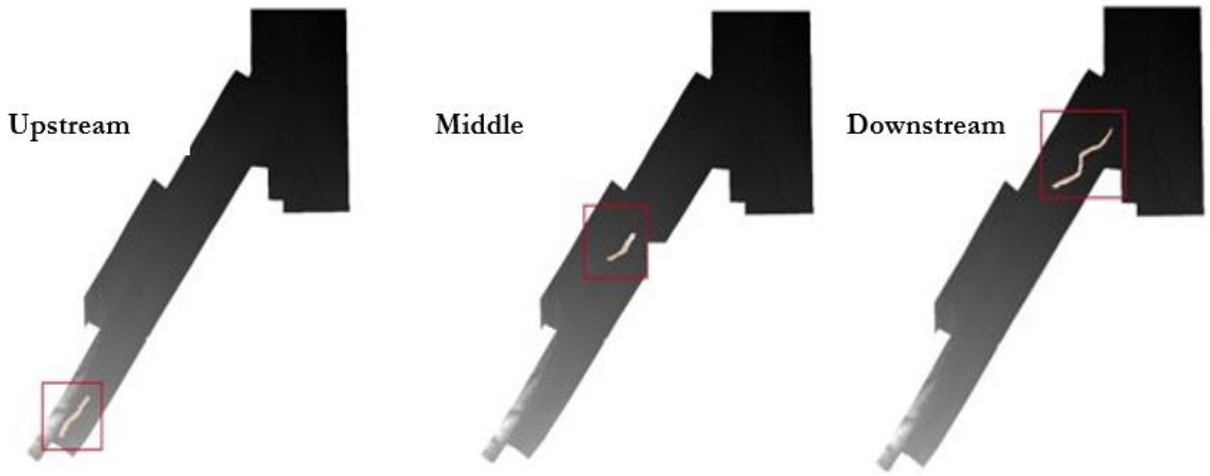

Figure 5.7 Reach segementation highlighted by upstream, middle, and downstream portion for analysis.

Table 5.1 Comparative analysis of observed and simulated changes in elevation

Raster	Description	Purpose
Raster 1	2014 DTM - 2008 DTM	Represents observed changes in elevation from 2008 to 2014
Raster 2	Simulation MPM - 2008 DTM	Represents simulated changes in elevation by MPM approach relative to 2008 DTM
Raster 3	Simulation SMART - 2008 DTM	Represents simulated changes in elevation by SMART approach relative to 2008 DTM

It is pertinent to mention here that by comparing the observed changes in elevation (Raster 1) with the simulated changes obtained from both the MPM and SMART approaches (Rasters 2 and 3, respectively), this study provides a comprehensive assessment of the performance of these sediment transport models.

In Figure 5.8 the net riverbed elevation changes Δz (m) expressed in terms of differences, showing erosion in orange and deposition in blue. In the first part of upstream stretch the Raster 1 based on measured results agrees with the simulated results of Raster 2 and 3, respectively, particularly near the left and right banks. However, in the middle portion the Raster 1 shows the erosional trend whereas the Raster 2 and 3 shows more depositional trend, this is because of the complexity of river braidedness in this portion and more natural variation in the riverbed topography at the local scale.

Figure 5.9 shows box plot showing the elevation change in (m) for upstream reach. In this Raster 1 is in good agreement with Raster 3. The mean value for both passes through centre meaning the net difference of erosion and deposition is zero. Whereas for Raster 2 this value is slightly at 0.2 m meaning the MPM simulation depicted that overall, this portion is in aggradation.

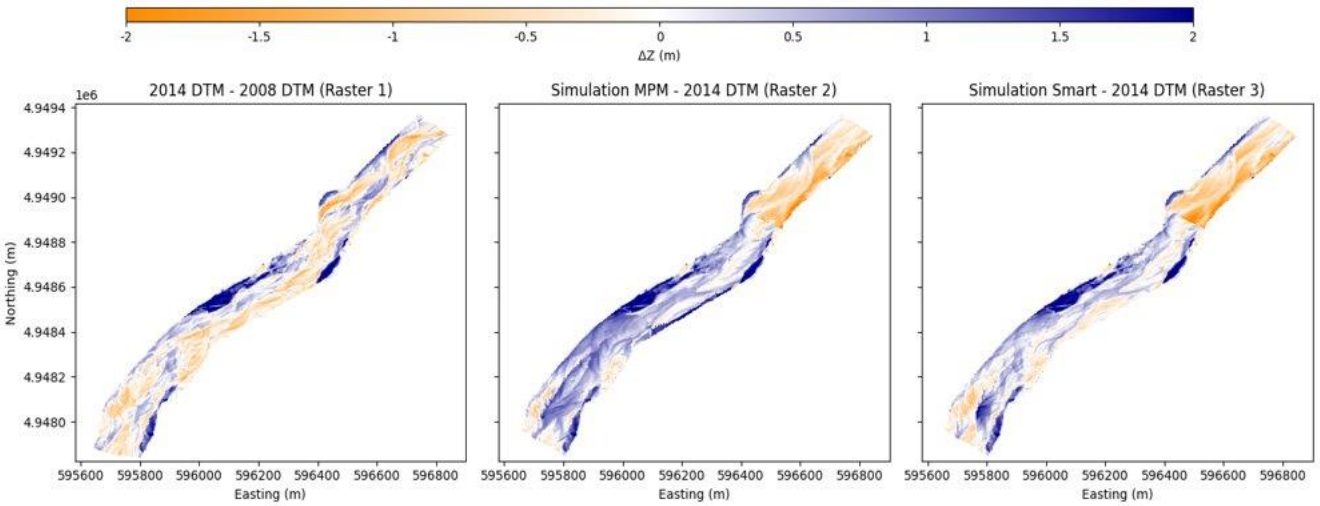

Figure 5.8 Results morphological modelling upstream reach.

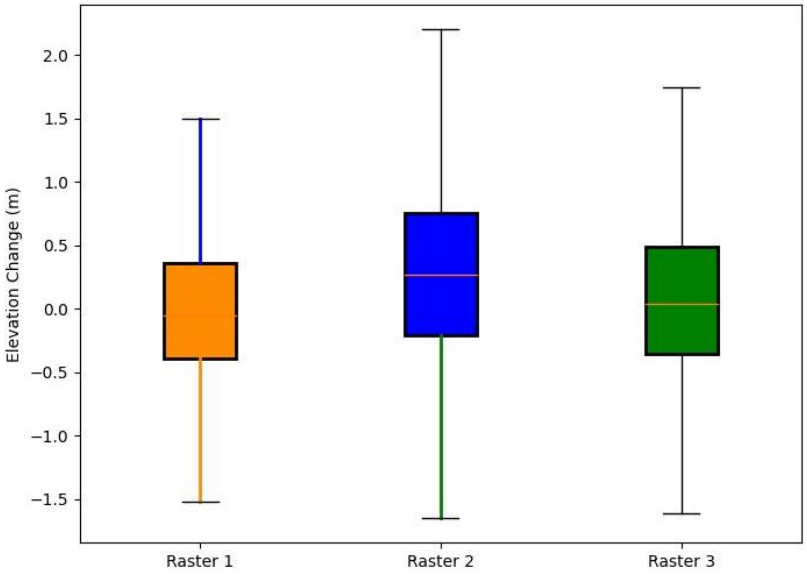

Figure 5.9 Box plot showing elevation change in upstream reach.

Figure 5.10 depicts the insights into the distribution of changes in elevation within the upstream reach. The distribution for Raster 1 and Raster 3 shown in orange and green color is evenly distributed around -2 m to 2 m whereas the Raster 2 is also within this range, but the distribution is slightly skewed to right side showing the depositional trend prediction by MPM simulation.

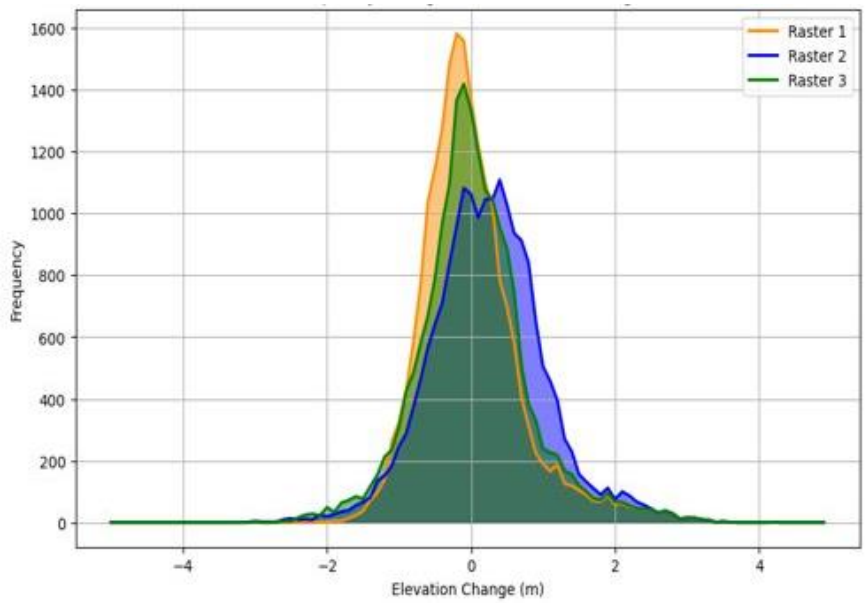

Figure 5.10 Frequency histogram showing distribution of elevation change for upstream area.

Contrary to the upstream reach, the middle reach as shown in Figure 5.11 shows both Raster 2 and Raster 3 are in good agreement with Raster 1. The centre portion of the middle reach is dominated by erosion that extends to the left bank on the lower side. On the downstream side more blues shows the deposition near the left bank that extends to the canter where the intensity of deposition is less as compared to bank. During the simulation the model remain stable, and no issue were reported. Furthermore, in the graphical representation some of the places are white in color that shows area where no sediment transport occurs hence the change in the bed elevation zero. Figure 5.12 shows box plot for dataset presents in the middle reach. Here it can be seen that again SMART outperforms the MPM as Raster 3 agrees with Raster 1 similar to previous case. Even though the 2D maps were showing that Raster 2 and Raster 3 are in agreement with Raster 1 but the detail investigation using box plot and frequency chart distribution as shown in Figure 5.13 shows otherwise. Therefore, only relying on the 2D maps can be an issue hence always supported through statistical analysis can be a good idea to check the hypothesis is correct or not.

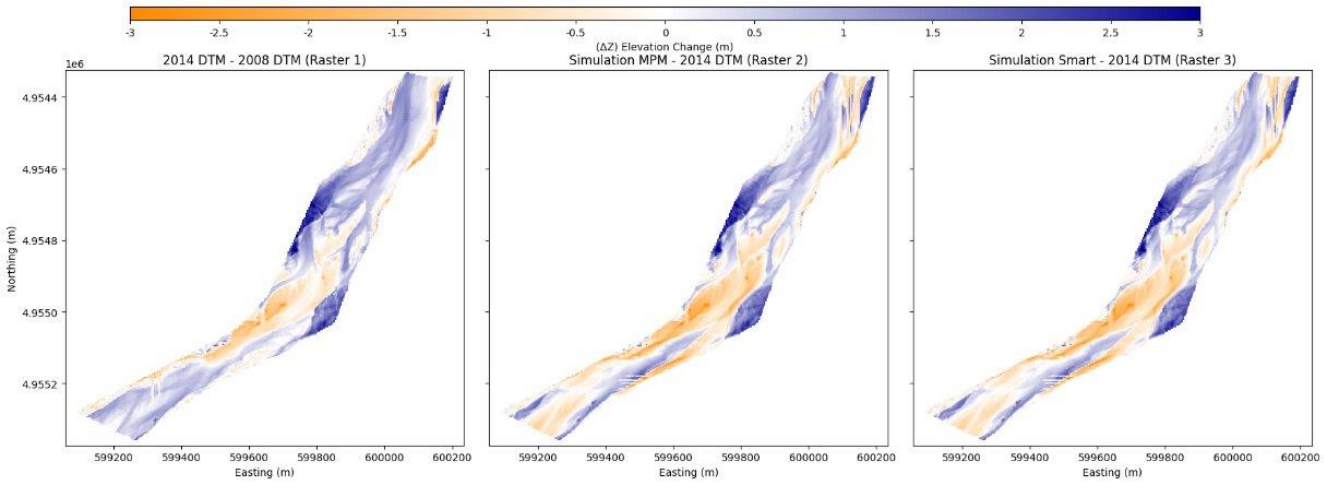

Figure 5.11 Results morphological modelling middle reach.

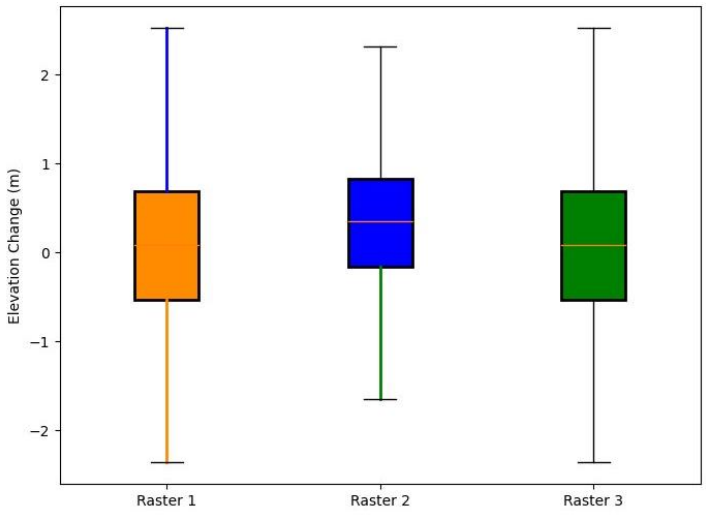

Figure 5.12 Box plot showing the elevation change in middle reach

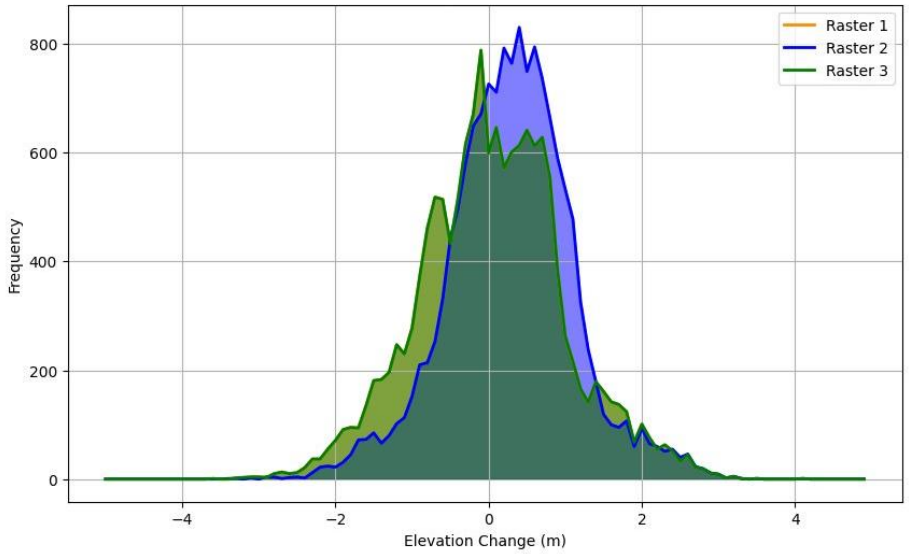

Figure 5.13 Frequency histogram of elevation change for middle area

In the downstream reach again Raster 3 is in more agreement with Raster 1 as compared to Raster 2 specially in the middle portion where the deposition is prominent in Raster 2 in contrast to Raster 3 and 1 where both deposition and erosion are visible (Figure 5.14, Figure 5.15 and Figure 5.16).

Overall, in all the segments depositional trend is prominent by SMART and MPM. Whereas, SMART outperforms MPM when comparison is made of numerical results with the measured one. The box plots show that for all the three sections the upper and lower whiskers vary between +2 m and –2 m. The median quartile for all sections for raster 1 and 3 (Measured and SMART) is almost zero whereas the median quartile for the MPM is positive in all the MPM simulations.

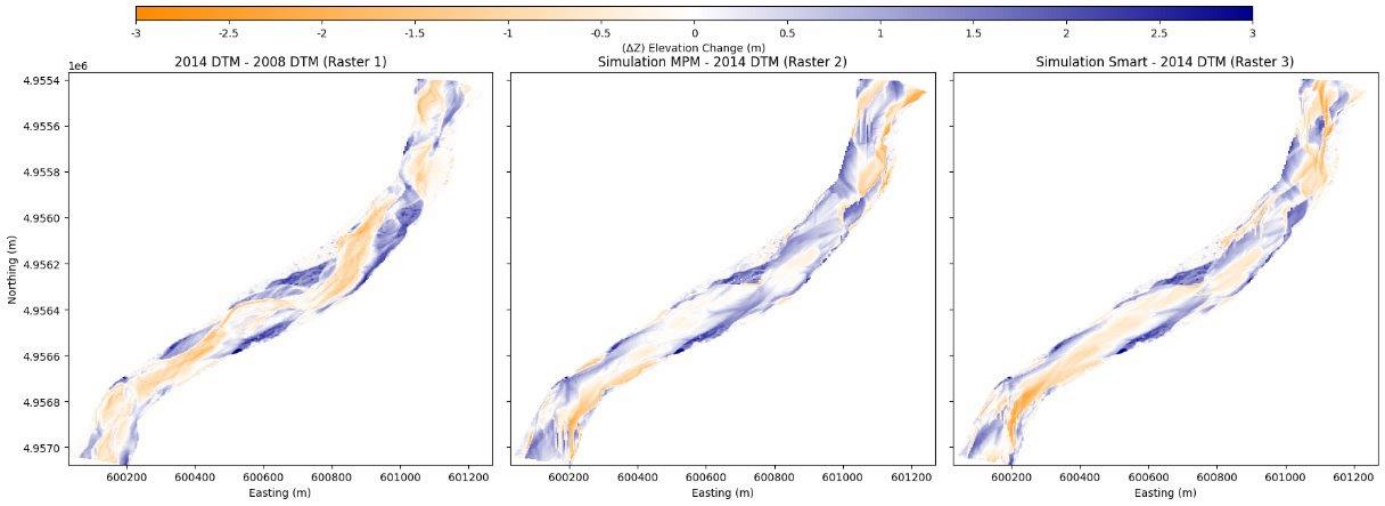

Figure 5.14 Results morphological modelling downstream reach.

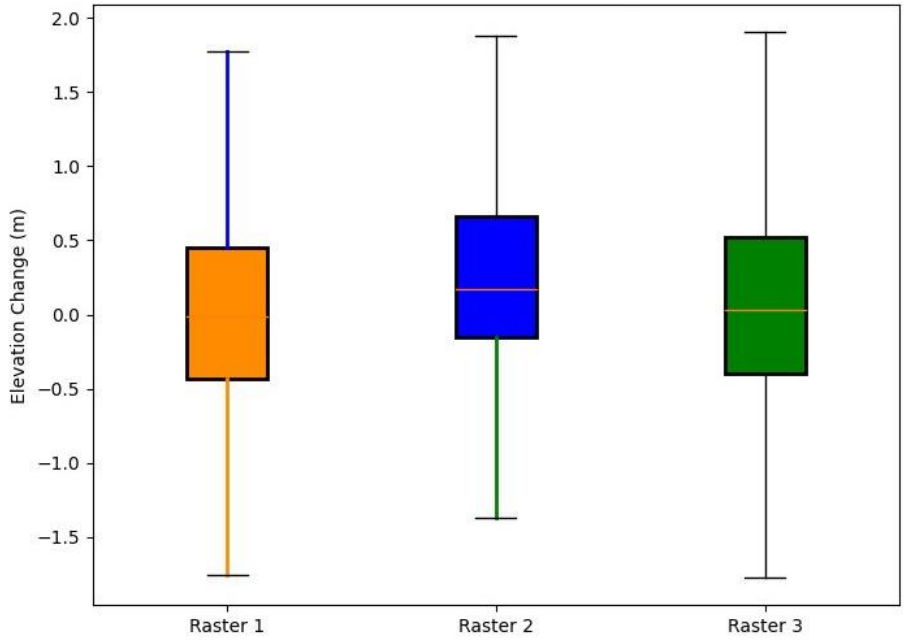

Figure 5.15 Box plot showing the elevation change in downstream reach

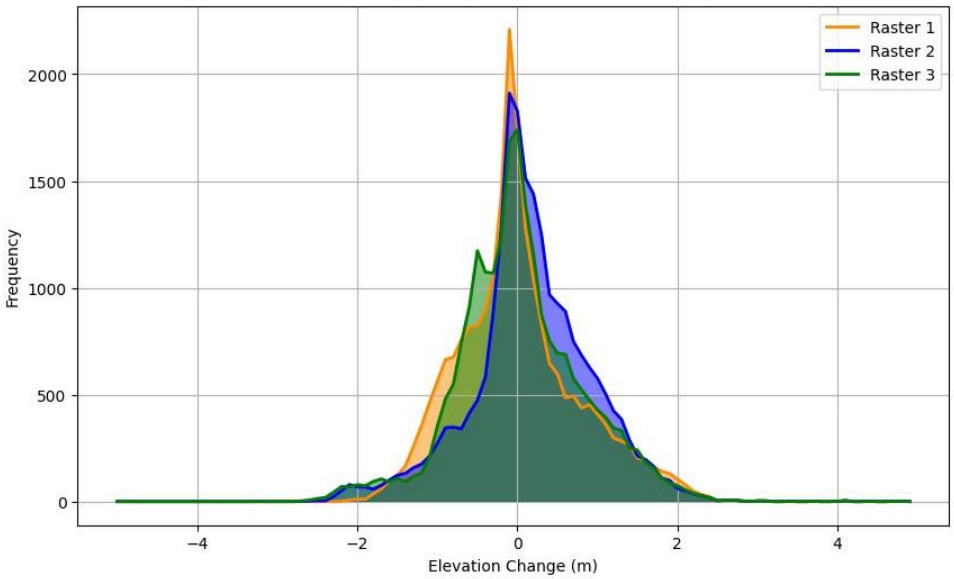

Figure 5.16 Frequency histogram of elevation change for downstream reach

5.4 Model Sensitivity Analysis

The sensitivity analysis plays a pivotal role in morphodynamic modelling. In this section, the aim is not only to validate bedload model and check it's reliability but also to assess the significance of each parameters i.e.

mean grain size (D50) and roughness (n). The analysis encompasses 14 simulations across three different cases. Furthermore, morphodynamic models, like the one employed in this study, are constructed based on a set of input parameters, often derived from measurements or empirical data. Sensitivity analysis serves as a powerful tool to quantify the uncertainty in model predictions stemming from uncertainties in these input parameters. This quantification of uncertainty is essential for characterizing the reliability of model forecasts. In this study, a comprehensive sensitivity analysis is performed to address the above critical aspects.

The analysis was structured around three distinct cases, each designed to investigate the influence of specific parameters while holding others constant. D50 grain size represents the median particle in the sediment size distribution, making it a critical factor in sediment transport modelling. The D50 particle size raster map of the Baganza River is obtained from combining field sampling and photogrammetry technique. In MPM approach, the only grain size used is D50 whereas SMART technique requires a different parameter i.e., D90/D30 ratio discussed already in section 5.2.4. The roughness parameter (n value) is computed based on grain size only (i.e., neglecting bedforms, vegetation, etc.) using empirical formula given in Equation 5.1

$$n = \frac{\mathrm{d}^{\frac{1}{6}}}{26} \qquad 5.1$$

MPM whereas d = D90 in this empirical equation. Throughout all the simulations where D50 is changed, n value remains constant, i.e., 0.025. In case 1, eight simulations were performed, four utilizing the MPM approach and four using the SMART approach. In four simulations, the values of particle equivalent diameter were increased by 20% and 10%, instead, in the remaining four simulations, those values were decreased by 20% and 10%. In case 2, a total of two simulations were performed and in third case four simulations were conducted, two employing the MPM approach and two using the SMART approach. In these simulations, n value is adjusted by 20% and 10%, resulting in n values of 0.03 and 0.02. The D50 value remained constant in these simulations. In case 3, the objective was to understand the influence of varying n values on the model's accuracy and the significance of n in representing real sediment transport dynamics. Summary of cases and relevant changes in input parameters are listed in Table 5.2

Table 5.2 Data showing summary for sensitivity analysis.

Sim	Case No.	Approach	D50 (m)	D90/D30	n
1	1	MPM	+20 %	-	0.025
2	1		+10 %	-	0.025
3	2		Constant	-	0.025
4	3		Constant	-	+20 %
5	3		Constant	-	-20 %
6	1		-10 %	-	0.025
7	1		-20%	-	0.025
8	1	SMART	20 %	4.43	0.025
9	1		10 %	4.43	0.025
10	2		Constant	+20 %	0.025
11	3		Constant	4.43	+20 %
12	3		Constant	4.43	-20 %
13	1		-10 %	4.43	0.025
14	1		-20 %	4.43	0.025

5.4.1 Results and Discussion

The analysis encompassed three distinct cases, each exploring the model's response to a specific input parameters (while holding others constant). The investigation involved modifications to the input parameters across six designated sub-reaches, excluding the reaches close to upstream and downstream boundary conditions termed as fixed bed. The simulations were conducted using both MPM and SMART approaches. Details on the performed analyses will be given in the following.

A comparison between the 2014 Digital Terrain Model (DTM) also referred to as measured DTM and the original 2008 DTM, which is also used as starting bathymetries for running the simulation, revealed variations in sediment dynamics. Simulated raster differences (MPM-2008 BTM and SMART-2008 BTM) are in agreement with measured differences (2014 DTM – 2008 DTM). The results of different simulations of the sensitivity analysis will be expressed by using these differences and using appropriate box plots.

The box plots expressed the distance between medians as a percentage of visible spread as shown in Figure 5.17. Generally, a value less than 10% or approaching zero indicated a strong similarity between measured and

simulation results, signifying good model performance. Conversely, higher percentages, even greater than 20%, indicated significant deviations between simulated and measured data.

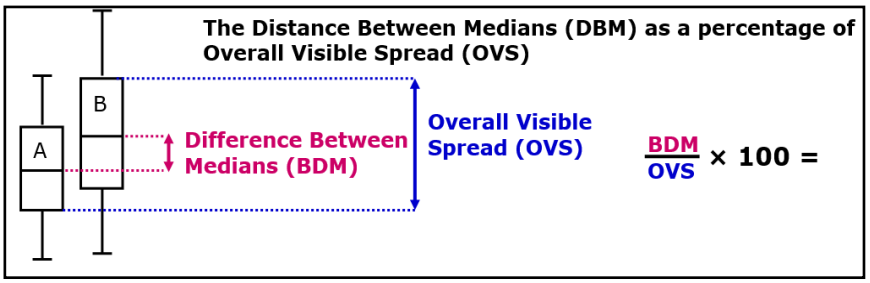

Figure 5.17 Difference between medians as a percentage of overall visible spread.

The frequency distribution plots provide insights into the distribution patterns of elevation changes across simulation scenarios, offering an overview of variation trends.

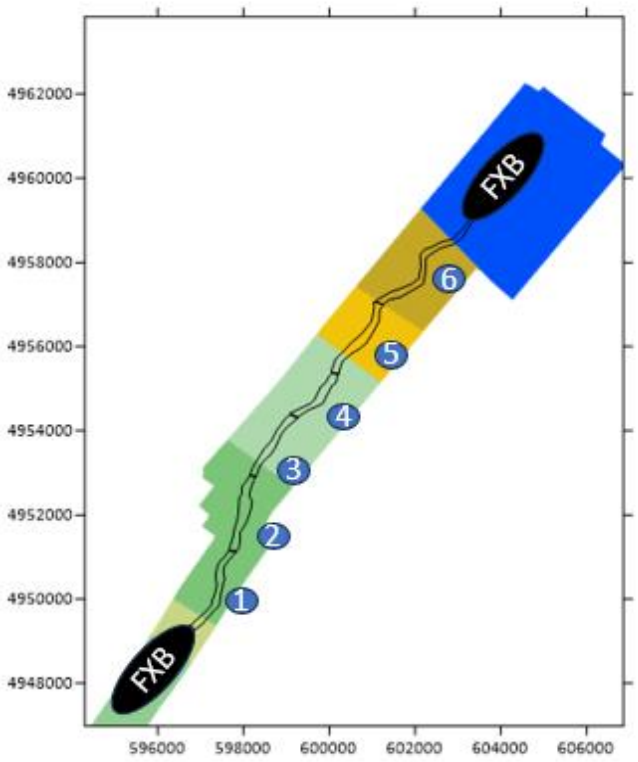

Figure 5.18 Spatial distribution of analysed Sub-reaches used in the sensitivity analysis.

Figure 5.18 illustrates the spatial layout of the study area, highlighting the six designated sub-reaches and the two fixed bed reaches positioned close to the upstream and downstream boundary conditions. The six reaches (labelled 1 to 6) were subjected to detailed analysis, while the two fixed bed reaches near the boundary

conditions were excluded from the analyses, to avoid bias in the result. The findings from each visualization provides nuanced insight into the model's responsiveness to changes in input parameters across different simulation scenarios. The study comprehensively captures the model's sensitivity to varying input parameter. However, the detail for only one case is provided for the sake of brevity.

- **20 % Increase in D50**

In analysing the impact of a 20% increase in median of the mean grain size (D50) on sediment dynamics within sub reach 1 of 6, significant insights emerged from the comparison between the 2014 measured Digital Terrain Model (DTM) and the original 2008 DTM, which is used as the initial bathymetry for simulations in both MPM and SMART approaches. Notably, both approaches showcased a dominance of deposition in the upstream section of the sub reach.

Interestingly, the comparison between 2014 DTM and 2008 DTM, indicative of actual measured differences in bathymetry, revealed erosion along the riverbanks and deposition in the first half of the sub reach. Consistent trends of bank erosion and in-channel deposition were observed in the latter half of reach 1, corroborating well with the differenced measured bathymetry. Furthermore, employing box plots to depict the differences between medians as a percentage of the visible spread, highlighted different patterns. In this context, the MPM approach exhibited a higher ratio of 25.04, while the SMART approach displayed a relatively lower ratio of 16.63 for reach 1 as shown in Figure 5.19 . In reach 2, the model accurately replicated the braided dynamics characterizing the riverbed. Both the MPM and SMART methodologies demonstrated a rather good accuracy in predicting changes, mirroring the braided pattern of the dominant flow.

The comparison between Raster 2 and Raster 3 highlighted a robust agreement, affirming the reliability of both approaches in this specific area. Notably, the models effectively identified upstream bank erosion. However, small differences emerged when examining the measured bathymetric changes in the Raster 1 data.

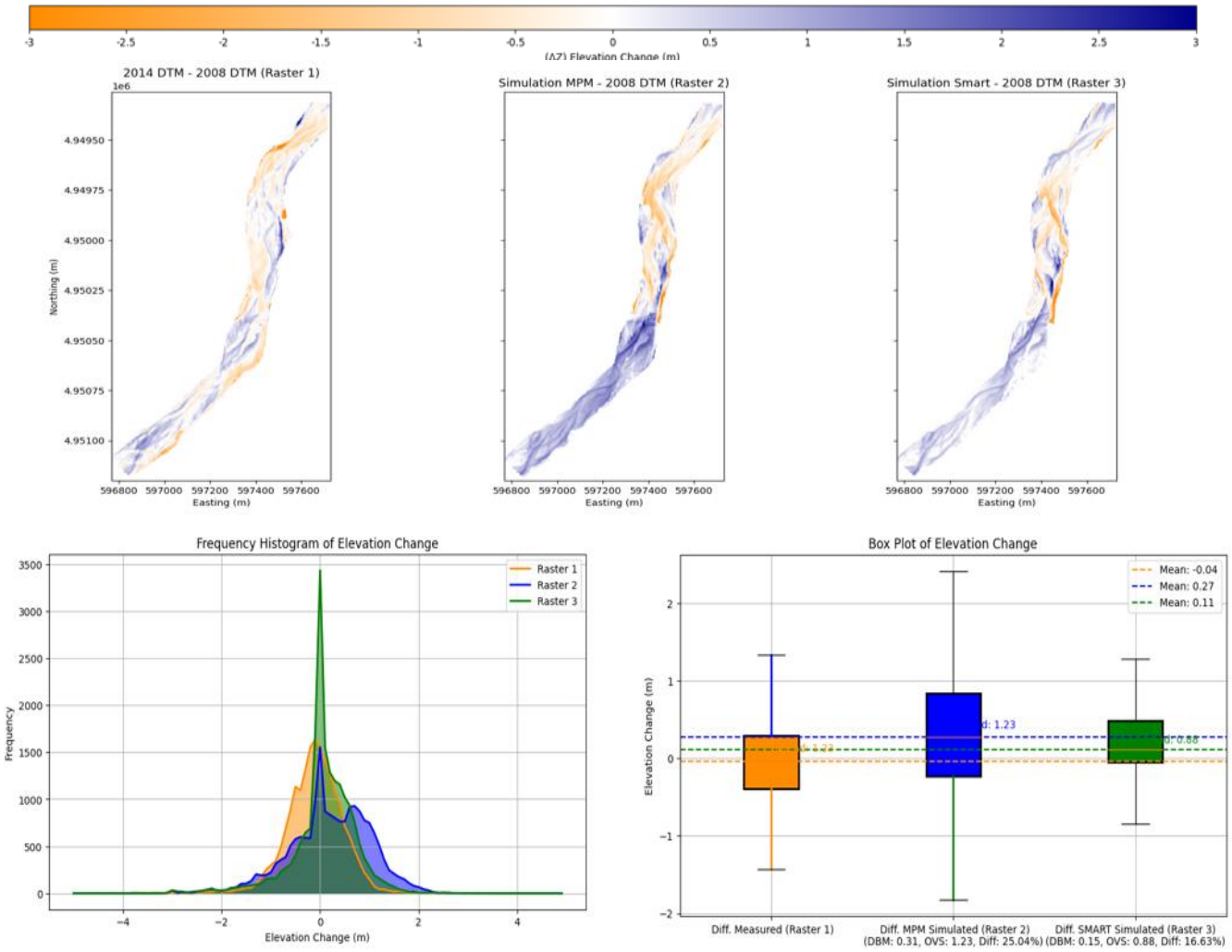

Figure 5.19 Comparison of mode outcomes with 20% increase in D50, shown through 2D maps, frequency histogram and box plot for elevation changes (Sub reach 1 of 6)

This comparison revealed heightened erosion in the centre section, an aspect slightly overlooked by the MPM approach, while the SMART approach captured some erosion along the left bank in the downstream zone. Statistical representations through box plots shows that the MPM approach showed a variance of 16.30%, while the SMART approach exhibited a marginally lower variance of 12.55% as shown in Sub-reach as shown below

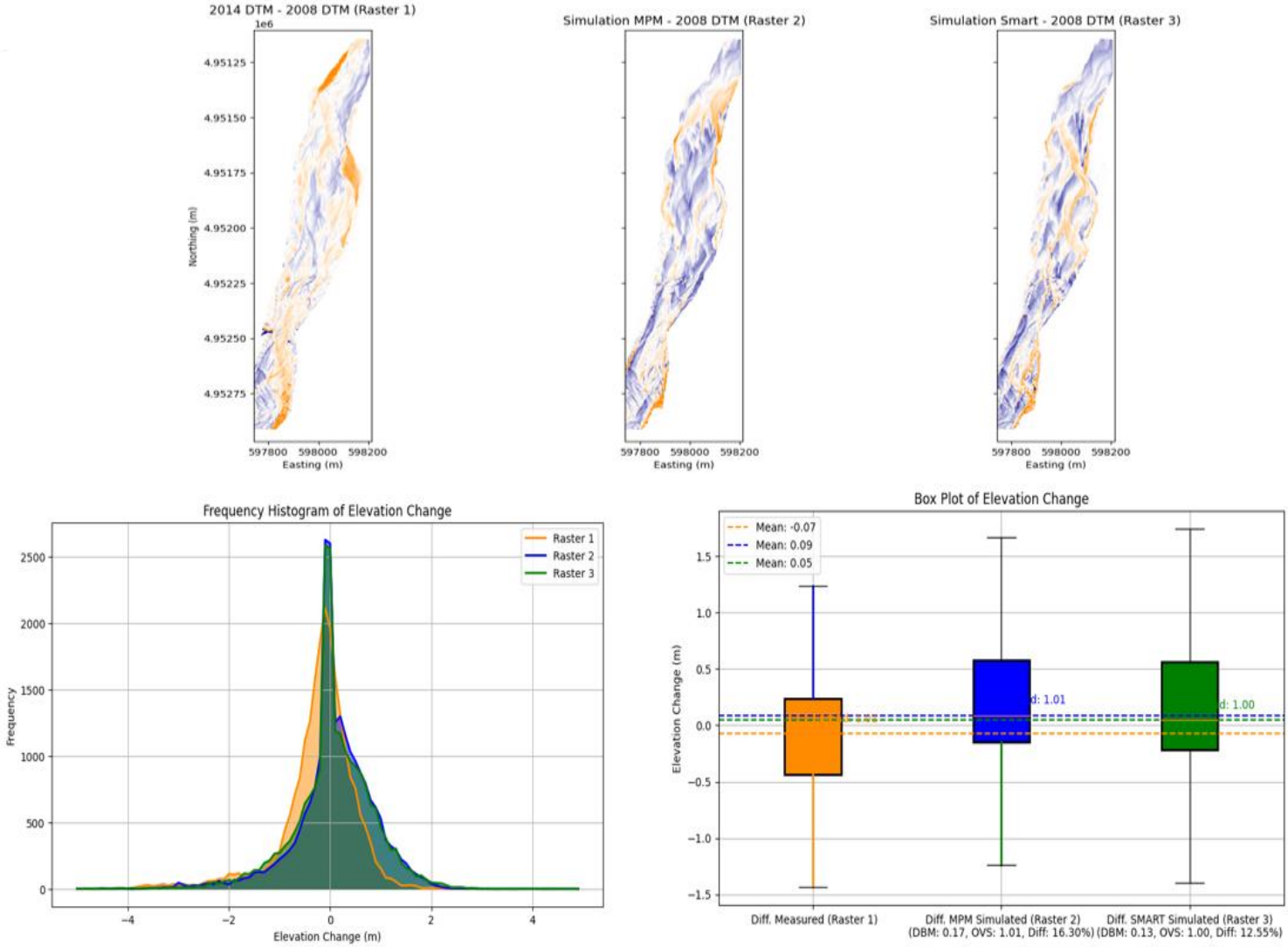

Figure 5.20 Comparison of mode outcomes with 20% increase in D50, shown through 2D maps, frequency histogram and box plot for elevation changes (Sub reach 2 of 6)

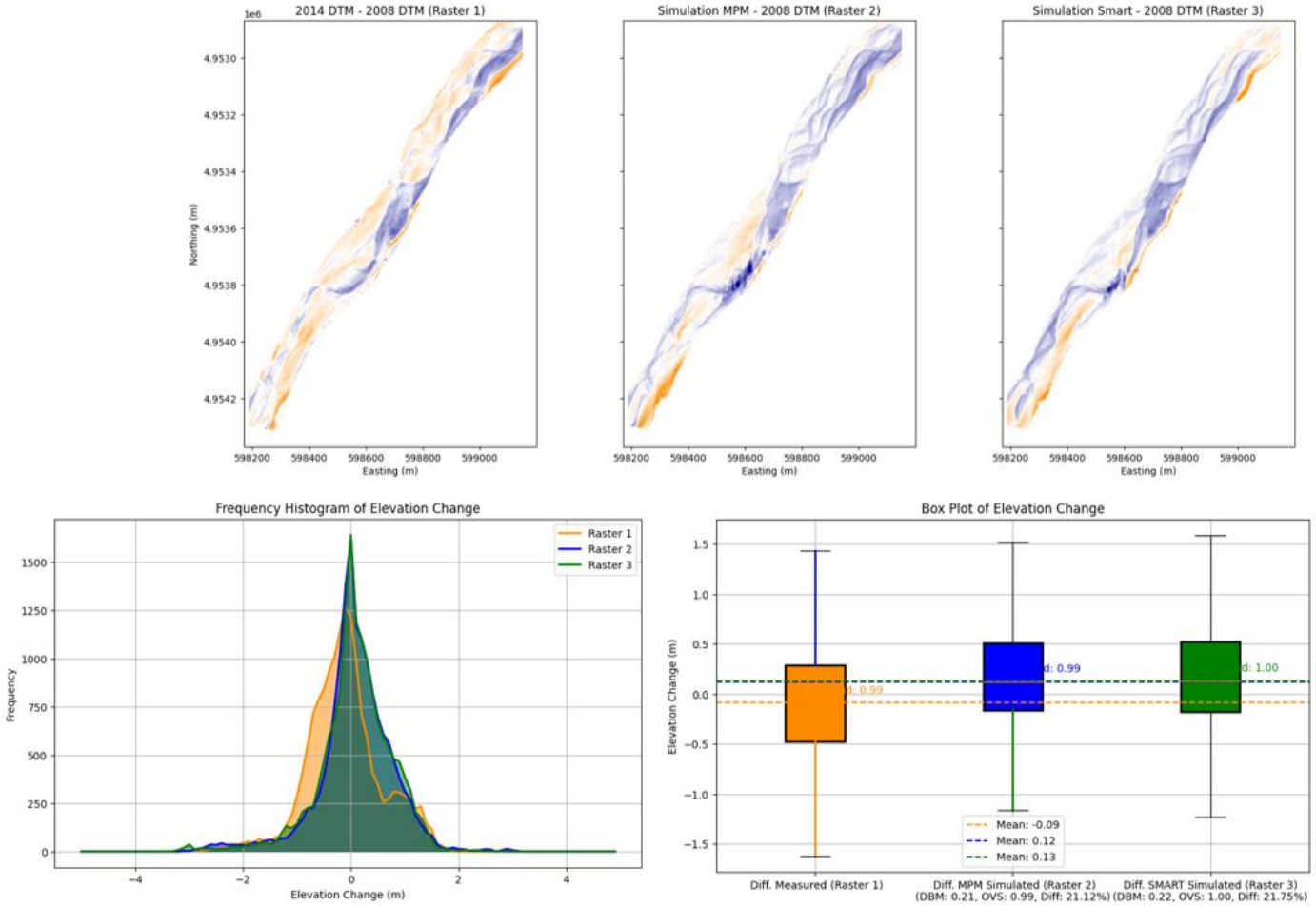

Figure 5.21 Comparison of model outcomes with 20% increase in D50, shown through 2D maps, frequency histogram and box plot for elevation changes (Sub reach 3 of 6)

In Sub-reach 3 as shown in Figure 5.21, there is a marginal shift where the MPM approach marginally leads with a variance of 21.12% as opposed to SMART"s variance of 21.75%.

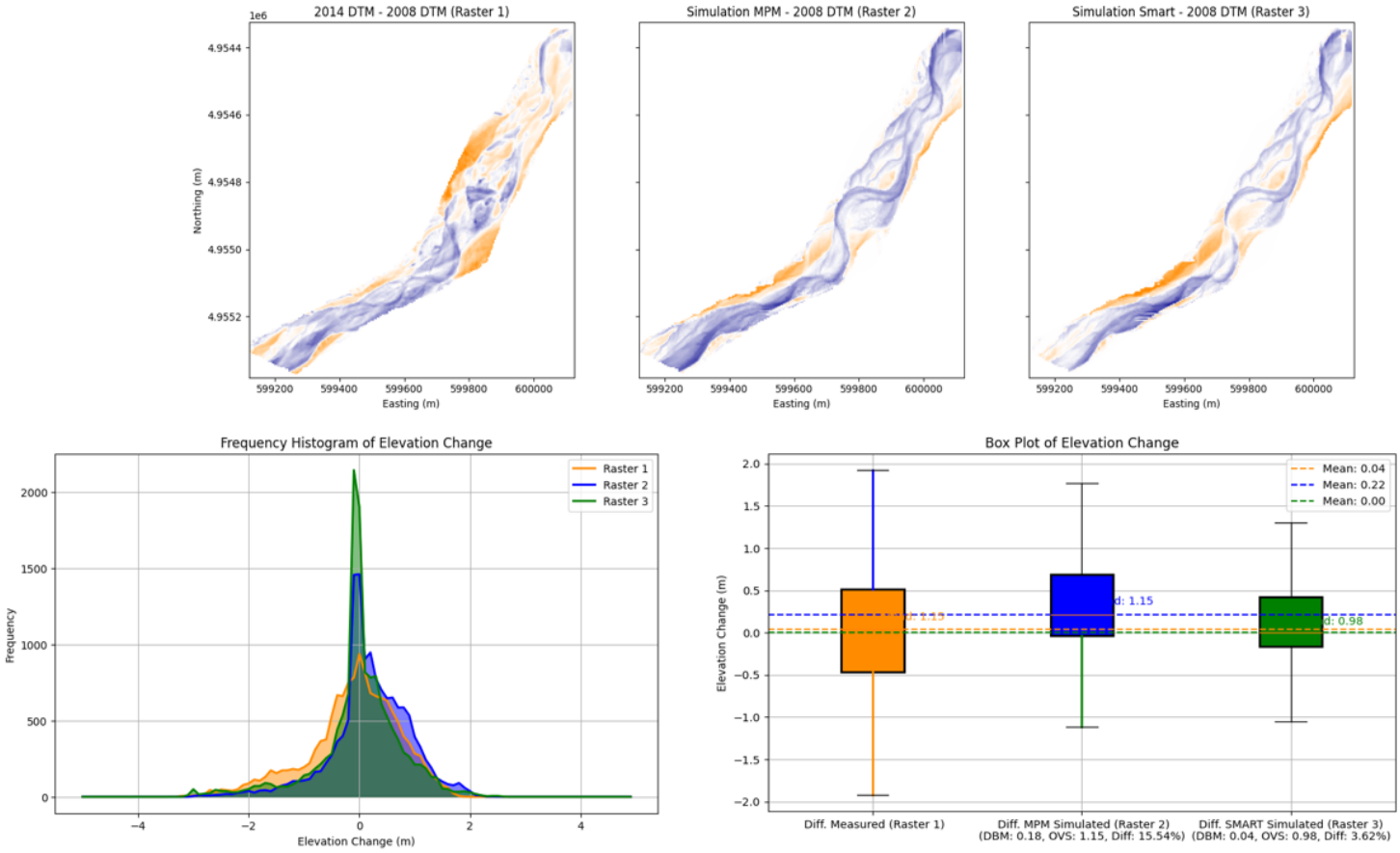

Figure 5.22 Comparison of mode outcomes with 20% increase in D50, shown through 2D maps, frequency histogram and box plot for elevation changes (Sub reach 4 of 6)

In reaches 4, 5, and 6, the SMART approach notably outperforms the MPM approach, showcasing significantly lower variances of 3.62%, 0.13%, and 9.47%, respectively. In contrast, the MPM approach exhibits higher variances of 15.54%, 2.90%, and 13.10% in these respective sub-reaches. These differences hint at the varying strengths of each approach across different sub-reaches, emphasizing the importance of considering their individual performance characteristics within distinct river segments.

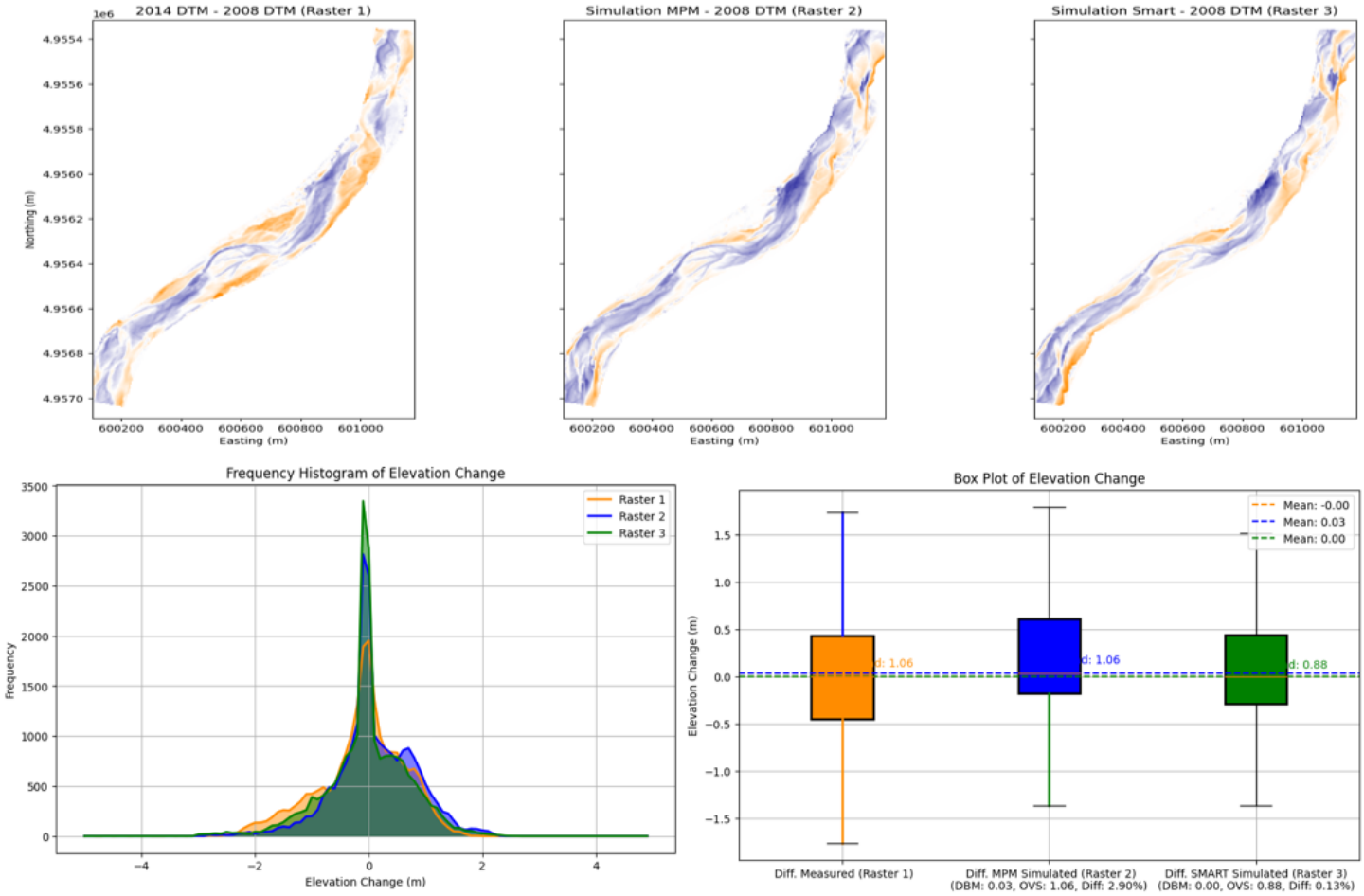

Figure 5.23 Comparison of mode outcomes with 20% increase in D50, shown through 2D maps, frequency histogram and box plot for elevation changes (Sub reach 5 of 6)

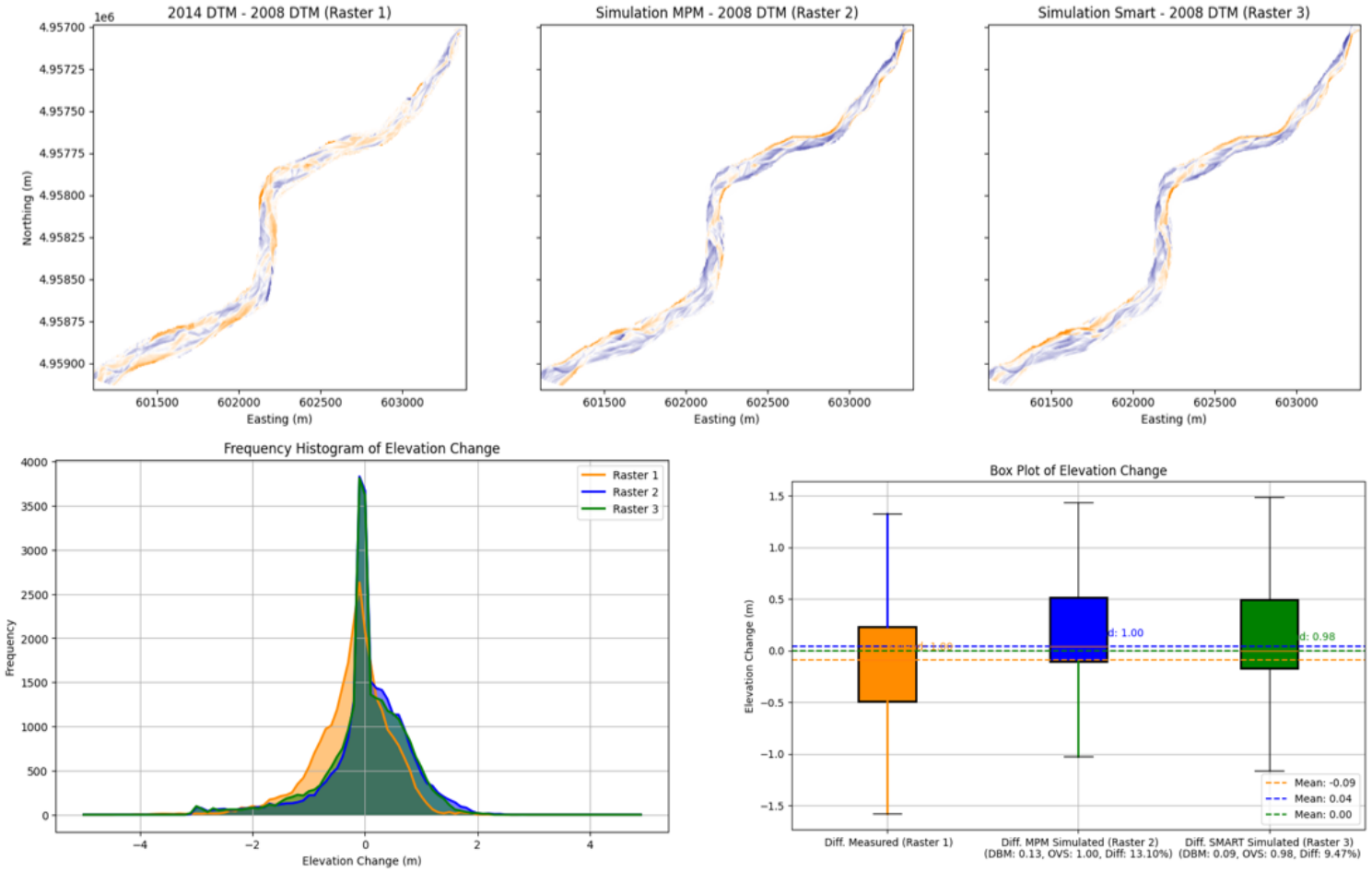

Figure 5.24 Comparison of mode outcomes with 20% increase in D50, shown through 2D maps, frequency histogram and box plot for elevation changes (Sub reach 6 of 6)

The investigation of mean grain size (D50) and Manning's roughness (n) parameter changes such as decreases, staying constant, or increase across all six sub-reaches led to results very similar to the trends observed with the initial +20% increase of D50, with small differences with respect to those discussed in previous section. Each adjustment showed similar patterns in results. These collective findings are presented in a heatmap for both MPM and SMART approaches as shown in Figure 5.25Figure 5.26 respectively. The heatmap uses colour variations to show difference in medians as a percentage of the visible spread. Lighter shades indicate minimal changes close to zero, while darker blues represent larger deviations from measured data. For instance, yellowish shades signify a 5% change, greenish to bluish denote 10%, and deeper blues indicate 25%.

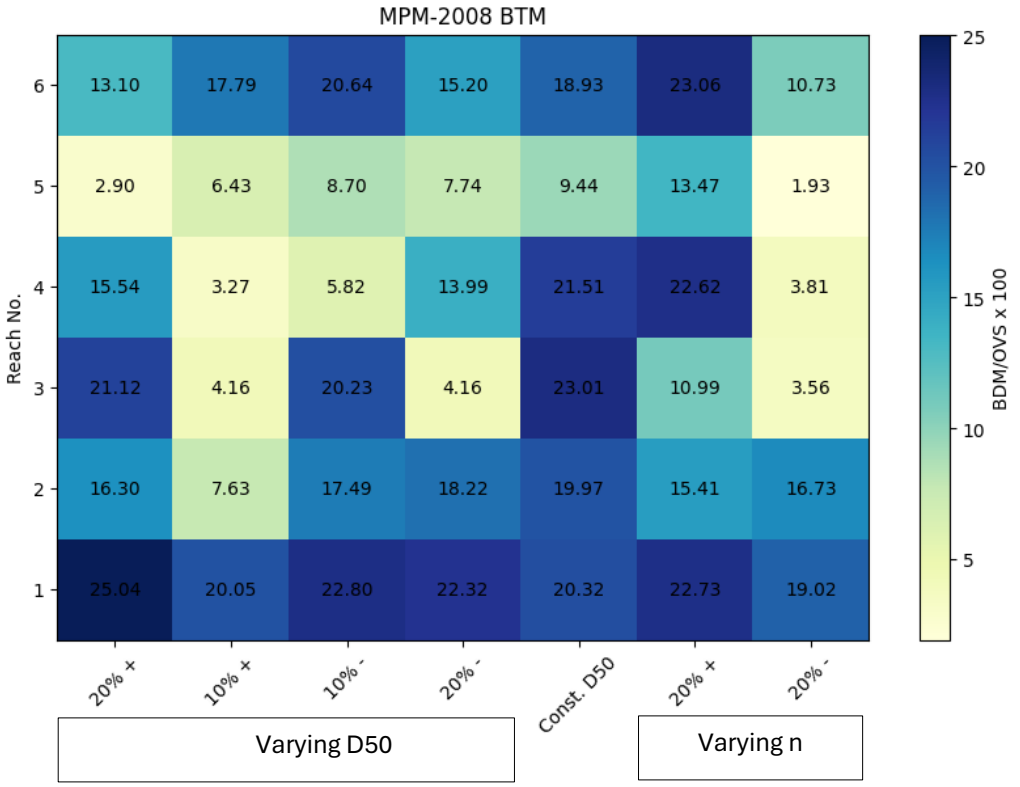

Figure 5.25 Difference in median elevation changes as a percentage of the visible spread along the river's sections for MPM approach.

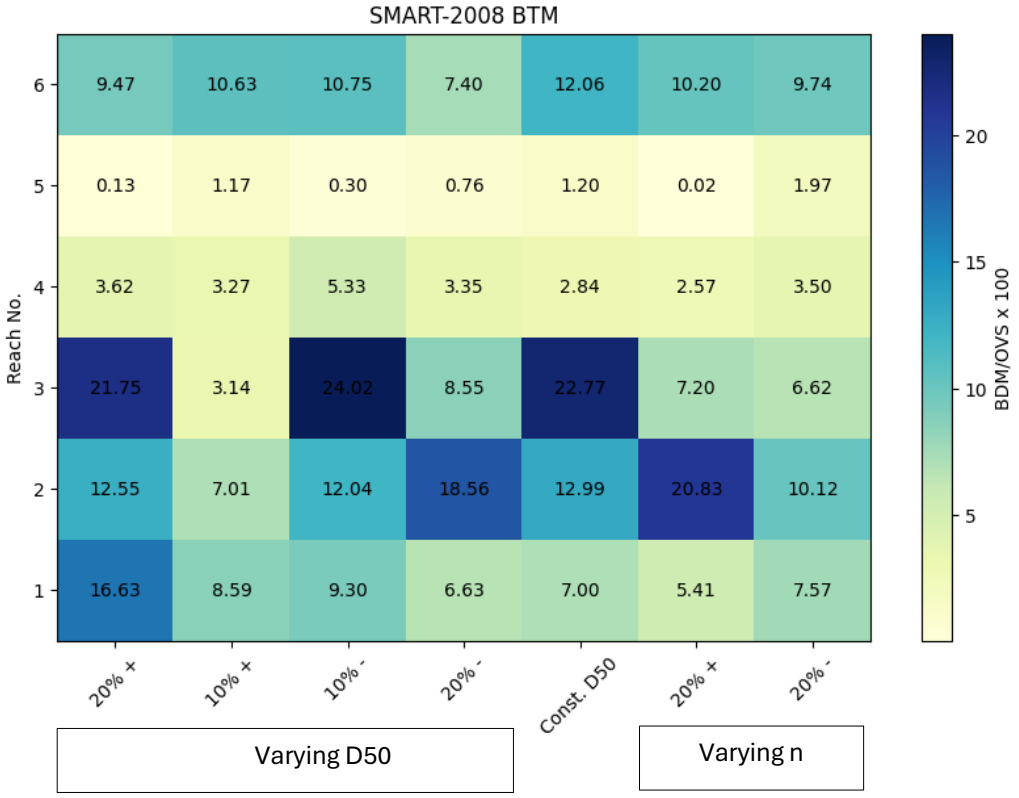

Figure 5.26 Difference in median elevation changes as a percentage of the visible spread along the river's sections for SMART approach.

A consistent pattern emerges when comparing SMART to MPM simulations: SMART consistently displays lighter shades, indicating better performance across all reaches. With parametric range variation expressed in percentages on the x-axis and different river segments (reaches) on the y-axis, intriguing insights arise as we move from upstream (Reach 1) to downstream (Reach 6). Notably, this signifies a shift from a wider, more intricately braided river morphology upstream to a narrower stretch near the Ponte Italia bridge, where the Baganza River meets the Parma River near reach 6 end.

A crucial trend emerges variance decreases as the river moves towards a straighter channel downstream. Both MPM and SMART models depict enhanced accuracy as the river shifts from upstream to downstream. This common trend underscores the improved modelling performance in straighter river sections, a characteristic observed consistently in both simulation approaches, which is rather obvious, since the braider and wider sections are more difficult to model mainly due to complex bathymetry.

Additionally, the largest difference from the 2008 Bathymetry in MPM is noted to be 25.04% in reach 1, resulting from a 20% increase in the D50 value. Conversely, the smallest variation is 1.93% in reach 5, derived from a 20% decrease in the n value. Comparatively, in SMART, the maximum difference from the 2008 Bathymetry is 24.02% in reach 3 due to a 10% decrease in the D50 value. The minimum difference is nearly zero, occurring in reach 5 due to a 20% increase in the n value. Overall, for both MPM and SMART, it was observed that a 20% decrease in roughness and a 10% increase in D50 was identified as the best case scenario.

5.4.2 Best case scenario

Simulation was completed using the best case scenario, which involves a 20% decrease in roughness (n value) and a 10% increase in D50, since this showed improved results overall for both the MPM and SMART simulations. Here it is important to note that in the best-case scenario the percentage adjustments were based on observed improvements in overall results for both the MPM and SMART simulations (see section 5.4.1.) However, it's essential to recognize that these modifications represent modelling choices and assumptions, and their impact should be considered in the context of our study. The BDM/OVS ratio decreases for both approaches across reaches 1-6, indicating enhanced model performance. Particularly notable is the significant reduction observed in the BDM/OVS x100 ratio in reach 5, where it decreases to 0.01% using MPM and 0.21% using SMART. This reduction suggests that the simulated results closely align with the measured values, indicating a high level of accuracy and reliability in the model predictions. Similar improvements are observed across other reaches, with a substantial decrease in the percentage of BDM/OVS for the best case scenario as shown in Figure 5.27and Figure 5.28,

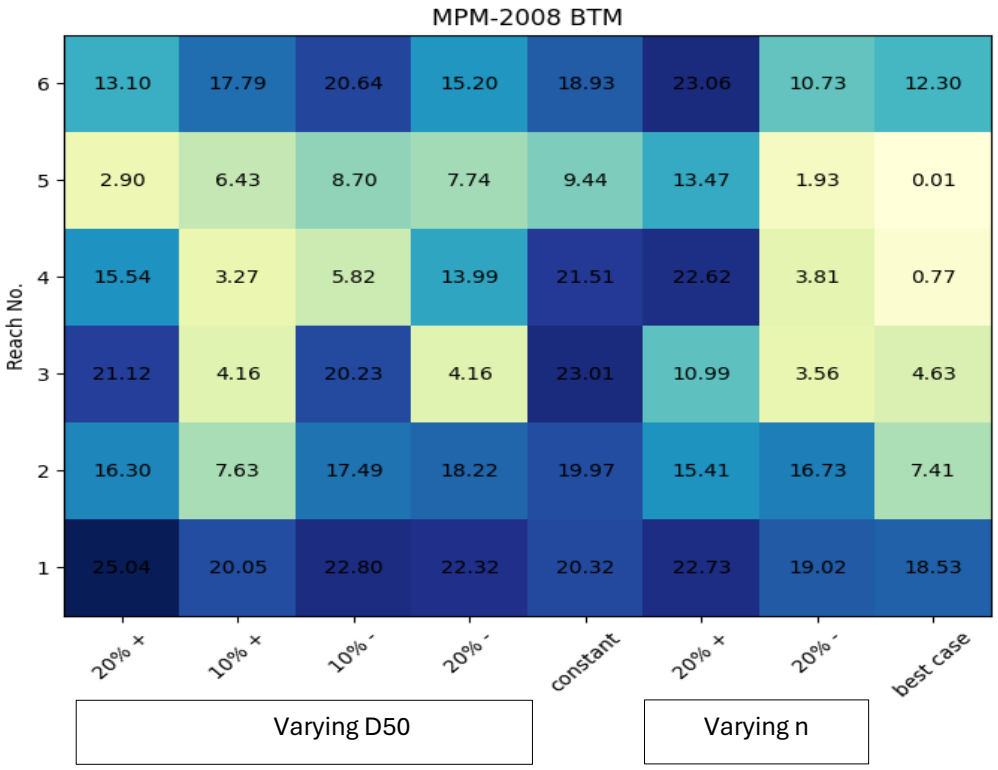

Figure 5.27 Difference in median elevation changes as a percentage of the visible spread using MPM approach with best case scenario.

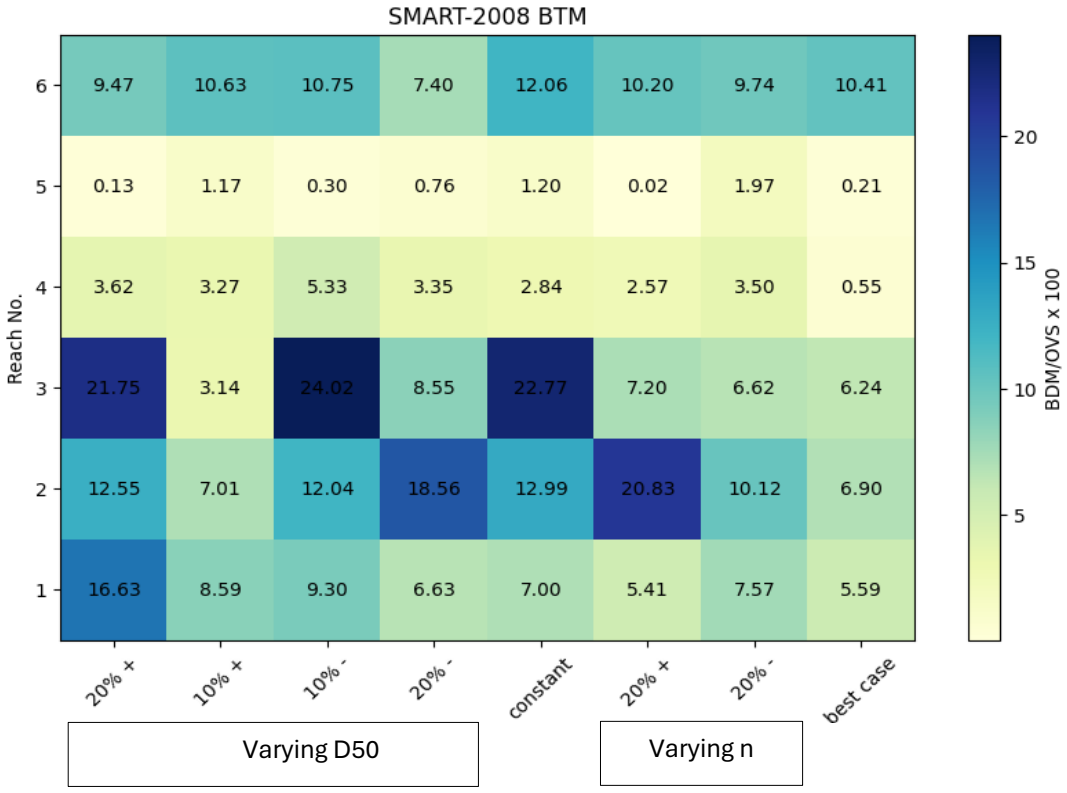

Figure 5.28 Difference in median elevation changes as a percentage of the visible spread using SMART approach with best case scenario.

5.4.2.1 Mass Balance for best case scenario

In order to ensure the quality and consistency of the sediment transport model mass balance is of prime importance. By comparing mass coming in and going out of a reach under investigation reflects the accuracy of model. Mass balance for the best-case scenario was performed and the results are shown from Figure 5.29 Figure 5.30, Figure 5.31Figure 5.32 respectively. The measured difference i.e. 2014 DTM -2008 DTM was compared with simulated difference both with MPM and SMART approaches. Volume of lowering, raising, net volume and cumulative volume was computed for each reach. The volume of lowering in m3 shows that maximum volume lowered in reach no.2 for all the three cases. While minimum volume lowered is in reach no 5. Therefore, the simulated and measured data is in agreement in terms of the reach wise assessment for volume lowering in (m3). Similarly, maximum raising occurs in reach 3 for measured difference case as compared simulated difference case which is more for MPM in reach 1 and SMART in reach 2. Furthermore, the minimum raising occurs in reach 5 for all the three cases.

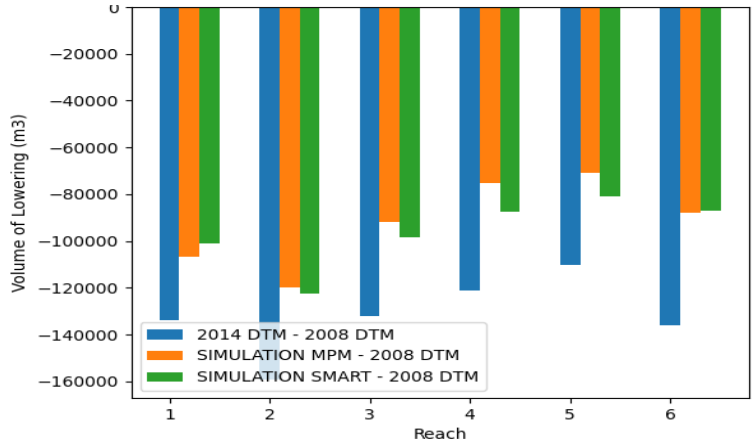

Figure 5.29 Reach wise volume of lowering of the riverbed.

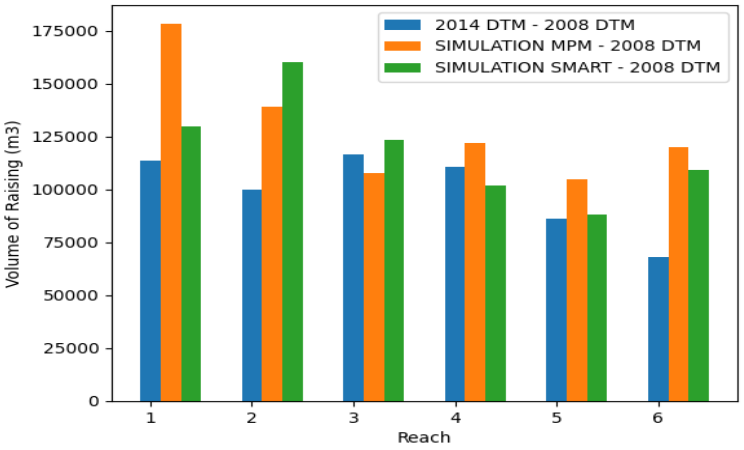

Figure 5.30 Reach wise volume of raising of the riverbed

Net volume as shown in Figure 5.31 highlights the significance of mass balance approach and here we can see the overall limitation from the model perspective. In all reaches the trend of deposition is significant for both MPM and SMART approaches whereas in the measured results the erosion is visible in all the reaches. The net volume of erosion in SMART approach is less as compared to the MPM approach that's why its performance is better for all the reaches.

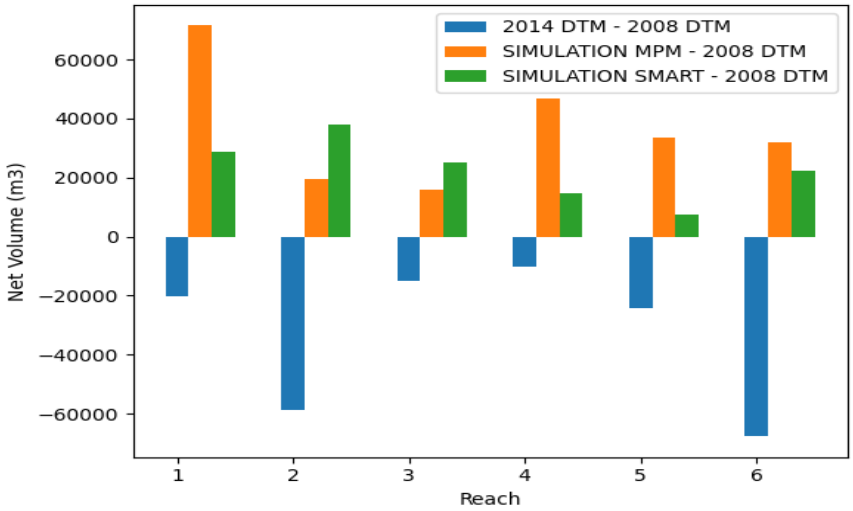

Figure 5.31 Net volume in cubic meter for all the reaches used in the analysis.

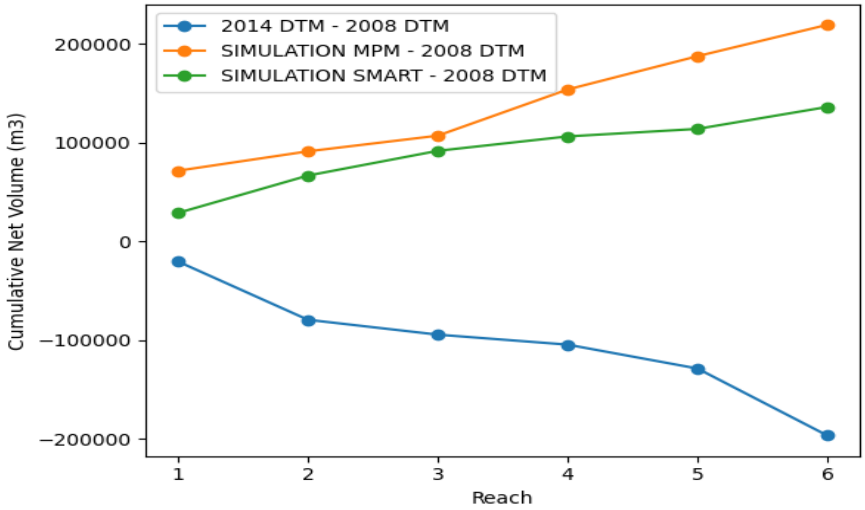

Figure 5.32 Cumulative net volume for all the reaches used in the analysis.

Furthermore, the cumulative volume as shown in Figure 5.32 highlights the progression of erosional trend in the measured data and depositional trend in the simulated data. Additionally, differences in raising and lowering volumes along with net and cumulative volume across various reaches indicate the importance of refining and validating the model parameters further. While the comparison of volume lowering and raising provides a metric for assessing overall model performance, quantifying net erosion and deposition presents challenges

due to model simplifications and weakly coupled approach, compounded by data gaps spanning six years (2008-2014). The weak coupling feedback's mechanism influence further, make difficult accurate quantitative assessments. Despite these limitations, the model presents efficacy in terms of qualitative results and captures broad trends despite quantitative constraints.

5.5 Simulation Complete Domain

5.5.1 Model Configuration

In the modelling of the entire domain, spanning from upstream of Calestano to the Ponte Italia bridge, the best case configurations are employed for both the MPM and SMART methodologies. Manning's roughness coefficient (n) is adjusted to 0.02, representing a 20% decrease from the baseline, while the median grain size (D50) map shown in Figure 5.5 is increased by 10%. Additionally, a bed porosity of 0.47, critical shear stress (tau_c) of 0.047, Courant number of 0.3 (with sediment) and 0.8 without sediment, sediment density ratio (s) of 1.683, and cell size of 4 m are utilized. Both approaches utilize a cell size of 4 x 4 m to ensure computational efficiency and accuracy. This configuration represents the optimized parameters obtained from the sensitivity analysis, aiming to achieve the best agreement between simulated and measured results across the entire river domain. The details are given Table 5.3

Table 5.3 Configuration for complete domain simulation

Manning's Roughness	Median Grain Size	Bed Porosity	Critical Shear Stress	Courant Number	Sediment Density Ratio	Cell Size
0.02 (20% decrease)	D50 (10% increase)	0.47	0.047	0.3 (with sediment)	1.683	4 m x 4 m

5.5.2 Synthetic Hydrographs

In complete domain scenario, the simulation employed synthetic hydrographs as upstream boundary condition, having return intervals of 5, 10, 20, and 50 years. Synthetic hydrographs provide a practical solution for incorporating upstream boundary conditions into simulations, especially in case of absence of long-term flow records. The peak discharge is at 13 hours for all the return periods as can be seen in Figure 5.33.

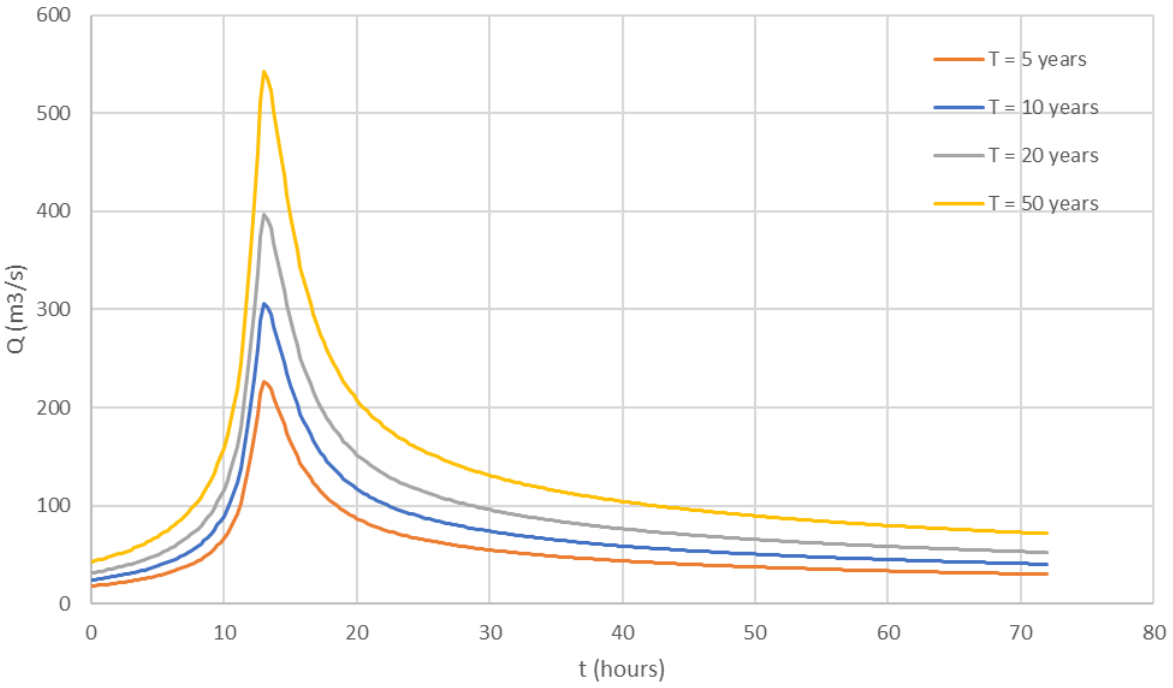

Figure 5.33 Synthetic hydrograph for 5, 10, 20, and 50 years respectively utilized in the simulation.

5.5.3 Results

5.5.3.1 Simulation Runtime

The runtime of the simulations with sediments varied across different return periods, with both MPM and SMART models demonstrating distinct computational requirements. For MPM simulations, the runtime increased progressively with higher return periods, ranging from 6.93 hours for RP=5 years to 9.96 hours for RP=50 years. Similarly, SMART simulations exhibited an escalation in runtime, from 6.87 hours for RP=5 years to 10.2 hours for RP=50 years. Notably, in the absence of sediments, simulations showed a considerable decrease in runtime, starting from 3.78 hours for RP=5 years and peaking at 5.14 hours for RP=50 years, indicative of the computational efficiency gained by eliminating sediment transport calculations as detailed in Table 5.4. Despite the computational complexities posed by sediment transport process, both MPM and SMART simulations exhibit reasonable computational efficiency across various return periods.

Table 5.4 Simulation runtime using grid size 4m × 4m.

Simulation	Approach	Runtime (hrs)			
With Sediments		RP=5 Y	RP=10 Y	RP=20 Y	RP=50 Y
	MPM	6.93 hrs	7.26 hrs	8.91 hrs	9.96 hrs
	SMART	6.87 hrs	7.80 hrs	8.92 hrs	10.2 hrs
Without Sediments	-	3.78 hrs	4 hrs	4.27 hrs	5.14 hrs

5.5.3.2 Simulation Stability

The numerical stability of the simulations was assessed by plotting the timestep against simulation runtime while adhering to Courant-Friedrichs-Lewy (CFL) restrictions of 0.3 with sediments and 0.8 without sediments. The resulting graph reported in Figure 5.34 depicts the evolution of timestep (dt) in seconds against simulation time (t) in hours. Initially, as the simulations commenced, the timestep for simulation without sediment was approximately 0.12 seconds, contrasting with around 0.04 seconds for simulation with sediment. As the simulations progressed, the timestep for simulation without sediment gradually decreased, reaching 0.07 seconds at approximately 13 hours when the flood peaked can be seen in Figure 5.34. In contrast, simulations with sediment maintained a relatively constant timestep throughout the duration of the flood simulation, hovering around 0.038 seconds until the end of the simulation. Subsequently, after the flood event subsided, simulations without sediment reverted to a timestep of approximately 0.12 seconds until the completion of the simulation. Although the timestep with sediments is less than that without sediments, however it allows large enough timesteps to complete the simulation in a reasonable time. This analysis provides insights into the temporal evolution of timestep dynamics during the simulation, highlighting the contrasting behaviours between simulations with and without sediment transport and underscoring the importance of numerical stability considerations. The little perturbation with sediments shows the bed activity during the simulation in contrast to without sediment where the line is smooth.

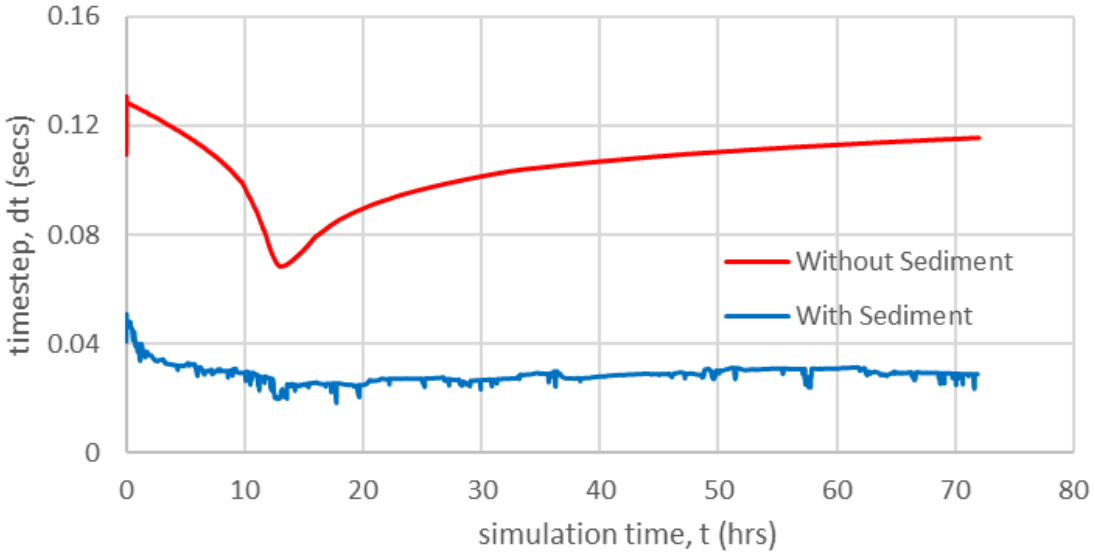

Figure 5.34 Timestep evolution with and without sediments.

5.5.3.3 Simulated Discharges and Water levels

The domain shown in Figure 5.35 is used for the simulation purpose. The bathymetry raster used for simulation having length of 30 km (4m x 4m) contains 7 x 10^6 cells. The simulation was run for the discharge hydrograph mentioned in previous section, having RP=5 Y, RP=10 Y, RP= 20 Y and RP= 50 Y, respectively. For analysis purpose, the domain is segmented in three portions such as upstream, in the middle part and downstream. Simulated water levels and discharges for MPM, SMART and no sediment were plotted.

Figure 5.35 Simulation Area started upstream at Calestano to downstream at Ponte Italia with demarcation of measuring discharge and WSE points.

Simulated discharges at section 1 as shown in Figure 5.36 show that the model accurately simulated the discharges for all return periods and effectively simulated peaks at 13 hours. The discharge measuring position is in upstream location, so the flood peak arrives with no time and the simulated graph shows smooth increase and decrease on rising limb and falling limb respectively.

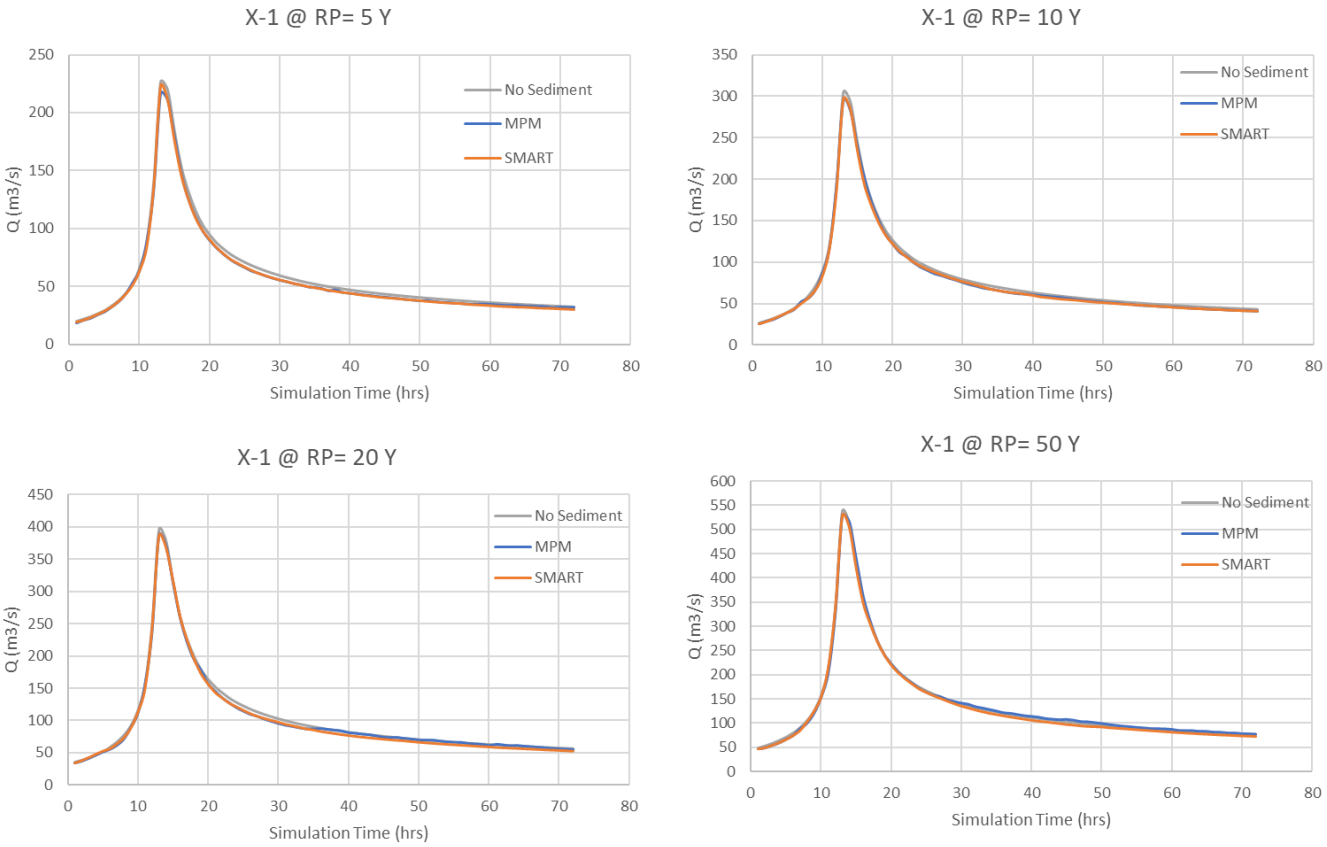

Figure 5.36 Simulated discharges for all return intervals without and with sediment (MPM, SMART) cases at point X-1

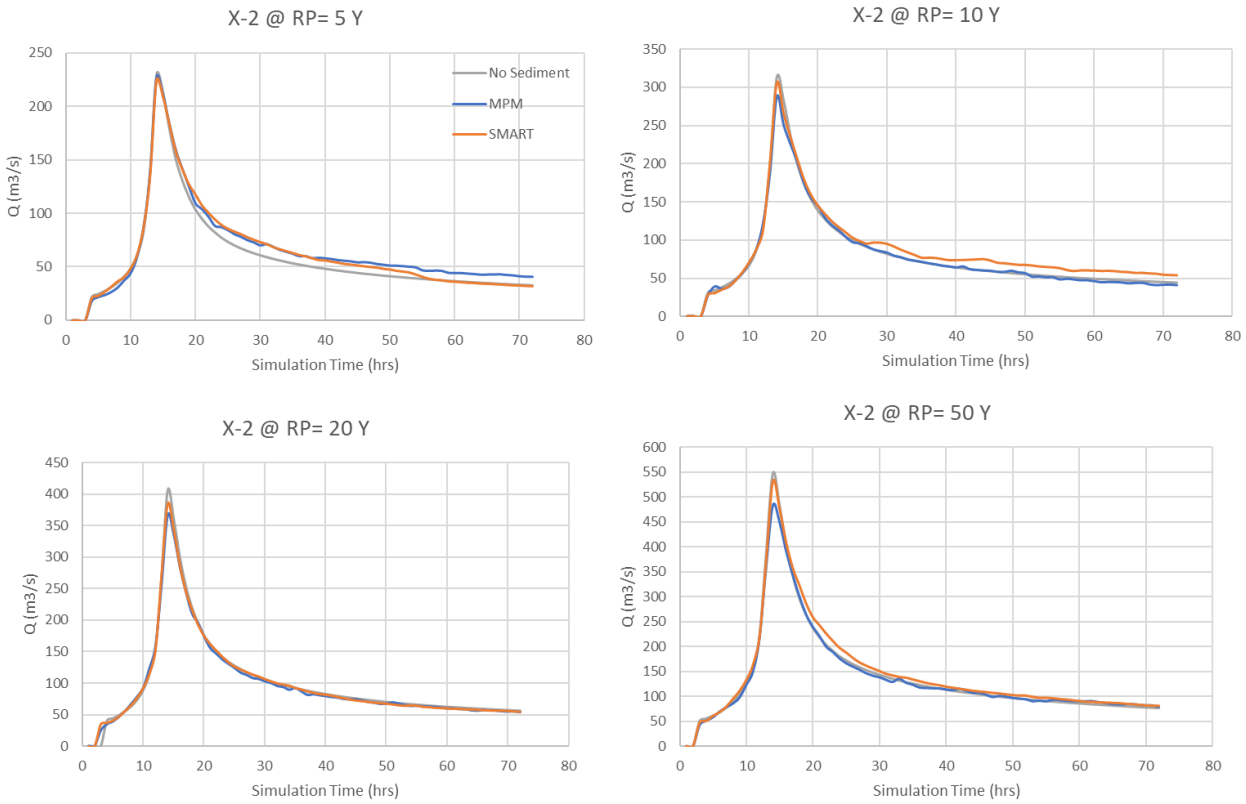

Figure 5.37 Simulated dischrages for all return intervals without and with sediment (MPM, SMART) cases at point X-2

At section 2 as depicted by Figure 5.37 Simulated dischrages for all return intervals without and with sediment (MPM, SMART) cases at point X-2 the simulated discharge shows a little abnormal trend in the start because the flood wave doesn't reach in the start, and it slowly peaks up at rising limb side. The falling limb is not smooth due to sediment transport phenomenon whereas in non-sediment case falling limb is smooth. If we compare MPM with SMART approach in this section it can be clearly seen that perturbations along the falling limb of discharge hydrograph are much more pronounced in case of SMART than MPM. Also, the discharge hydrograph peaks are well captured by the SMART approach than that of MPM approach at all 5, 10, 20 and 50 years return period, respectively. Simulated discharges for section 3 are shown in Figure 5.38 Like section 2, this section also shows different behaviours for rising and falling limb of discharge hydrograph. The interesting aspect here is that at RP=20 years and RP=50 years the falling limb of the discharges for the case with sediment is higher than the case where there is no sediment, contrary to section 2. The reason could be the reduced width of the section near the urban stretch in section 3.

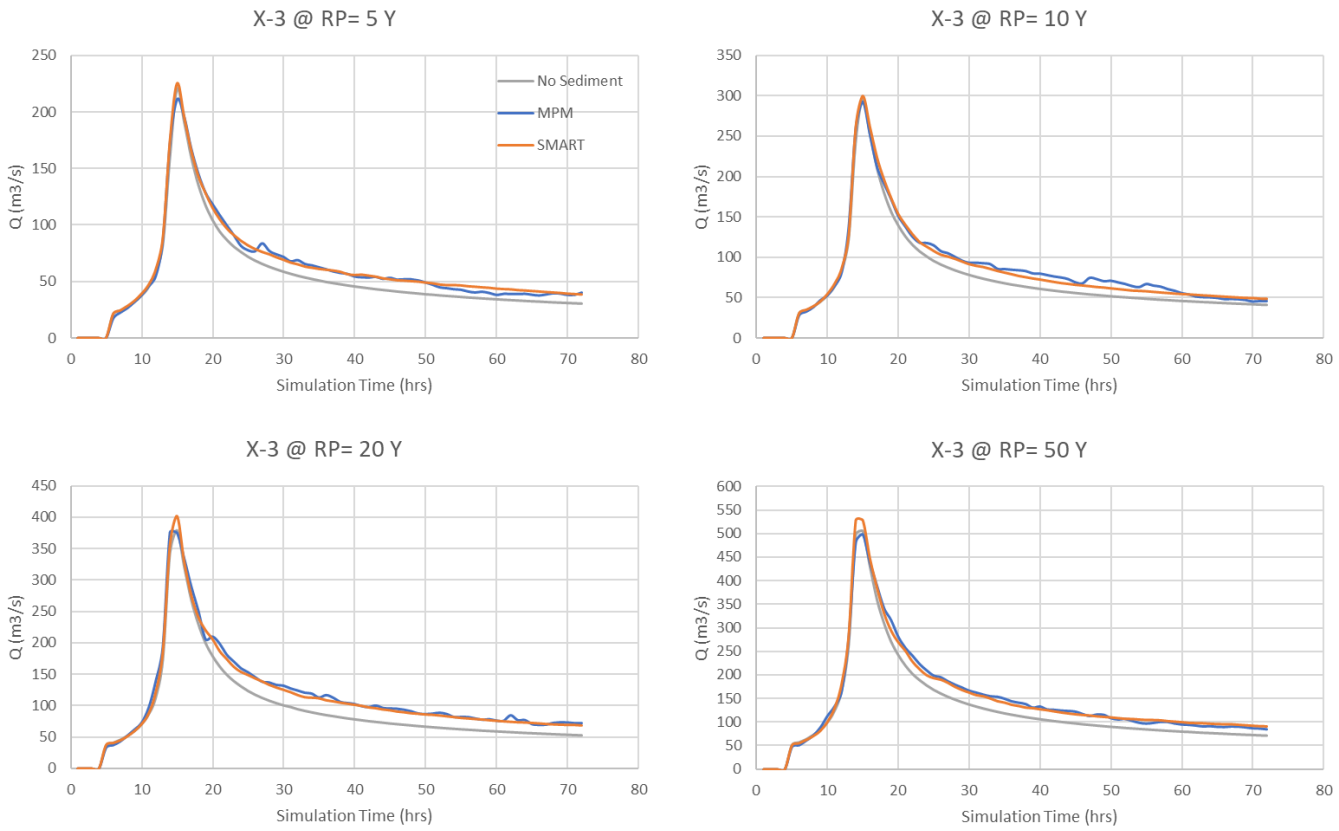

Figure 5.38 Simulated discharges for all return intervals with MPM, SMART and no sediment case at X-3

The simulated water levels recorded at P1(located on upstream side can be seen in Figure 5.35). Further, Figure 5.39 showcase distinct patterns across different scenarios, including cases with no sediment, MPM, and SMART simulations, encompassing various return periods. In scenarios without sediment, the water levels exhibit fluctuations, typically peaking from 249 to 249.2 m across all return periods before reverting to 249 m by the simulation's conclusion. Conversely, in MPM and SMART simulations the maximum water level can be seen in RP=50 Y where the level went up to 249.8 m., notable variations in water levels are observed throughout the simulations can , indicative of the dynamic nature of bed level fluctuations attributed to sediment transport processes see Figure 5.39. These fluctuations underscore the influence of sediment dynamics on water level behaviour. Results suggest that once the flood wave passed, erosion and deposition continue and during the simulation, there is always an alternation between both processes.

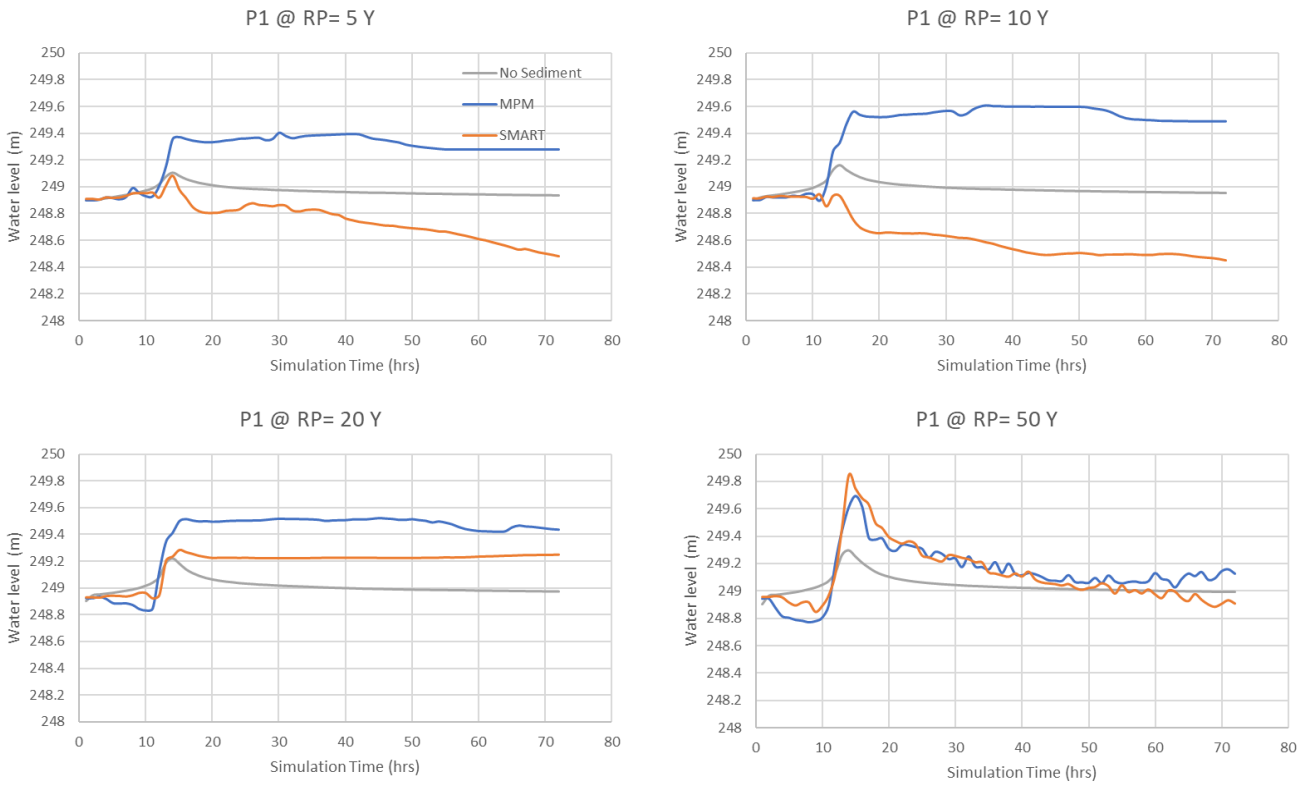

Figure 5.39 Simulated water levels for all return intervals with MPM, SMART and no sediment case at P-1

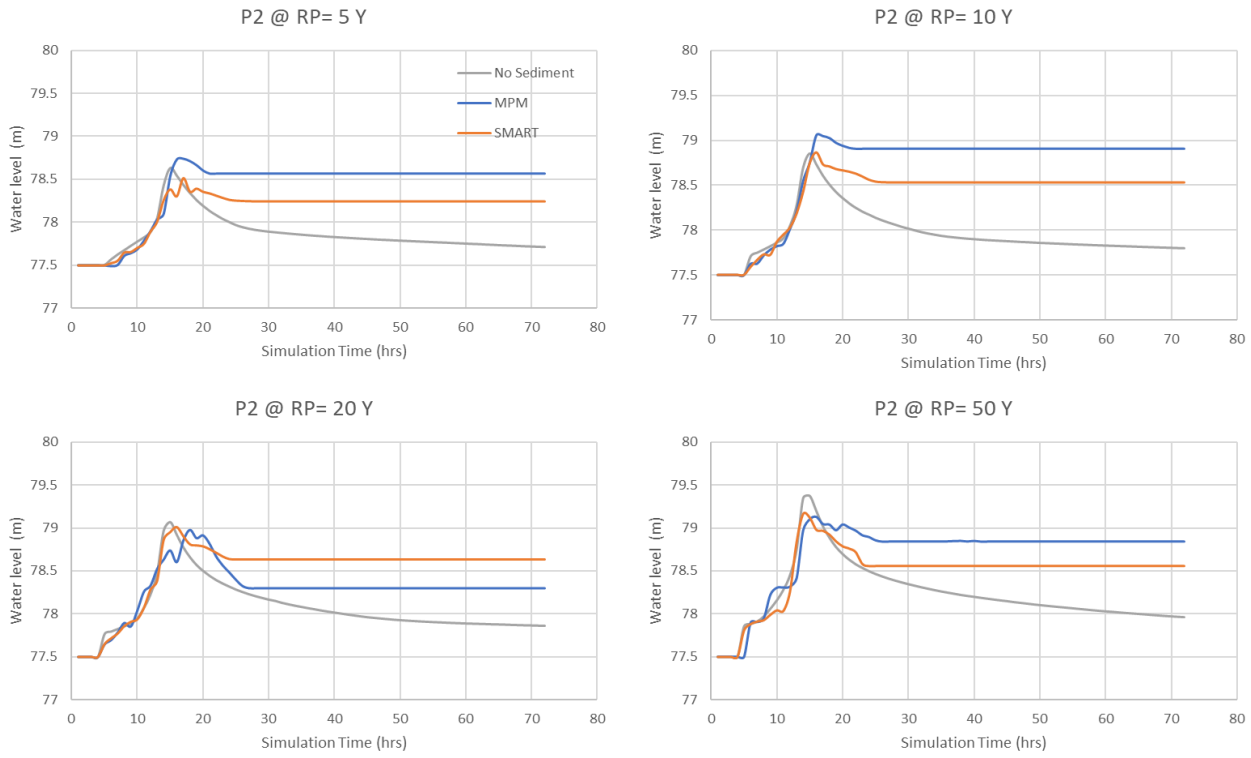

Figure 5.40 Simulated water levels for all return intervals with MPM, SMART and no sediment case at P-2

Figure 5.40 shows the simulated water levels at P2 location at downstream location.. The level shows distinct patterns across different scenarios. In scenarios without sediment, the water levels exhibit fluctuations, typically peaking from 77.5 m to 79 m across all return periods. Conversely, in MPM and SMART simulations, variations in water levels are observed throughout the simulations. The peak water levels are when the flood wave arrive at 13 hours and then the level tend to recede this phenomenon is observed under all the return periods.

5.5.4 2D Maps of Physical Quantities

5.5.4.1 Maximum Water Surface Elevation

The provided maps in Figure 5.41 to Figure 5.44 in depict the maximum water surface elevation (WSE) for return periods (RP) of 5, 10, 20, and 50 years across the entire domain from Calestano to Ponte Italia Bridge near Parma. The color palette ranges from dark blue to very light blue, with maximum water surface elevation marked as 390 (m.a.s.l) and minimum as 60 (m.a.s.l). Notably, as the return period increases, there is a discernible expansion of the river outside its channel in nearby areas. This is evident by the spill of river water beyond the boundaries of the domain, particularly notable in the first half and last half of the domain. Despite marginal differences in elevation values across the return periods, the primary observation is the amplification of river spillage outside the riverbed as the return period increases. Furthermore, each map for return periods of 5, 10, 20, and 50 years presents simulations under three scenarios: without sediments, using the MPM approach, and SMART approach. Notably, the presence of sediments in the simulations results in a more pronounced spillage of the river beyond its channel compared to scenarios without sediments. Moreover, upon comparison between the MPM and SMART simulations, it becomes evident that the spillage is consistently greater in the MPM approach compared to the SMART approach.

5.5.4.2 Maximum Velocity

The velocity maps shown from Figure 5.45 to Figure 5.48 exhibit variations in flow velocity across the domain for return periods of 5, 10, 20, and 50 years. The color scheme ranges from purple representing 0 m/s to red indicating 5 m/s, with intermediate velocities depicted in green, yellow, and orange. Within the channel, higher velocities, indicated by red, are observed along the bends and banks, reflecting the accelerated flow dynamics characteristic of these regions. Conversely, areas surrounding spill zones and the far channel exhibit lower velocities, depicted by colours such as purple and green. This spatial variability in flow velocity highlights the influence of channel morphology

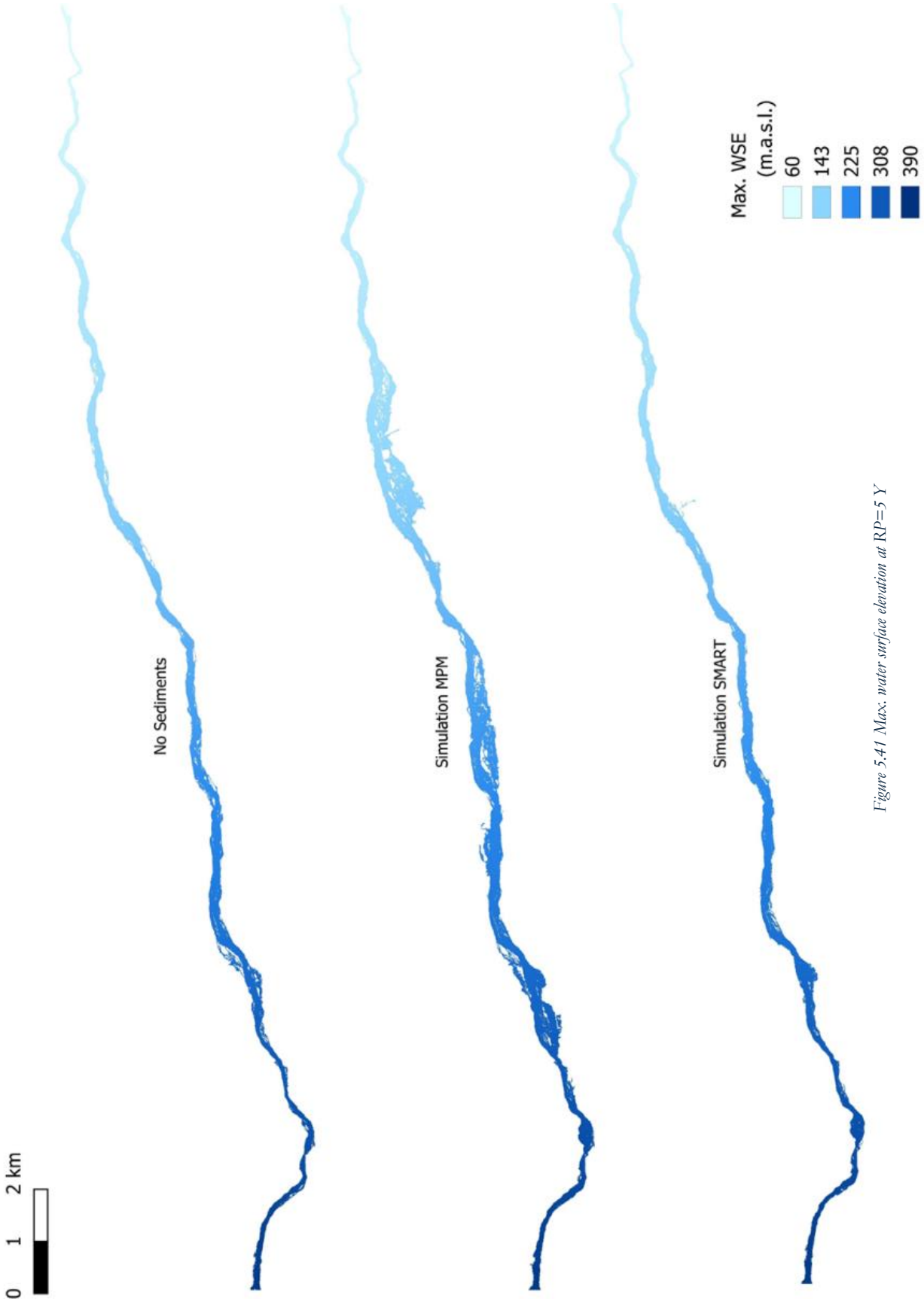

Figure 5.41 Max. water surface elevation at RP=5 Y

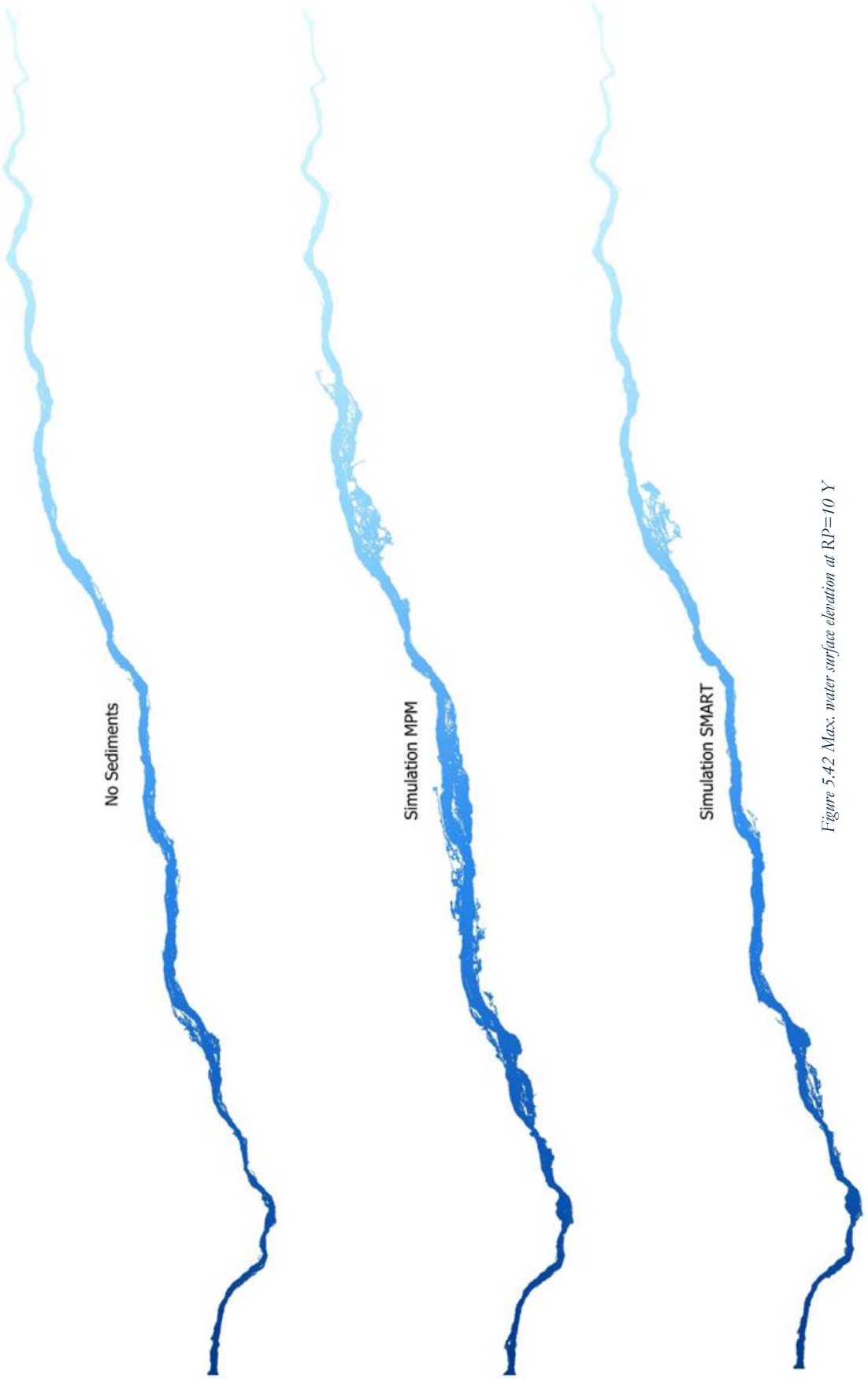

Figure 5.42 Max. water surface elevation at RP=10 Y

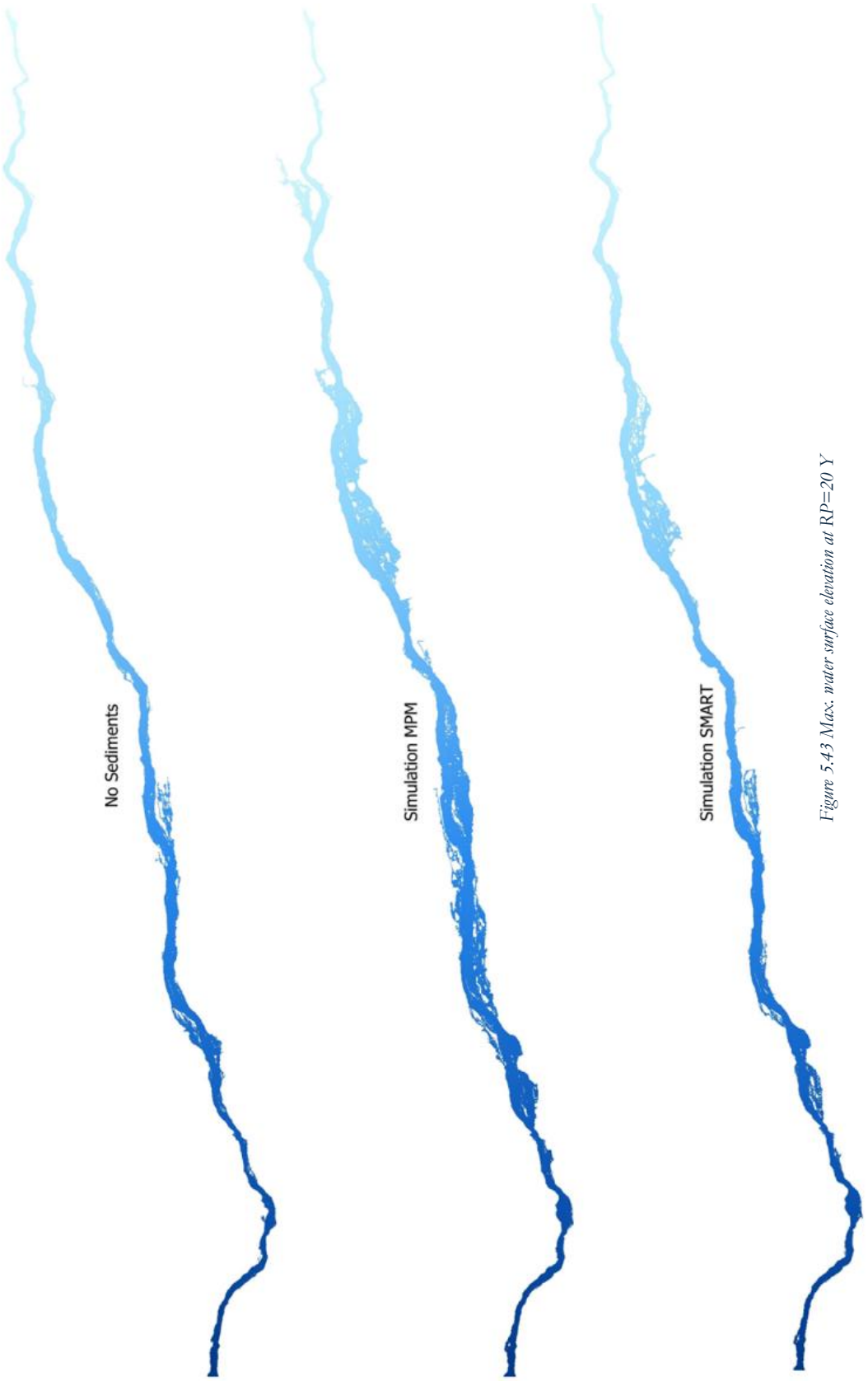

Figure 5.43 Max. water surface elevation at RP=20 Y

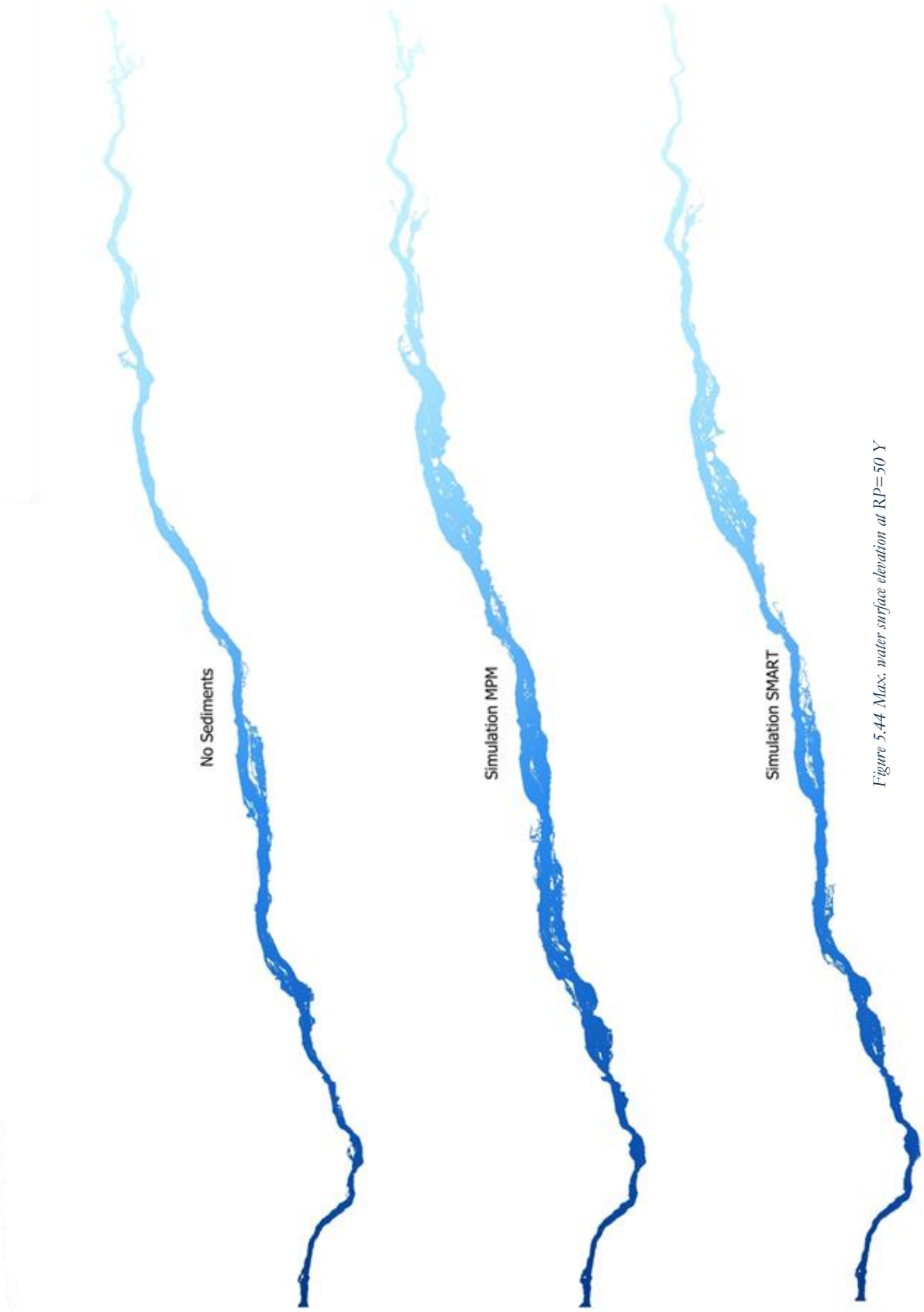

Figure 5.44 Max. water surface elevation at RP=50 Y

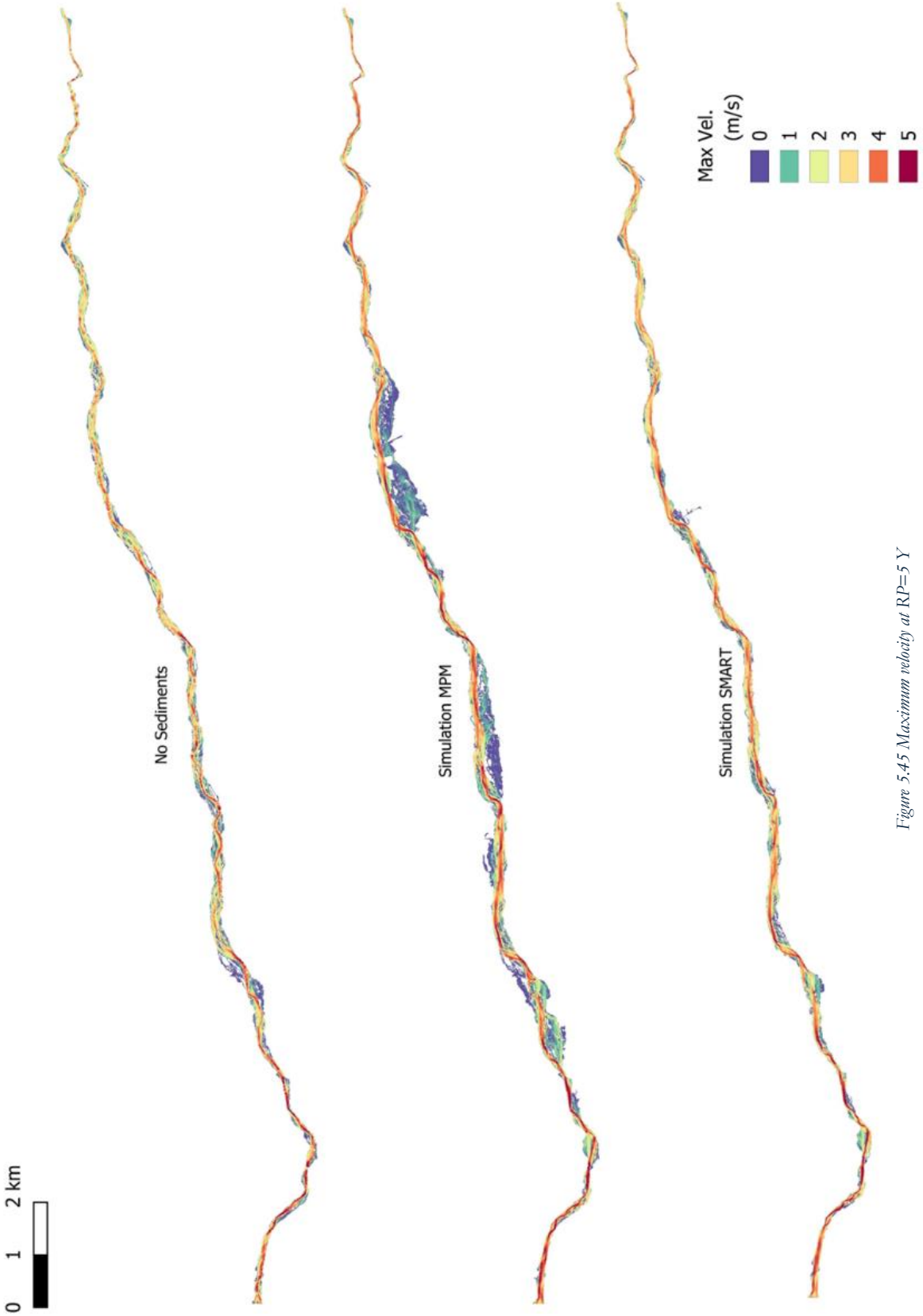

Figure 5.45 Maximum velocity at RP=5 Y

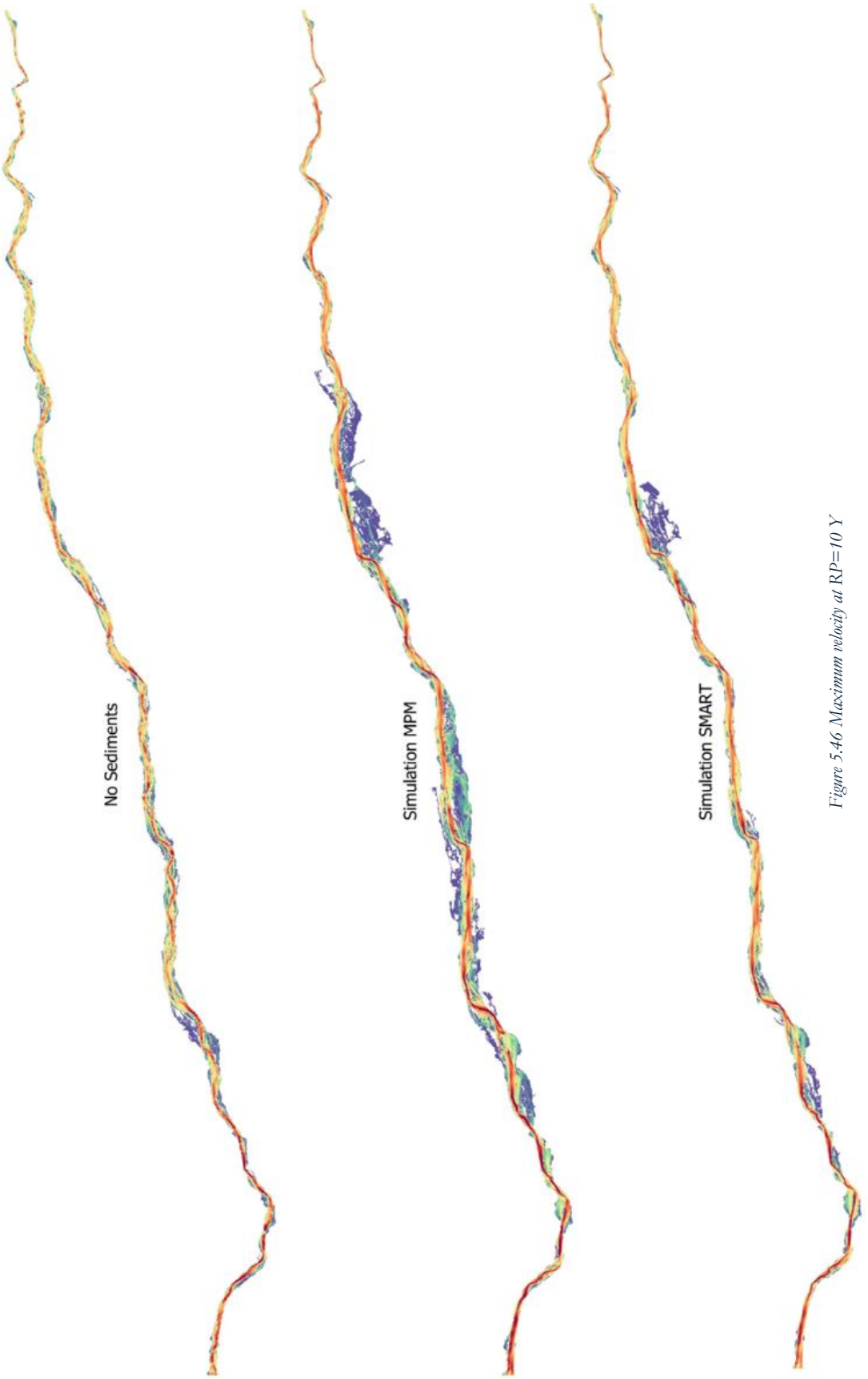

Figure 5.46 Maximum velocity at RP=10 Y

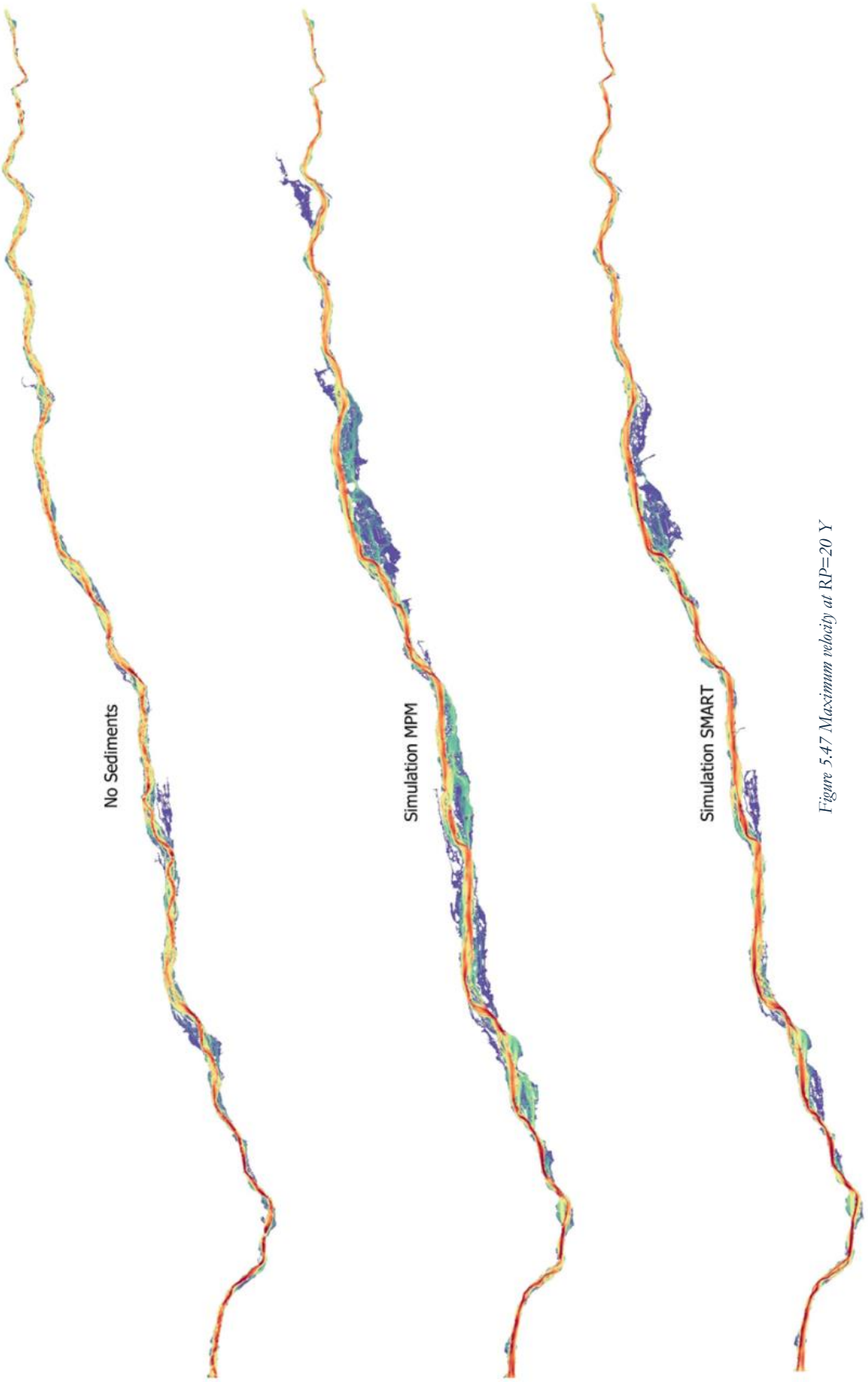

Figure 5.47 Maximum velocity at RP=20 Y

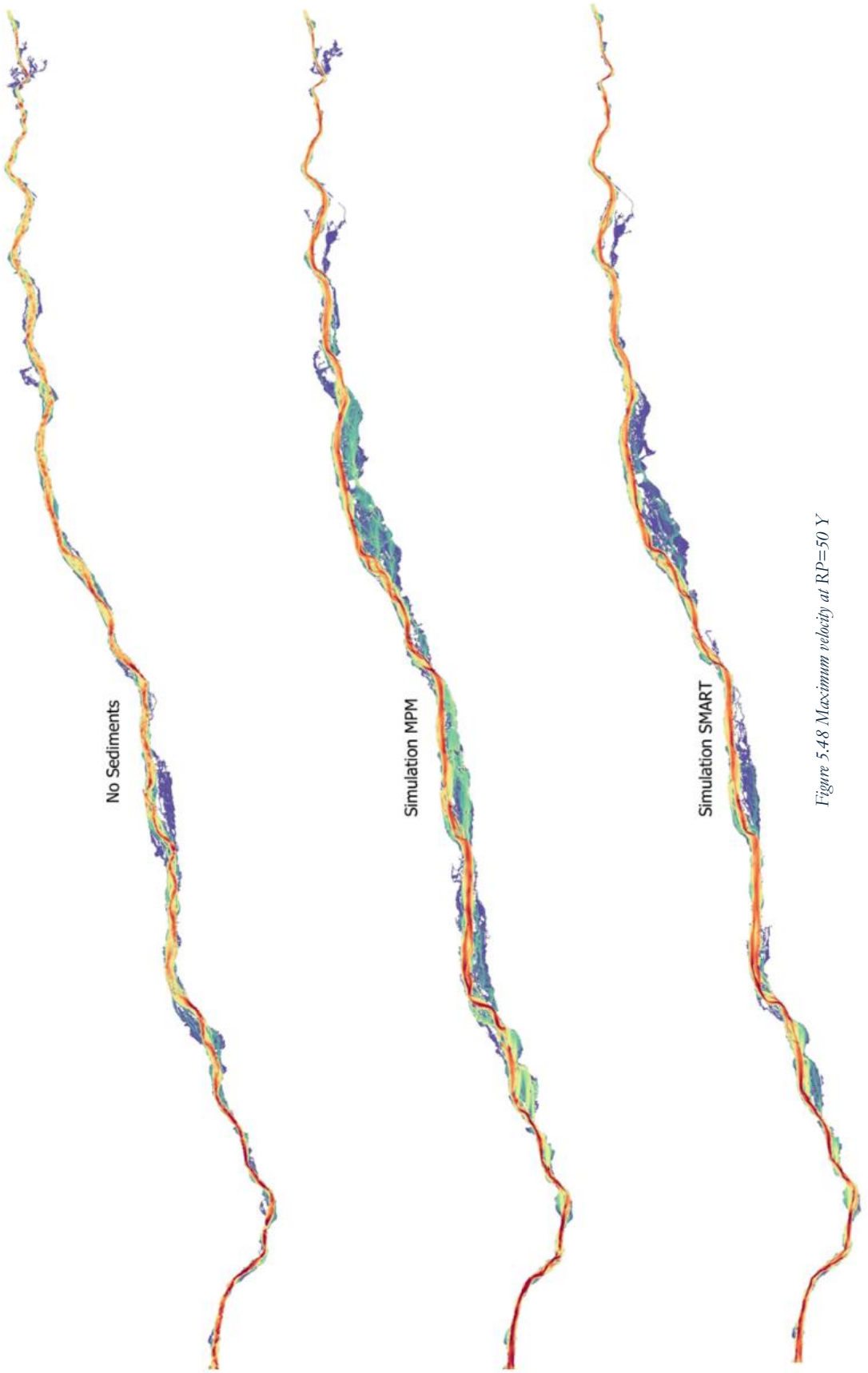

Figure 5.48 Maximum velocity at RP=50 Y

5.5.4.3 Erosion and Deposition

Figure 5.49 Net erosion and deposition trend at the end of simulation

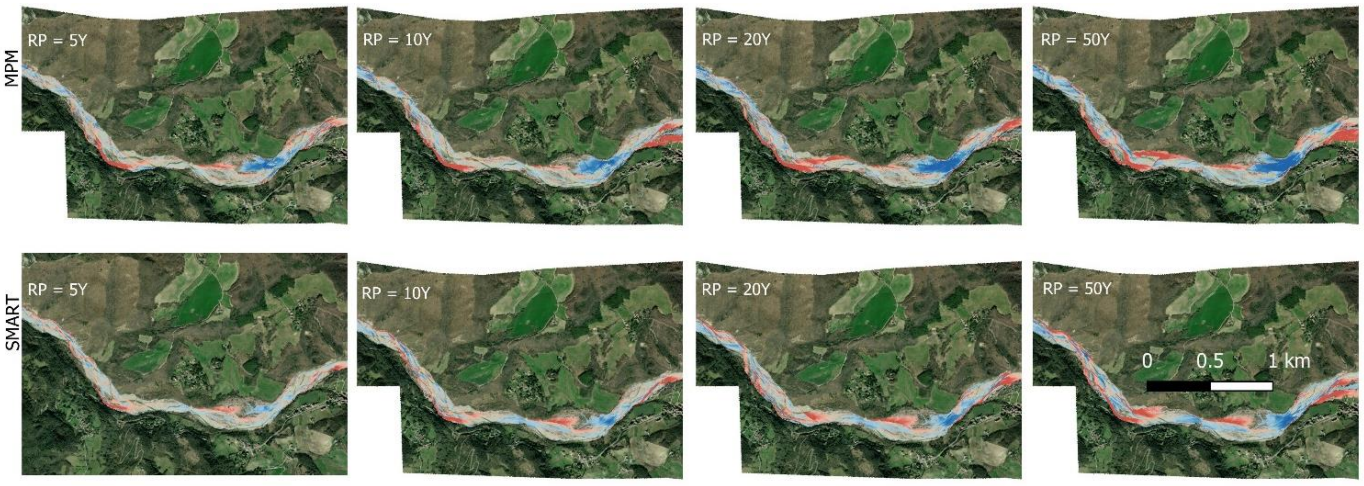

Figure 5.50 Net erosion and deposition progression under different return periods with MPM and SMART approach at location 1.

Figure 5.51 Net erosion and deposition progression under different return periods with MPM and SMART approach at location 3.

The basic results of the sediment simulations are changes in channel geometry therefore, general bahaviour of the bedload transport in terms of erosion and deposition inside Baganza catchment will be discussed. The erosion and deposition maps depict morphological changes across the domain for return periods of 5, 10, 20, and 50 years. The complete map as shown in Figure 5.49 offers an overarching view of erosion and deposition patterns, while smaller zoom-in windows, denoted as a-1, a-3, b-1, and b-3, allow for detailed examination of local morphological changes in Figure 5.50 and Figure 5.51. These correspond to simulations using the MPM approach (a-1 and a-3) and the SMART approach (b-1 and b-3). The maps illustrate net erosion and deposition, calculated by subtracting the initial bathymetry from the bathymetry obtained after simulation completion.

The findings indicate a persistent trend of erosion and deposition following the passage of the flood wave, with a continual alternation between these processes observed throughout the simulation. Analysis of solid bedload transport behaviour in the Baganza River reveals a predominant erosive action along the banks, particularly pronounced on the left side during the rising limb of the hydrograph. As the flood begins to recede, the intensity of erosion diminishes.

5.6 Baganza River Morphological Units

5.6.1 Introduction

Fluvial landforms within river channels, known as river morphological units (MU), significantly shape riverine ecosystems and influence sediment transport dynamics. These units, typically spanning the scale of 10 channel widths. Traditionally, these units have been delineated through field observation, which tends to be more qualitative than quantitative as indicated by Belletti et al. (2017). Furthermore, Weber et al. (2017) introduced a methodology aimed at overcoming the limitations of traditional in-situ delineation methods. Their approach

focused on leveraging near-census topographic and bathymetric data alongside hydrodynamic modelling techniques to delineate and map channel landforms at the morphological unit scale. In this research, a novel approach is adopted by employing water depth and the Froude number for delineation and classification purposes. The aim is to capture the intricate interplay between flow velocity and channel morphology, providing understanding of sediment transport dynamics within the river channel. This methodological adjustment enhances the accuracy of morphological unit classification, contributing to a deeper insight into riverine geomorphology.

5.6.2 Methodology

Based on Pasternack (2011), a distinct methodology for delineating in-channel riverbed morphological units is employed. Pasternack's classification provides valuable insights into MUs, but their bahaviour varies based on the specific bed material and environmental context. While the classification applies well to gravel/cobble rivers, it may not be valid for mountain streams, where different morphological units (such as cascades and steps) develop due to irregular bed morphology. Here it is pertinent to mention that he used velocity and water depth to categorize the bed morphological units. In this research, water depth rasters have been derived from base-flow and high-flow scenarios, representing flood return periods of 5 years. Additionally, velocity rasters were employed in conjunction with water depth to calculate Froude numbers, aiding in the classification process as shown in Figure 5.52. Froude number is a dimensionless number used in fluid mechanics to quantify the relative importance of inertial forces to gravitational forces in a flow. Mathematically it can be expressed in Equation 5.2

$$F_r = \frac{v}{\sqrt{gh}} \qquad 5.2$$

Whereas v is the velocity in (m/s). g is acceleration due to gravity in m/s² and h is the water depth in (m). Analysing the Froude number in conjunction with water depth provides valuable insights into flow stability within morphological units. Subcritical flow regimes, characterized by low Froude numbers, typically exhibit stable flow conditions conducive to sediment deposition and habitat formation

In contrast, supercritical flow regimes, indicated by high Froude numbers, may experience flow instabilities such as hydraulic jumps or downstream erosion, influencing morphological unit stability and channel morphology.

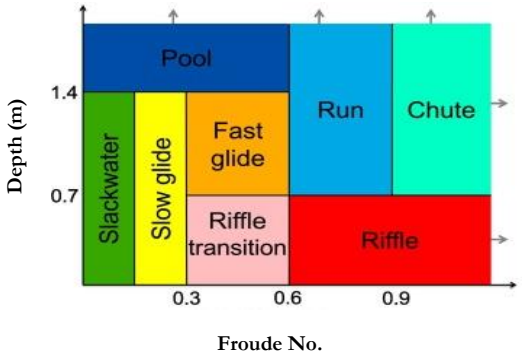

Figure 5.52 Criteria for classification of river morphological unit based on Pasternack (2011)

Eight distinct morphological units were delineated based on thresholds of water depth and Froude numbers, as specified by Figure 5.52. Each unit was defined by specific ranges of water depth and Froude numbers, capturing variations in flow velocity and morphology conditions within the channel. This methodology allowed for a comprehensive characterization of morphological units. Analysing the Froude number aids in assessing flow stability within morphological units. Subcritical flow regimes typically exhibit stable flow conditions conducive to sediment accumulation and habitat formation. In contrast, supercritical flow regimes may experience instabilities such as hydraulic jumps or downstream erosion, impacting morphological unit stability. Within the river reach spanning from Calestano to Ponte Italia, detailed examination of morphological units and sediment dynamics is crucial for effective river management.

5.6.3 Results and Discussion

This study divides the reach into seven sub-reaches as shown in Figure 5.53 to facilitate a comprehensive analysis of these factors. Morphological units were classified based on both flow conditions, i.e. "base flow" (low flows with a return period of 5 years), and "maximum flow" (high flows with a return period of 5 years) (Figure 5.53). Additionally, sediment was assessed by comparing initial and final bathymetry data after high flow simulations, allowing for the quantification of erosion and deposition processes. All morphological unit maps from subreach 1 to 7 are formed using combination of water depth and Froude No. raster maps containing value at each cell.

Figure 5.53 Sub-reaches from Calestano to Ponte Italia for river morphological units' classification.

Under the "base flow" scenario, sub-reach 1 exhibits a dominant presence of slack water (dark green), with pockets of riffle (red) along left bank and central part and little riffle transition (pink) areas, along with slow glide (yellow) features. However, upon classification based on high flows, notable changes occur. As the Froude number exceeds 0.6, areas previously identified as slack water transition into riffle formations, represented by a significant expansion of red hues across the sub-reach. Subsequently, most sub-reach 1 transforms into a combination of riffle (red) and fast glide (orange) units, indicating heightened flow velocities and alterations in channel morphology. Under "high flows", the erosion is along the left bank and deposition along the centre and on right side as shown in Figure 5.54

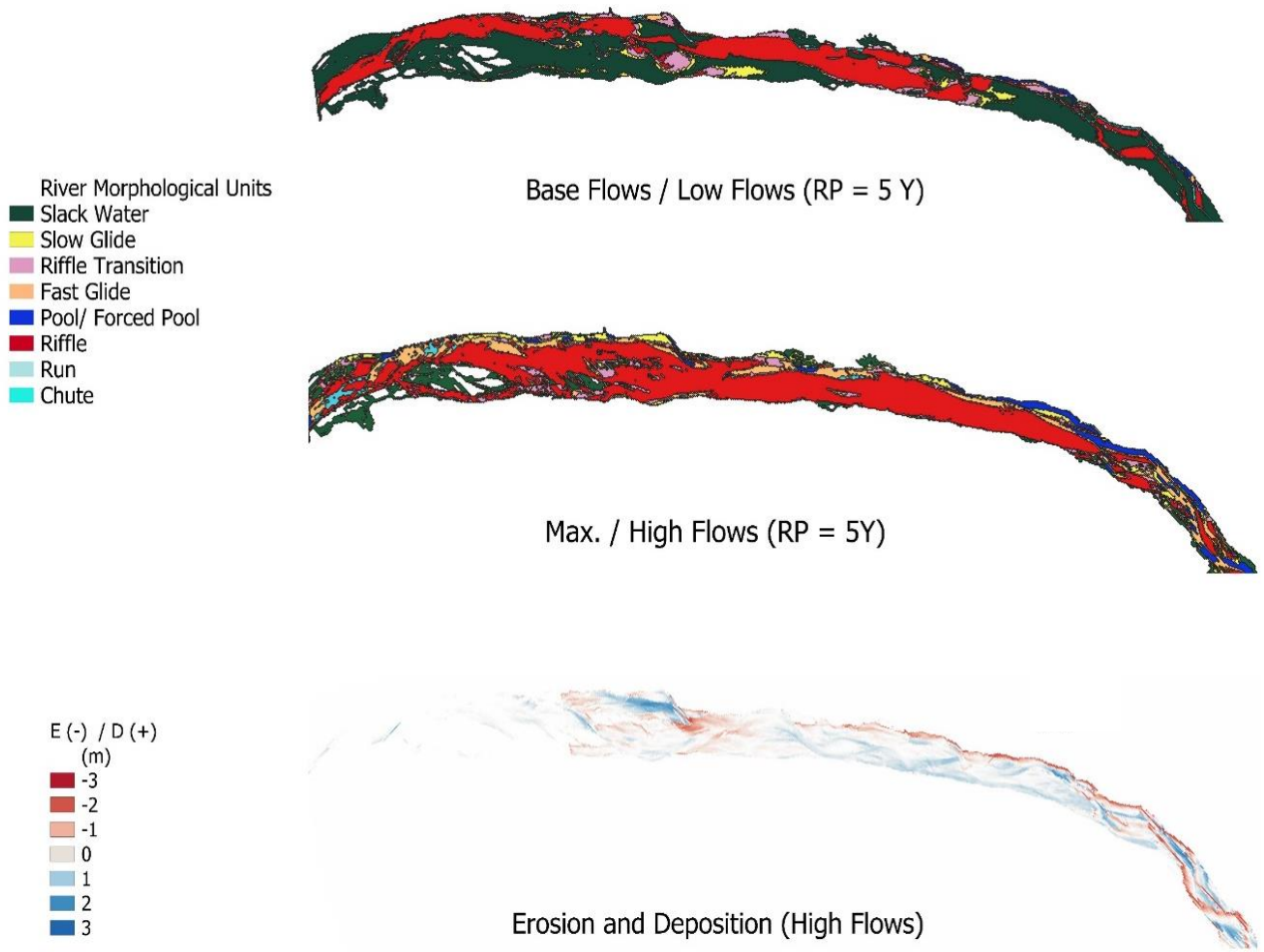

Figure 5.54 Sub-reach 1 Baganza River morphological unit.

In sub-reach 2, like sub-reach 1, a dominant presence of slack water (dark green) characterizes the landscape under "base flow" conditions. Riffle (red) formations, along with riffle transition, also contribute significantly to the morphological composition.

However, upon classification based on high flows, notable transformations occur. As the flow increases, all morphological units within this section undergo changes, indicating a pronounced impact of the increased flow regime, as shown in Figure 5.55. It is worth noting that erosion predominantly occurs along the right bank in this sub-reach, differing from the erosion patterns observed in the previous section. Additionally, a distinct feature in this sub-reach is the presence of white patches in the central portion, indicative of rare to no sediment transport occurrence.

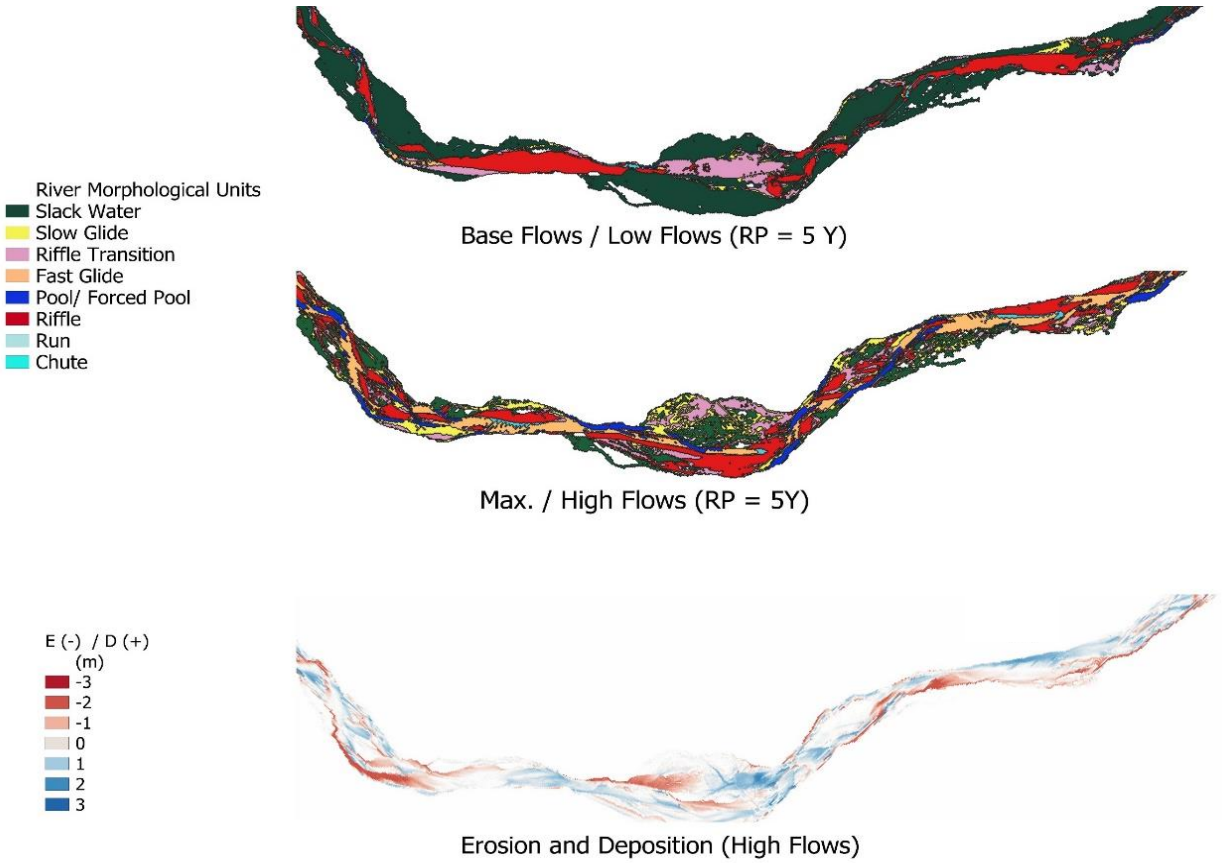

Figure 5.55 Sub-reach 2 Baganza River morphological unit.

In sub-reaches 3, 4, and 5, the morphology under "base flow" conditions follows a distinct pattern, characterized by an upstream area dominated by slack water, changes into riffles transition, and then into riffles features. Conversely, the lower downstream portion primarily consists of riffles, with minimal presence of slack water. During "high flow" scenarios, the sub-reach experiences a notable shift, with riffles dominating

almost the entire area, complemented by sporadic occurrences of fast glide and slow glide units along the periphery of the main river channel. Erosion and deposition trends exhibit an alternating pattern under high flow conditions, highlighting the dynamic nature of sediment transport processes in this sub-reach.

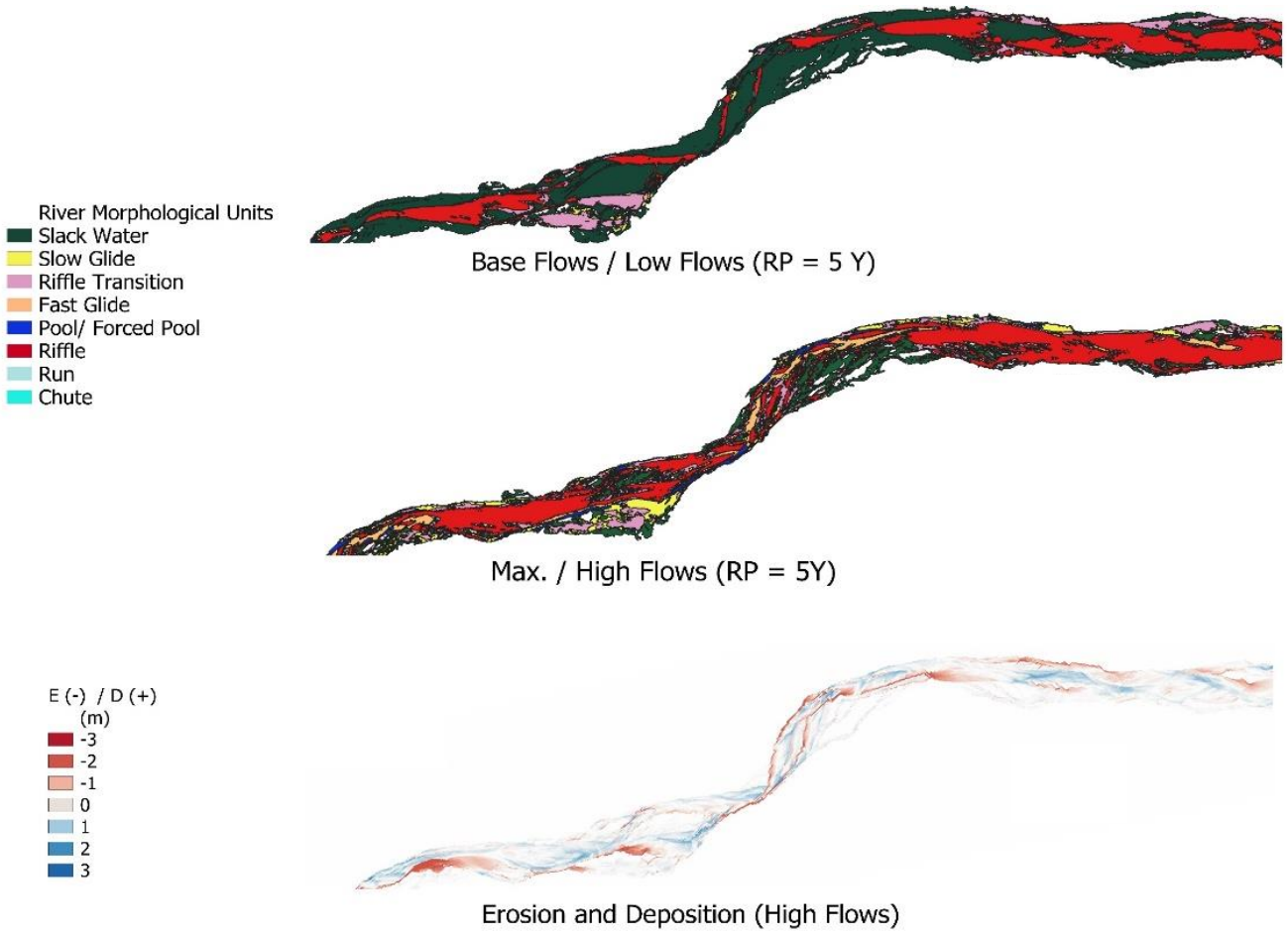

Figure 5.56 Sub-reach 3 baganza River morphological unit.

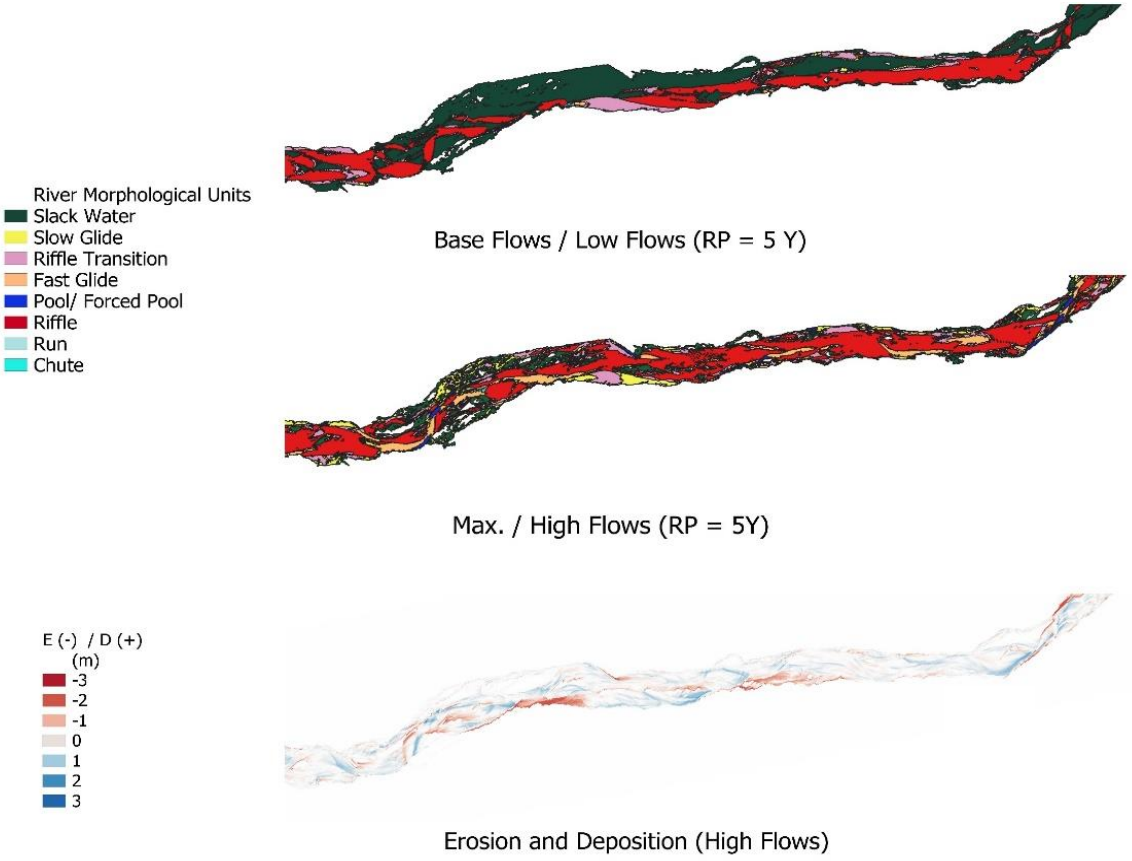

Figure 5.57 Sub-reach 4 Baganza River morphological unit.

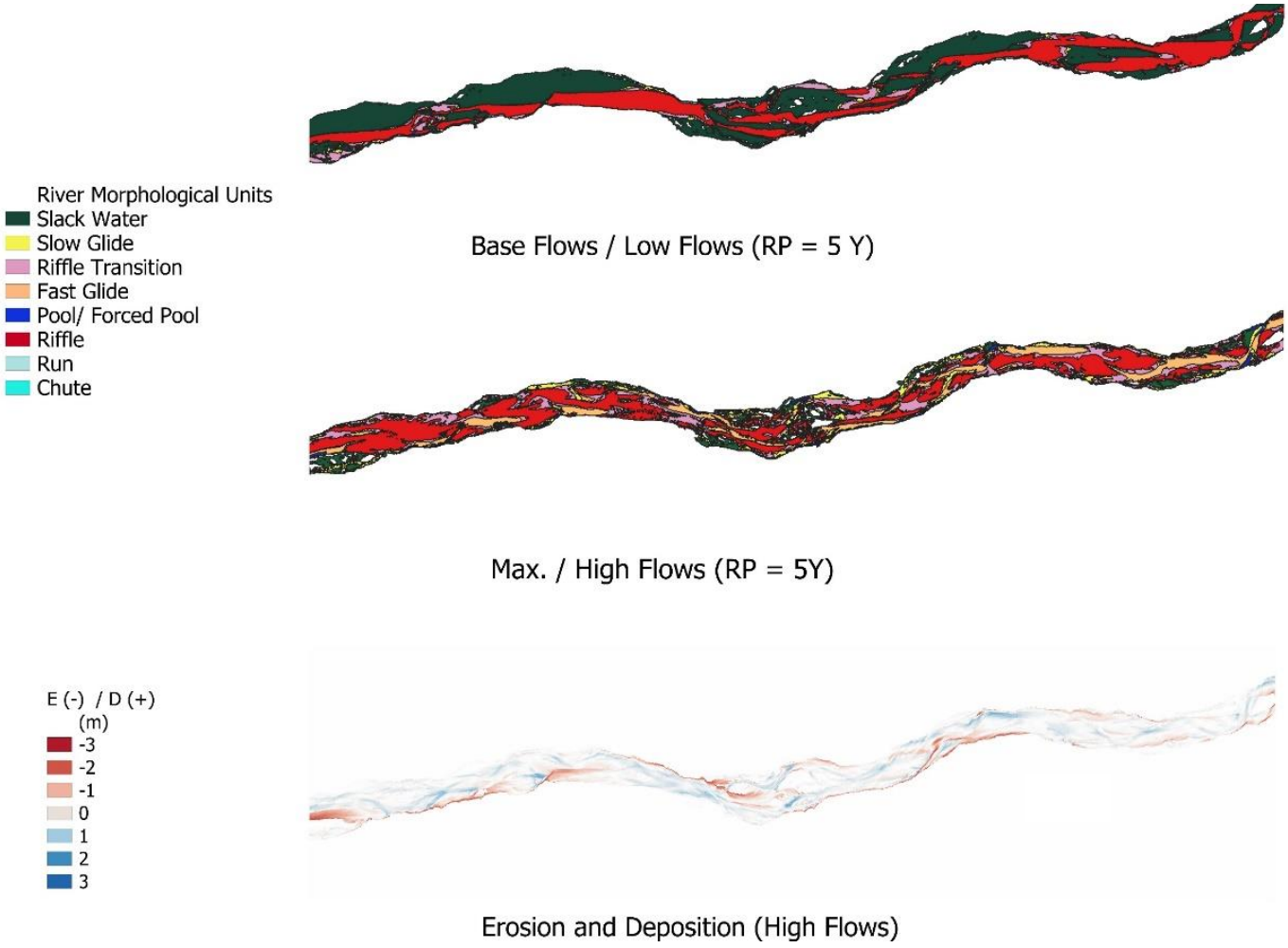

Figure 5.58 Sub-reach 5 Baganza River morphological unit.

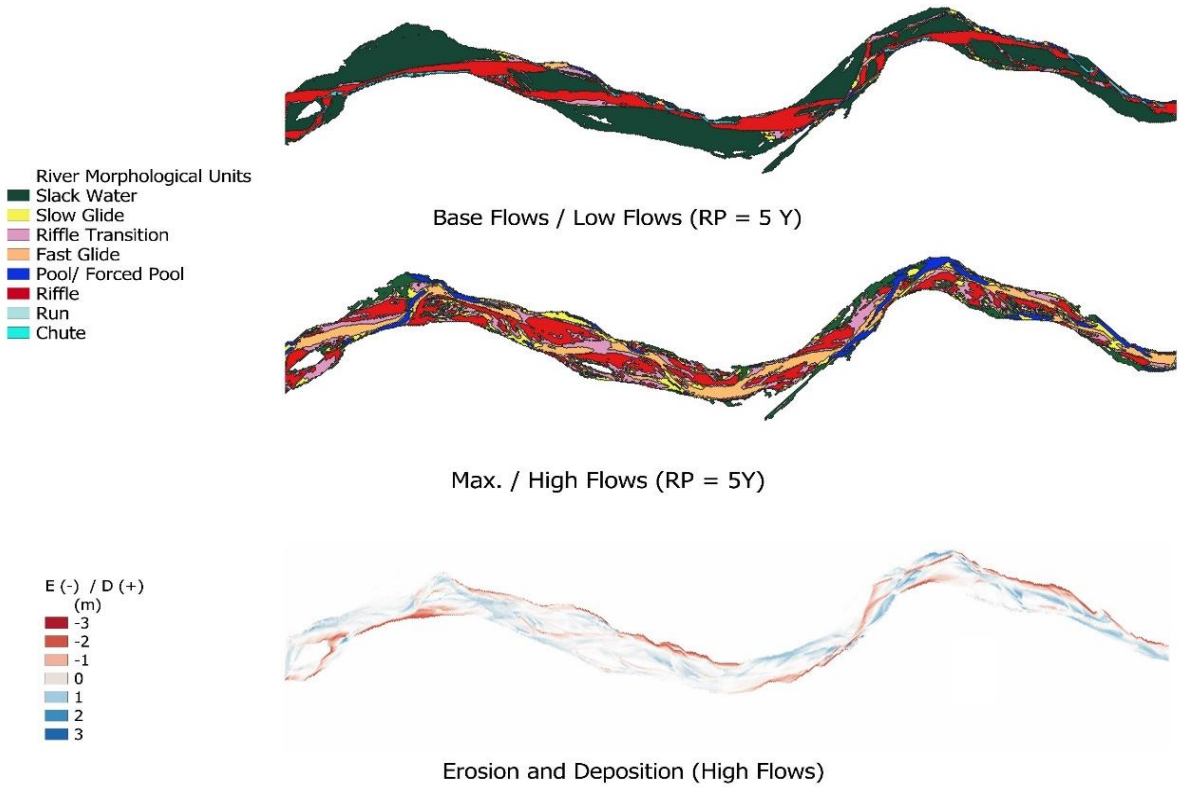

Figure 5.59 Sub-reach 6 Baganza River morphological unit.

Sub-reach 6 represents a transitional phase, as the Baganza River reach traverses more urbanized areas, resulting in a consistent morphology with reduced braidedness. Under "base flow" conditions, slack water is the most prominent morphological unit, followed by riffles. Conversely, high flow scenarios reveal a diverse array of morphological units, with fast glide and riffles dominating the landscape. Notably, dark blue areas emerge, indicating the presence of pool/forced pool formations, emphasizing areas of increased water depth and habitat diversity. This sub-reach demonstrates a unique aspect of urban river morphology, showcasing a combination of natural and anthropogenic influences on channel dynamics and habitat distribution. The last sub-reach 7 represents the reach where the downstream boundary condition is imposed near the Ponte Italia bridge. Here it is imperative to note that slack water and riffle are dominated in the "low flow" regimes whereas in "high flow" regimes, morphological units are dominated by pool/forced pool with dark blue colour. This is because in this section water remains stagnant and have high water depth as compared to any other section in the domain. The second prominent feature after pool is slow glide shown in Figure 5.60.

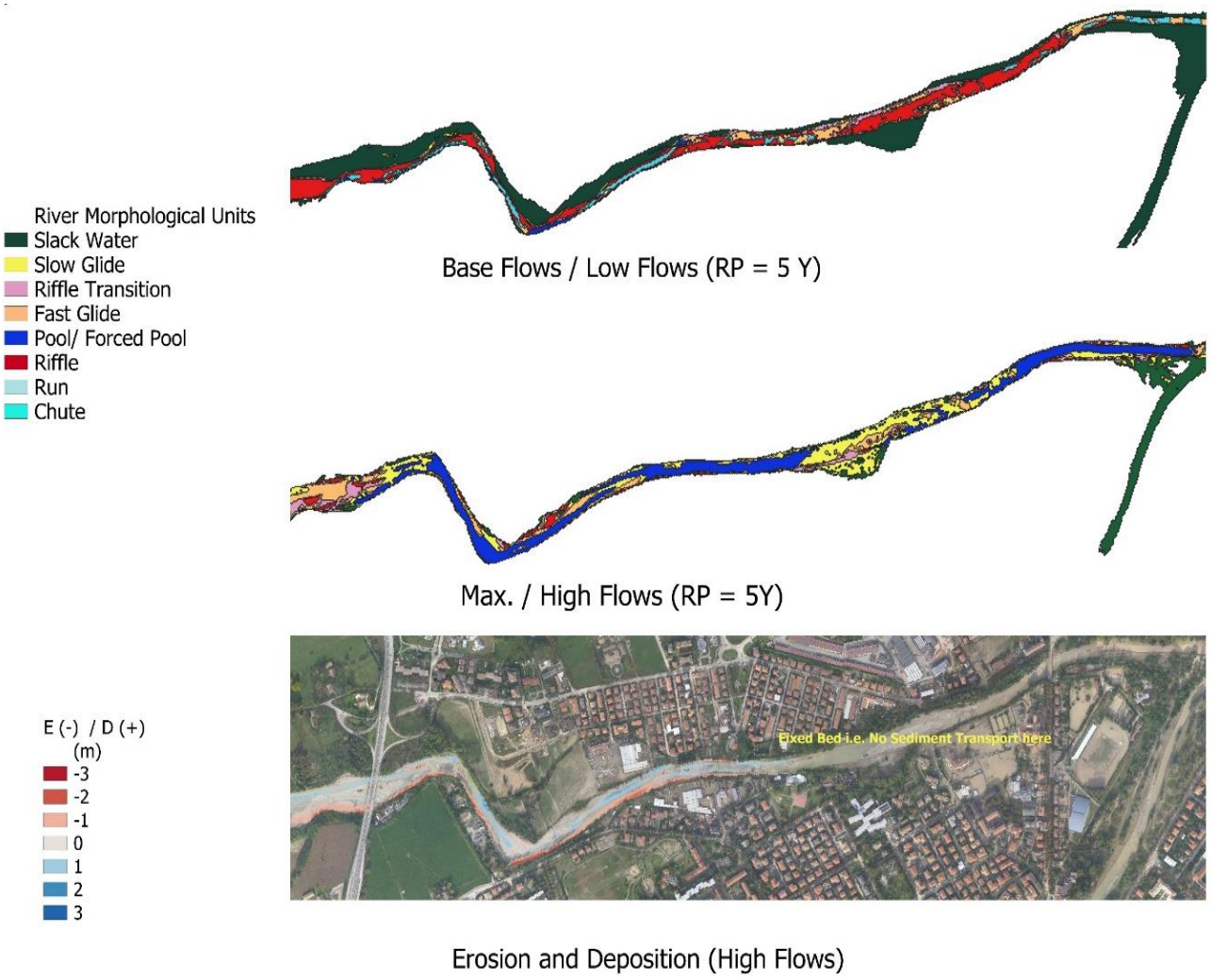

Figure 5.60 Sub-reach 7 Baganza River morphological unit.

Considering the general bahaviour of solid bedload transport in river baganza we can say that more erosive action occurs along the banks mostly on the left side during the rising limb of the hydrograph whereas the intensity become less once the flood starts to recede. Another important point is no sediment transport occurs in the last section can be seen in Figure 5.60 here the shear stress value remain less than the critical shear stress value which restrict the solid movement inside the channel.

Chapter 6: CONCLUSIONS

The investigation undertaken in this research aimed to deepen understanding of the morphodynamic modelling through a multidisciplinary approach. Preliminary, both geomorphological and granulometric analyses were conducted on the case study of the Baganza River catchment. The main part of the research was the numerical integration of previously built hydrodynamic model by (Vacondio et al., 2014, 2017) and morphodynamic model by Juez et. al. (2014). The new sediment transport model was subjected to benchmark tests, by referring to laboratory experiments from literature. By considering the application of the new sediment transport model to the real case study, its responsiveness against input parameters and high-resolution topographical data was assessed. Throughout this systematic exploration, key findings and limitations that provide valuable insights for future research were uncovered and detailed as below. In examination of the geomorphological characterization, the mature geomorphic stage of the Baganza catchment was revealed. This involved identifying critical morphometric parameters such as basin relief, slope, stream order, bifurcation ratio and stream length ratio that are essential for understanding river system dynamics. These insights hold significant implications for applications such as flood risk assessment.

Granulometric classification of river sediments involved the adoption of a hybrid technique, merging photogrammetry and sieving methods. Through this approach, we conducted robust granulometric distribution analysis, highlighting the prevalence of gravel content within the catchment within range 2-32 mm. Additionally, the hybrid technique proved efficient in streamlining data collection processes, which was eventually utilized for the sediment transport model.

Incorporating sediment effects into hydrodynamic models was a crucial aspect of this study. Through benchmark testing of sediment transport model using MPM and SMART approaches, we demonstrated their accuracy in replicating known dam break experimental scenarios. However, identified limitations, such as overlooking vertical velocities and the evolution of grain size distribution over time, present significant challenges. The model results predict the experimental results accurately even with the limitations just discussed, however the mass balance results show the otherwise.

The impact of high-resolution bathymetry on sediment dynamics and model responsiveness to alterations in input parameters was also assessed. Exploration of sediment dynamics and model performance across various sub-reaches underscored the complexities of river morphology. While both MPM and SMART approaches exhibited strengths and weaknesses, the findings emphasized the importance of considering individual performance characteristics for precise predictions. In most of the simulation scenarios, SMART approach outperforms the MPM approach as shown by the heatmaps produced in section 5.4.1and 5.4.2. This difference appears prominent in the region where the river passes by the urban areas with relatively straight stretches.

Despite these constraints, the findings of the study make significant contributions to the comprehension and management of river systems, with implications for devising flood mitigation strategies and fostering environmental sustainability.

References

Aberle, J., & Nikora, V. (2006). Statistical properties of armored gravel-bed surfaces. Water Resources Research, 42, W11414. https://doi.org/10.1029/2005WR004674

Agenzia Interregionale per il fiume Po (AIPo). (2016). Relazione finale piano delle indagini propedeutiche alla progettazione definitiva (PR-E-1047). Progettazione definitiva dei lavori di realizzazione della cassa di espansione del T. Baganza nei comuni di Felino (PR), Sala Baganza (PR), Collecchio (PR) e Parma. (https://www.agenziapo.it/documentazione/115 accessed on 10/01/2022)(In Italian).

Albaroot, M., et al. (2018). Quantification of Morphometric Analysis using Remote Sensing and GIS Techniques in the Qa' Jahran Basin, Thamar Province, Yemen. International Journal of New Technology and Research, 4(8), August.

Arabameri, A., Tiefenbacher, J. P., Blaschke, T., Pradhan, B., & Bui, D. T. (2020). Morphometric analysis for soil erosion susceptibility mapping using novel GIS-based ensemble model. Remote Sensing, 12(5). https://doi.org/10.3390/rs12050874

Arnaud-Fassetta, G., et al. (2009). Fluvial geomorphology and flood-risk management. Géomorphologie: Relief, Processus, Environnement, 15(2), 109–128. https://doi.org/10.4000/geomorphologie.7554

Awasthi, A. K. (1970). Skewness as an environmental indicator in the Solani river system, Roorkee (India). Sedimentary Geology, 4(1-2), 177–183.

Ayad Ali Faris Beg (2015). Morphometric Toolbox: A New Technique in Basin Morphometric Analysis Using ArcGIS. Global Journal of Earth Science and Engineering, 2(2), 21–30. https://doi.org/10.15377/2409-5710.2015.02.02.1

Bellal, M., Iervolino, M., & Zech, Y. (2004). Knickpoint migration process: Experimental and numerical approaches. Proceedings of the 12th conference on Sediment and Sedimentation Particles, Prague, Czech Republic, September 2004, pp. 185-195.

Belletti, B., Rinaldi, M., Bussettini, M., Comiti, F., Gurnell, A., Mao, L., Nardi, L., Vezza, P. (2017). Characterising physical habitats and fluvial hydromorphology: A new system for the survey and classification of river geomorphic units. Geomorphology. 283. 10.1016/j.geomorph.2017.01.032.

Brush, L. M., & Wolman, M. G. (1960). Knickpoint bahaviour in non-cohesive material: A laboratory study. Bulletin of the Geological Society of America, 71(1), 59-73.

Bunte, K., & Abt, S. R. (2001). Sampling surface and subsurface particle-size distributions in wadable gravel- and cobble-bed streams for analyses in sediment transport, hydraulics, and streambed monitoring. US Department of Agriculture, Forest Service, Rocky Mountain Research Station.

Bunte, K., & Abt, S. R. (2001). Sampling Surface and Subsurface Particle-Size Distributions in Wadable Gravel- and Cobble-bed Streams for Analyses in Sediment Transport, Hydraulics, and Streambed Monitoring. USDA Rocky Mountain Research Station, General Technical Report RMRS-GTR-74.

Caleffi, V., Valiani, A., & Zanni, A. (2003). Finite volume method for simulating extreme flood events in natural channels. Journal of Hydraulic Research, IAHR, 41(2), 167-177.

Cavalli, M., Trevisani, S., Comiti, F., & Marchi, L. (2013). Geomorphometric assessment of spatial sediment connectivity in small Alpine catchments. Geomorphology, 188, 31–41. https://doi.org/10.1016/j.geomorph.2012.05.007

Church, M. A., McLean, D. G., & Wolcott, J. F. (1987). River bed gravels: Sampling and analysis. In Sediment Transport in Gravel-Bed Rivers, Thorne, C. R., Bathurst, J. C., & Hey, R. D. (eds.), John Wiley and Sons, Chichester, 43–88.

Clerici, A., Perego, S., Tellini, C., & Vescovi, P. (2002). A procedure for landslide susceptibility zonation by the conditional analysis method. Geomorphology, 48, 349-364. https://doi.org/10.1016/S0169-555X(02)00079-X

Dade, W.B. (2000). Grain size, sediment transport and alluvial channel pattern. Geomorphology, 35(1-2), 119–126. https://doi.org/10.1016/S0169-555X(00)00030-1

Dazzi, S., Vacondio, R., & Mignosa, P. (2019). Integration of a levee breach erosion model in a GPU-accelerated 2D shallow water equations code. Water Resources Research, 55, 682–702. https://doi.org/10.1029/2018WR023826

Dazzi, S., Vacondio, R., Dal Palù, A., & Mignosa, P. (2018). A local time-stepping algorithm for GPU-accelerated 2D shallow water models. Advances in Water Resources, 111, 274-288.

Di Francesco, S., Biscarini, C., & Manciola, P. (2016). Characterization of a flood event through a sediment analysis: The Tescio River case study. Water, 8(7), 308.

Dottori, F., Kalas, M., Salamon, P., Bianchi, A., Alfieri, L., & Feyen, L. (2017). An operational procedure for rapid flood risk assessment in Europe. Natural Hazards and Earth System Sciences, 17(7), 1111–1126. https://doi.org/10.5194/nhess-17-1111-2017

Ferrari, A., Viero, D. P., Vacondio, R., Defina, A., & Mignosa, P. (2019). Flood inundation modeling in urbanized areas: A mesh-independent porosity approach with anisotropic friction. Advances in Water Resources, 125, 98-113.

Folk, R. L., & Ward, W. C. (1957). Brazos River bar [Texas]: A study in the significance of grain size parameters. Journal of Sedimentary Research, 27(1), 3–26.

Fripp, J., & Diplas, P. (1993). Surface Sampling in Gravel Streams. Journal of Hydraulic Engineering, 119(4), 473-482. https://doi.org/10.1061/(ASCE)0733-9429(1993)119:4(473)

Graham, D. J., & Reid, I. (2005). Automated sizing of coarse-grained sediments: Image-processing procedures. Mathematical Geology, 37(1), 1–28.

Graham, D. J., & Rice, S. P. (2005). A transferable method for the automated grain sizing of river gravels. Water Resources Research, 41, W07020.

Hassan, M. A., & Church, M. (2000). Experiments on surface structure and partial sediment transport on a gravel bed. Water Resources Research, 36(7), 1885–1895.

Hutton, C. J. (2012). Modelling Geomorphic Systems: Numerical Modelling. In Geomorphological Techniques, 13.

Juez, C., Murillo, J., & García-Navarro, P. (2014). A 2D weakly-coupled and efficient numerical model for transient shallow flow and movable bed. Advances in Water Resources, 71, 93-109. https://doi.org/10.1016/j.advwatres.2014.05.014

Kabir, M. A., Dutta, D., & Hironaka, S. (2015). Evaluation of sediment transport capacity equations using basin scale process-based sediment dynamic modelling approach. Water Resources Management, 29(4), 1097–1116. https://doi.org/10.1007/s11269-014-0863-0

Khan, U. A., & Valentino, R. (2022). Investigating the granulometric distribution of fluvial sediments through the hybrid technique: Case study of the Baganza River (Italy). Water, 14(9), 1511.

Kondolf, G. M., Lisle, T. E., & Wolman, G. M. (2007). Bed sediment measurement. In G. M. Kondolf & H. Piegay (Eds.), Tools in Fluvial Geomorphology (pp. 333-353). John Wiley & Sons Ltd.

Korup, O., Strom, A. L., & Weidinger, J. T. (2006). Fluvial response to large rock-slope failures: Examples from the Himalayas, the Tien Shan, and the Southern Alps in New Zealand. Geomorphology, 78(1–2), 3–21. https://doi.org/10.1016/j.geomorph.2006.01.020

Kurganov, A., & Petrova, G. (2007). A second-order well-balanced positivity-preserving central-upwind scheme for the Saint-Venant system. Communications in Mathematical Sciences, 5(1), 133–160.

Le Roux, J. P., & Rojas, E. M. (2007). Sediment transport patterns determined from grain size parameters: Overview and state of the art. Sedimentary Geology, 202, 473–488.

Liang, Q., & Borthwick, A. G. (2009). Adaptive quadtree simulation of shallow flows with wet-dry fronts over complex topography. Computers & Fluids, 38, 221–234.

Mahala, A. (2019). The significance of morphometric analysis to understand the hydrological and morphological characteristics in two different morpho-climatic settings. Applied Water Science, 10, 156. https://doi.org/10.1007/s13201-019-1118-2

Mandarino, A., Pepe, G., Maerker, M., Cevasco, A., & Brandolini, P. (2020). Short-term GIS analysis for the assessment of the recent active-channel planform adjustments in a widening, highly altered river: The Scrivia River, Italy. Water, 12(2), 514.

Meyer-Peter, E., & Müller, R. (1948). Formulas for bed load transport. Proceedings of the 2nd IAHR Congress, Stockholm, Sweden.

Palumbo, A., Frazao, S. S., Goutière, L., Pianese, D., & Zech, Y. (2008). Dam-break flow on mobile bed in a channel with a sudden enlargement. Journal of Hydraulic Engineering, 134(2), 206–218.

Pasternack, G. B. (2011). 2D modeling and ecohydraulic analysis. University of California at Davis.

Reid, I., Graham, D., Laronne, J., & Rice, S. (2010). Essential ancillary data requirements for the validation of surrogate measurements of bedload: non-invasive bed material grain size and definitive measurements of bed-load flux. U.S. Geological Survey Scientific Investigations Report 2010–5091.

Roberts, R. G., & Church, M. (1986). The sediment budget in severely disturbed watersheds, Queen Charlotte Ranges, British Columbia. Canadian Journal of Forest Research, 16(5), 1092–1106.

Rogers, B. D., Borthwick, A. G., & Taylor, P. H. (2003). Mathematical balancing of flux gradient and source terms prior to using Roe's approximate Riemann solver. Journal of Computational Physics, 192(2), 422–451.

Salim, A. H. A. (2014). Geomorphological analysis of the morphometric characteristics that determine the volume of sediment yield of Wadi Al-Arja, South Jordan. Journal of Geographical Sciences, 24(3), 457–474. https://doi.org/10.1007/s11442-014-1100-8

Smart, G. (1984). Sediment transport formula for steep channels. Journal of Hydraulic Engineering, 110(3), 267–276. https://doi.org/10.1061/(ASCE)0733-9429(1984)110:3(267)

Smart, G. M. (2003). The influence of roughness structure on flow resistance in mountain streams. Journal of Hydraulic Research, 41(3), 259–269.

Soares-Frazão, S., & Zech, Y. (2011). HLLC scheme with novel wave-speed estimators appropriate for two-dimensional shallow-water flow on erodible bed. International Journal for Numerical Methods in Fluids, 66(8), 973–989.

Spinewine, B., & Zech, Y. (2007). Small-scale laboratory dam-break waves on movable beds. Journal of Hydraulic Research, 45(sup1), 73-86. https://doi.org/10.1080/00221686.2007.9521834

Strom, K. B., Kuhns, R. D., & Lucas, H. J. (2010). Comparison of automated image-based grain sizing to standard pebble-count methods. Journal of Hydraulic Engineering, 136(4), 461–473.

Su, Q., Peng, C., Yi, L., Huang, H., Liu, Y., Xu, X., Chen, G., & Yu, H. (2016). An improved method of sediment grain size trend analysis in the Xiaoqinghe Estuary, southwestern Laizhou Bay, China. Environmental Earth Sciences, 75(15), 1185. https://doi.org/10.1007/s12665–016-5924–7

Syvitski, J. P. M. (1991). Principles, Methods, and Application of Particle Size Analysis. Cambridge University Press.

Toro, E. F. (2001). Shock-capturing methods for free-surface shallow water flows. John Wiley & Sons Ltd.

Vacondio, R., Dal Palù, A., & Mignosa, P. (2014). GPU-enhanced finite volume shallow water solver for fast flood simulations. Environmental Modelling & Software, 57, 60–75. https://doi.org/10.1016/j.envsoft.2014.02.003

Vanzo, D., Peter, S., Vonwiller, L., Buergler, M., Weberndorfer, M., Siviglia, A., Conde, D., & Vetsch, D. F. (2021). BASEMENT v3: A modular freeware for river process modeling over multiple computational backends. ArXiv:2102.12862 [Physics]. https://doi.org/10.48550/arXiv.2102.12862

Variante al Piano per l'assetto idrogeologico del bacino del fiume Po (PAI): torrente Baganza da Calestano a Confluenza Parma e torrente Parma da Parma a confluenza Po, 2015, pp-12.

Venditti, J. G., Dietrich, W. E., Nelson, P. A., Wydzga, M. A., Fadde, J., & Sklar, L. (2010). Effect of sediment pulse grain size on sediment transport rates and bed mobility in gravel bed rivers. Journal of Geophysical Research, 115(F3), F03039.

Williams, R. D., Brasington, J., & Hicks, D. M. (2016). Numerical modelling of braided river morphodynamics: Review and future challenges. Geography Compass, 10(3), 102–127. https://doi.org/10.1111/gec3.12260

Wolman, M. G. (1954). A method of sampling coarse river-bed material. American Geophysical Union, Transactions, 35(6), 951–956.

Zavattero, E., Du, M., Ma, Q., Delestre, O., & Gourbesville, P. (2016). 2D sediment transport modeling in high energy river: Application to Var River, France. Procedia Engineering, 154, 536–543. https://doi.org/10.1016/j.proeng.2016.07.549

Zech, Y., Soares-Frazão, S., Spinewine, B., et al. (2008). Dam-break induced sediment movement: Experimental approaches and numerical modelling. Journal of Hydraulic Research, 46(2), 176–190. https://doi.org/10.1080/00221686.2008.9521854

Ziliani, L., & Surian, N. (2012). Evolutionary trajectory of channel morphology and controlling factors in a large gravel-bed river. Geomorphology, 173, 104-117.